Max-Planck-Institut für Meteorologie
Max Planck Institute for Meteorology

MAX-PLANCK-GESELLSCHAFT

Tropical Pacific/Atlantic Climate Variability and the Subtropical-Tropical Cells

Katja Lohmann

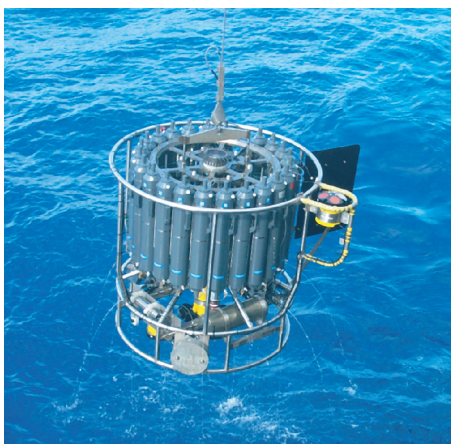

Berichte zur Erdsystemforschung 11/2005

Reports on Earth System Science

Hinweis

Die Berichte zur Erdsytemforschung werden vom Max-Planck-Institut für Meteorologie in Hamburg in unregelmäßiger Abfolge herausgegeben.

Sie enthalten wissenschaftliche und technische Beiträge, inklusive Dissertationen.

Die Beiträge geben nicht notwendigerweise die Auffassung des Instituts wieder.

Die "Berichte zur Erdsystemforschung" führen die vorherigen Reihen "Reports" und "Examensarbeiten" weiter.

Notice

The Reports on Earth System Science are published by the Max Planck Institute for Meteorology in Hamburg. They appear in irregular intervals.

They contain scientific and technical contributions, including Ph. D. theses.

The Reports do not necessarily reflect the opinion of the Institute.

The "Reports on Earth System Science" continue the former "Reports" and "Examensarbeiten" of the Max Planck Institute.

Anschrift / Address

Max-Planck-Institut für Meteorologie
Bundesstrasse 53
20146 Hamburg
Deutschland

Tel.: +49-(0)40-4 11 73-0
Fax: +49-(0)40-4 11 73-298
Web: www.mpimet.mpg.de

Layout:

Bettina Diallo, PR & Grafik

Titelfotos:
vorne:
Christian Klepp - Jochem Marotzke - Christian Klepp
hinten:
Clotilde Dubois - Christian Klepp - Katsumasa Tanaka

Berichte zur Erdsytemforschung 11/2005

Variabilität im tropischen Pazifik/Atlantik und die subtropisch-tropischen Zellen

Tropical Pacific/Atlantic Climate Variability and the Subtropical-Tropical Cells

Dissertation zur Erlangung des Doktorgrades der Naturwissenschaften
im Fachbereich Geowissenschaften der Universität Hamburg
vorgelegt von

Katja Lohmann

aus Weiden

Hamburg 2005

Reports on Earth System Science 11/2005

ISSN 1614-1199

Katja Lohmann
Max-Planck-Institut für Meteorologie
Bundesstrasse 53
20146 Hamburg
Germany

Als Dissertation angenommen
vom Fachbereich Geowissenschaften der Universität Hamburg

auf Grund der Gutachten von
Prof. Dr. Jens Meincke
und
Prof. Dr. Mojib Latif

Hamburg, den 1.Februar 2005
Professor Dr. Helmut Schleicher
Dekan des Fachbereiches Geowissenschaften

ISSN 1614-1199

Tropical Pacific/Atlantic Climate Variability and the Subtropical-Tropical Cells

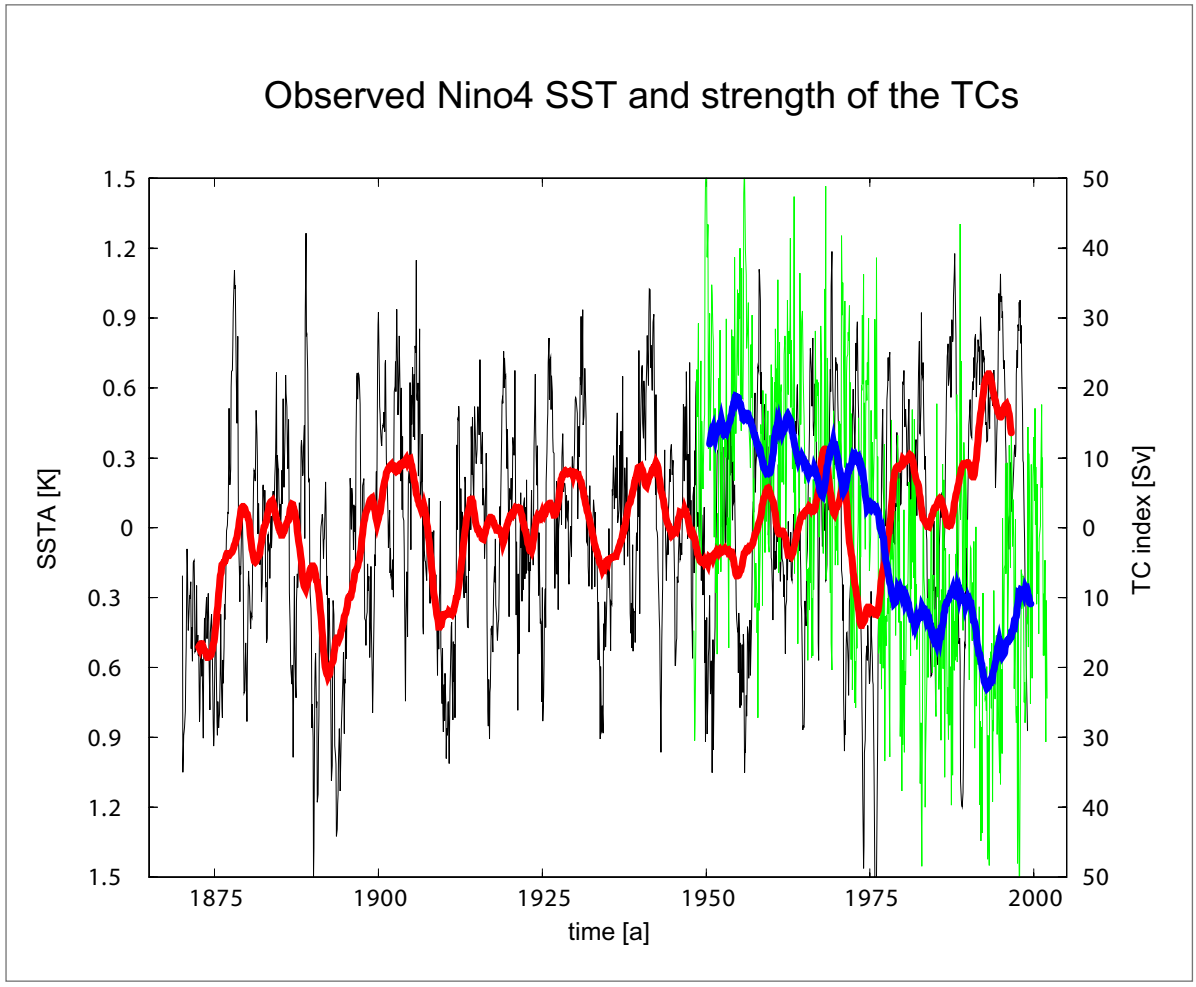

Katja Lohmann

Hamburg 2005

Table of contents

Abstract

In this study the variability in the tropical Pacific and Atlantic Ocean connected to the wind driven shallow tropical and subtropical overturning cells is investigated.

The leading sea surface temperature (SST) mode in the western equatorial Pacific (the Niño4 region) is a decadal mode. The analysis of observed SST and simulations with the MPI-OM model forced with the NCEP reanalysis suggests that the decadal SST variability is closely correlated with the variability of the tropical (TCs) and subtropical (STCs) cells. Changes in the strength of the cells lead the changes in SST. The lag becomes larger with increasing latitude, indicating that the STCs adjust slower than the narrow TCs. The correlation pattern between indices for the strength of the (S)TCs and the SST in the tropical Pacific shows an equatorial horseshoe-like pattern, which indicates that the influence of the cells is larger in the Niño4 than in the Niño3 region. For the TCs, a correlation between the cell strength and the SST is also found on interannual timescales.

Different processes play important roles in the connection between the cells and the SST. Apart from the anomalous upwelling of colder subsurface water, the zonal and meridional advection of water from the cold tongue by anomalous currents contributes to the changes in SST. In the warm pool area, where the vertical temperature gradient in the upper layer is relatively weak, the horizontal temperature advection is of the same order as the vertical one. The surface heat flux acts in most regions as a damping. Thus, it is the ocean dynamics that drive the decadal SST variability in large regions of the tropical Pacific.

The analysis of a multi-century integration with the coupled atmosphere-ocean model ECHAM4/OPYC supports the results obtained from the simulations forced with the NCEP reanalysis. The coupled integration suggests the existence of a coupled feedback loop between the SST and the STCs, which can also be seen in the coupled model ECHAM5/MPI-OM.

Considering the influence of the Atlantic (S)TC onto the tropical SST, no uniform results are found for the different models and timescales. Since the variability in the tropical Atlantic is relatively small compared to the tropical Pacific, one reason might be that mainly noise is considered here.

Some influence from the tropical Pacific onto the Atlantic (S)TC via changes in the trade winds over the Atlantic Ocean can be found. During years with anomalously warm (cold) Niño3 SST the strength of the cells increases (decreases).

The results of a scenario integration of the ECHAM4/OPYC model show a relativ complex response of the (S)TCs to greenhouse warming. The analysis of the 1% integrations from the coupled model intercomparison project CMIP2 shows different responses of the cells within the different models, making a prediction of (S)TC sensitivity to an increase in the CO_2 concentration difficult.

Zusammenfassung

In dieser Arbeit wird die Variabilität im tropischen Pazifik und Atlantik untersucht, die mit den windgetriebenen flachen tropischen und subtropischen Zellen verknüpft ist.

Der führende Meeresoberflächentemperatur(SST)-Mode im westlichen äquatorialen Pazifik (Niño4-Region) ist dekadisch. Die Analyse von beobachteter SST und Simulationen mit dem MPI-OM-Modell angetrieben mit der NCEP Reanalyse zeigt, daß die dekadische SST-Variabilität eng mit der Variabilität der tropischen (TCs) und subtropischen (STCs) Zellen korreliert ist. Änderungen in der Zellstärke gehen Änderungen in der SST zeitlich voraus, wobei der Zeitlag mit steigender Breite zunimmt. Letzteres läßt vermuten, daß sich die STCs langsamer ändern als die TCs. Das Korrelationsmuster zwischen der SST im tropischen Pazifik und Indices für die Stärke der (S)TCs zeigt ein äquatoriales hufeisenförmiges Muster, welches darauf schließen läßt, daß der Einfluß der Zellen in der Niño4-Region größer ist als in der Niño3-Region. Für die TCs findet man eine Korrelation zwischen der Zellstärke und der SST auch auf zwischenjährlichen Zeitskalen.

Bei der Verknüpfung von Zellen und SST sind verschiedene Prozesse von Bedeutung. Neben dem anomalen Upwelling von kälterem tieferem Wasser, trägt auch die zonale und meridionale Advektion von Wasser aus der relativ kalten Zunge im Osten durch anomale Strömungen zu den Änderungen in der SST bei. In der Warmpoolregion, wo der vertikale Temperaturgradient in der oberen Schicht relativ schwach ist, ist die horizontale Temperaturadvektion von gleicher Größenordnung wie die vertikale. Der Wärmefluß durch die Oberfläche wirkt überwiegend dämpfend. Es ist daher die Ozeandynamik, die die dekadische SST-Variabilität in großen Bereichen des tropischen Pazifiks antreibt.

Die Analyse einer mehrere hundert Jahre langen Integration mit dem gekoppelten Atmosphären/Ozeanmodell ECHAM4/OPYC ergibt ähnliche Ergebnisse wie die Simulationen, die mit der NCEP-Reanalyse angetrieben wurden. Die gekoppelte Integration weist auf eine Rückkopplungsschleife zwischen der SST und den STCs hin, welche auch im gekoppelten Modell ECHAM5/MPI-OM existiert.

Betrachtet man den Einfluß der atlantischen (S)TC auf die tropische SST, so finden sich für die unterschiedlichen Modelle und Zeitskalen keine übereinstimmenden Ergebnisse. Ein Grund dafür könnte die Tatsache sein, daß die Variabilität im tropischen Atlantik im Vergleich zum tropischen Pazifik relativ klein ist, so daß überwiegend Rauschen betrachtet wird. Man findet einen Einfluß vom tropischen Pazifik auf die atlantische (S)TC durch Änderungen in den Passatwinden über dem Atlantik. In Jahren mit anomal warmer (kalter) Niño3-SST nimmt die Zellstärke zu (ab).

Die Ergebnisse eines Szenarienlaufs mit dem ECHAM4/OPYC-Modell zeigen ein relativ komplexes Verhalten der (S)TCs bei globaler Erwärmung. Die Analyse der 1%-Läufe des gekoppelten Modellvergleichsprojektes CMIP2 zeigt ein unterschiedliches Verhalten der Zellen in den unterschiedlichen Modellen. Dieses erschwert eine genaue Vorhersage der Änderungen der (S)TCs bei einer Zunahme der CO_2-Konzentration.

1. Introduction

The sea surface temperature (SST) in the tropical Pacific exhibits pronounced decadal-scale variability. Studies investigating the origin of the SST variability include the tropical Pacific itself (e.g. *Trenberth and Hurrell, 1994* and *Graham, 1994*) and atmospheric teleconnections from midlatitudes (e.g. *Barnett et al., 1999*). Several studies suggest an influence of the shallow subtropical overturning cells (STCs) onto the SST variability in the tropical Pacific .

The STCs are mainly wind driven meridional overturning cells which were first described by *McCreary and Lu (1994)* and *Liu (1994)*. Figure 1 shows the meridional overturning streamfunction for the upper subtropical-tropical Pacific Ocean taken from an ocean general circulation model (OGCM) forced with the NCEP/NCAR reanalysis. In the zonal integral the STCs appear as closed cells with an upwelling at the equator, a poleward Ekman transport at the surface, subduction in the subtropics and an equatorward return flow within the thermocline. It is unclear, however, if these cells are really closed. *Johnson (2001)*, for instance, suggests from drifter data analysis that the poleward surface limb does not reach the subduction areas in the east.

The equatorial upwelling is partly balanced by downwelling within the tropics (at about 5^{o}S and 5^{o}N) forming relatively narrow recirculation cells which are referred to as tropical cells (TCs, *Lu et al., 1998*). The appearance of the TCs, however, can depend on the way the meridional overturning streamfunction is calculated (*Hazeleger et al., 2003*). The strength of the cells in our ocean model - 45 Sv and 25 Sv (1 Sverdrup = 10^6 m^3/s) for the southern and northern cell respectively - is in the order of what is suggested from observations and other model integrations (e.g. *Nonaka et al., 2002, McPhaden and Zhang, 2002* and *Sloyan et al., 2003*).

Considering the zonal structure shows that part of the equatorward flow is concentrated in the western boundary currents, the Mindanao Current and New Guinea Coastal Undercurrent

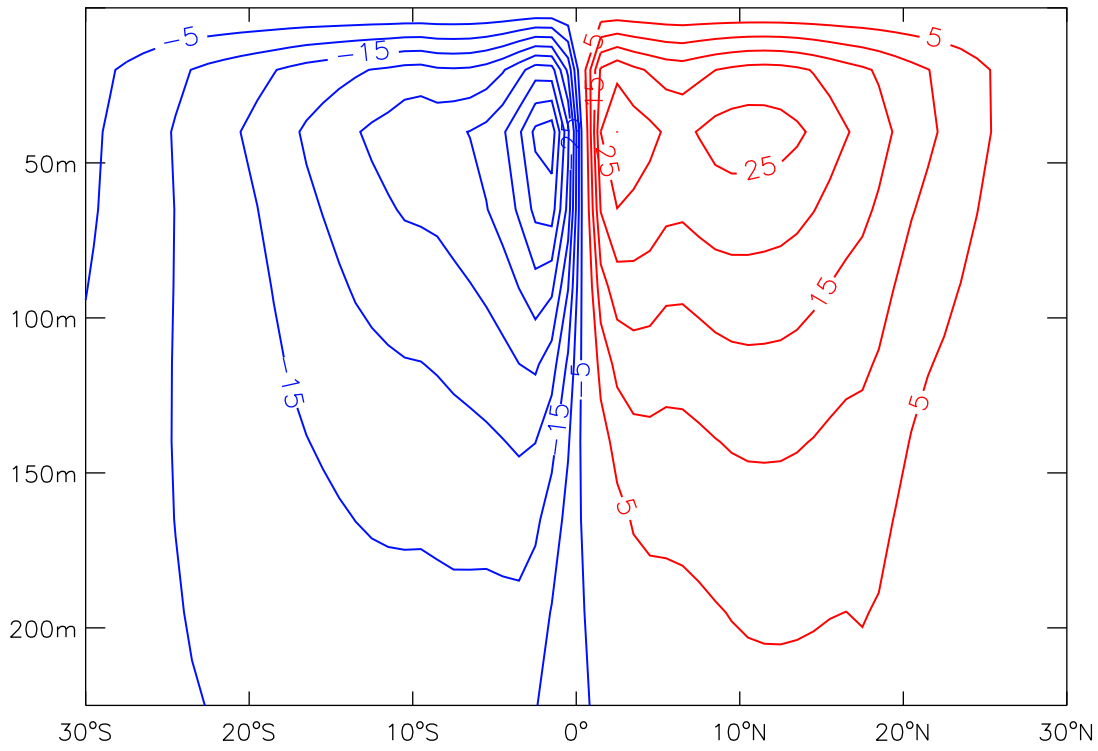

Figure 1: *Mean Pacific meridional overturning streamfunction in the MPI-OM model integration forced with the NCEP reanalysis (see chapter 2), averaged over the length of the run (1948-2001). Red (blue) lines represent clockwise (anticlockwise) flow. The contour interval is 5 Sv (1 Sv = 10^6 m^3/s).*

for the northern and southern hemisphere respectively. These currents feed into the Equatorial Undercurrent along which the upwelling occurs. The maximum upwelling velocities are found in the central to eastern Pacific.

The proposed influence of the STCs onto the SST is due to (1) the spin-up and -down of the cells leading to anomalies in the equatorward transport and upwelling strength of cold subsurface water and (2) due to the advection of temperature anomalies from the subtropical subduction areas by the mean flow. These two mechanisms are often referred to as (1) $v' \overline{T}$ and (2) $\bar{v} T'$ mechanism, respectively.

The first mechanism was suggested by *Kleeman et al. (1999)* from analysis of the tropical decadal variability simulated by a 3 1/2 layer ocean model coupled to a statistical atmosphere. Further supporting model studies were performed by *Klinger et al. (2002)* and *Solomon et al. (2003)* using the same ocean model and by *Nonaka et al. (2002)* who used an OGCM forced with observed wind stresses. *Merryfield and Boer (2004, submitted)* analyzed a coupled general circulation model (CGCM) simulation and found the $v' \overline{T}$ mechanism to be the

dominating one. *McPhaden and Zhang (2002)*, using hydrographic data and observed SST, reported that the warming of the tropical Pacific in the last decades was associated with a decrease in the strength of the STCs.

The second mechanism was described by *Gu and Philander (1997)* using a simple box model, by *Zhang et al. (1998)* analyzing the Levitus data and by *Giese et al. (2002)* using an OCGM. *Schneider et al. (1999)*, however, suggest from OGCM experiments that the subducted temperature anomalies from the subtropics do not affect the equatorial SST. This is supported by *Hazeleger et al. (2001)* who did not find any propagation of temperature anomalies to the equator in a combined model and observational study. *Yang and Liu (2004, submitted)* find both mechanisms of importance in their CGCM experiments. In a recent study, *Boccaletti et al. (2004, submitted)* proposed that a heat loss in higher latitudes leads via wave propagation to changes in the depth of the thermocline and thus to a heat gain at low latitudes.

In the tropical Atlantic Ocean the SST is dominated by two main modes of variability, the meridional or ‚dipol' mode (e.g. *Moura and Shukla, 1981*) and an ENSO-like mode (e.g. *Zebiak, 1993*).

Only very few studies consider an influence of the STC onto the SST variability. *Goes and Wainer (2003)* find a strengthening (weakening) of the (sub)surface currents during phases of cold (warm) equatorial SST using an OGCM forced with the NCEP reanalysis. *Lazar et al. (2001)* describe the propagation of temperature anomalies from the subtropics to the tropics using an Atlantic OGCM.

Comparing the mean STC in the Atlantic (figure 2) to that in the Pacific (figure 1) shows that while in the Pacific the cells are symmetric, only a southern STC exists in the Atlantic. Model studies suggest that the northern STC is canceled out due to the strong thermohaline overturning circulation (e.g. *Fratantoni et al., 2000*). A TC, however, seems to exist also in the northern hemisphere.

The strength of the Atlantic cell is relatively weak (12 Sv in the NCEP forced OGCM integration). *Zhang et al. (2003)* suggest from observations a transport of 10 Sv within the pycnocline branch, of which about half is concentrated in the western boundary current (North Brazil Undercurrent).

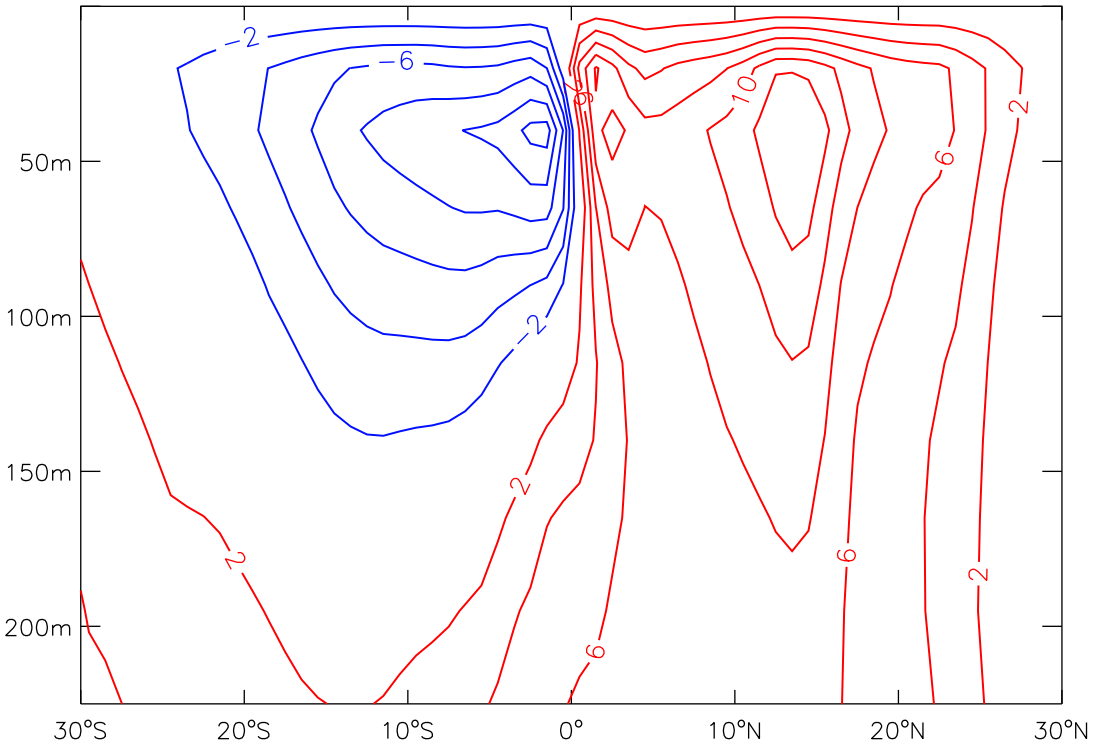

Figure 2: *Mean Atlantic meridional overturning streamfunction in the MPI-OM model integration forced with the NCEP reanalysis (see chapter 2), averaged over the length of the run (1948-2001). Red (blue) lines represent clockwise (anticlockwise) flow. The contour interval is 2 Sv (1 Sv = 10^6 m^3/s).*

In this study the variability in the tropical Pacific and Atlantic Ocean connected to the subtropical (STCs) and tropical (TCs) cells is investigated. Special attention is given to the Niño4 region and the decadal timescale.

The work is organized as follows: An overview over the data on which the study is based is given in chapter 2. In chapter 3 and 4 the results for the Pacific and Atlantic Ocean are discussed respectively. The main conclusions and an outlook are given in chapter 5.

2. Data

In this chapter the observations and model integrations, on which this study is based, are shortly described.

The observed SST is taken from the Hadley Centre Ice and Sea Surface Temperature (HadISST1.1) dataset encompassing the years 1870 to 1998 (*Rayner et al., 2003*).

To get insight into the dynamics of the observed SST variability a 54 year integration of the ocean general circulation model MPI-OM forced by the NCEP/NCAR reanalysis (*Kalnay et al., 1996*) for the years 1948 to 2001 is analyzed. The MPI-OM model, described by *Marsland et al. (2003)*, is a new version of the Hamburg Ocean Primitive Equation model HOPE using a C-grid and orthogonal curvilinear coordinates. For the integration used in this study the poles are located at 30^{o}W and 80^{o} north and south respectively. The horizontal resolution amounts to 2.5^{o} to 3^{o} in the tropical regions. The grid has a meridional refinement at the equator with a resolution of 0.5^{o} between about 10^{o}S and 10^{o}N. Vertically, 23 levels were used, of which nine are in the upper 250 meters. The surface heatflux was not taken from the NCEP reanalysis, but calculated according to Bulk formulae (see *Marsland et al., 2003*). Initial conditions were obtained from an extended-range integration with climatological forcing.

Six ensemble members exist for an integration with a different horizontal and vertical resolution (about 1.5^{o} horizontally without equatorial refinement and 40 vertical levels of which 13 are in the upper 250 meters). The initial conditions for each ensemble member were taken from the state simulated at the end of the previous member.

To separate the effect of the equatorial and off-equatorial winds onto the TC and STC variability, two wind sensitivity experiments were performed taking the MPI-OM model set-up of the third ensemble member. In the ‚no equator' experiment the wind stress forcing from the NCEP reanalysis is set to the climatological annual cycle between 5^{o}S and 5^{o}N. In the ‚only

equator‘ experiment climatological wind stress forcing is prescribed poleward of 5^o latitude. Both experiments contain transition zones between 5^o and 8^o latitude in which the anomalies (from the climatological annual cycle) change linearly.

Additionally, two existing wind sensitivity experiments are used in which climatological wind stress forcing and climatological forcing except wind stress respectively are applied globally. These experiments (plus the control run) were performed with a model set-up with a horizontal resolution of 3^o.

Apart from the MPI-OM integrations forced with the NCEP reanalysis results from a 300 year integration of the coupled general circulation model ECHAM4/OPYC3 are analyzed. The atmosphere model is ECHAM4 (*Roeckner et al., 1996*) with 19 vertical levels and a horizontal resolution of T42 corresponding to about 2.8^o x 2.8^o. The OPYC model (*Oberhuber, 1993*) is an isopycnal ocean model based on the primitive equations and has an embedded mixed layer model. The OGCM has a horizontal resolution of 2.8^o with a gradual meridional refinement in the subtropical/tropical region up to about 0.5^o in the equatorial region. The integration was run with 11 vertical density layers, and the output was interpolated onto fixed depth levels, 48 for the meridional overturning (17 in the upper 250 meters) and 10 for the other variables (5 in the upper 250 meters). The ECHAM4/OPYC3 integration was performed using flux correction.

Some of the analyses were additionally performed with the output (last 70 years) of a coupled integration of the MPI-OM model (1.5^o horizontal resolution and 40 vertical levels) with the atmosphere model ECHAM5 (horizontal resolution of T63 or about 2^o and 31 vertical levels). This integration runs without flux correction and a wind stress adaptation taking into account the ocean surface currents. In contrast to coupled integrations without wind stress adaptation, the Pacific and Atlantic STCs are represented more realistically (due to a reduction of the temperature bias in the equatorial region).

To investigate the behaviour of the TCs and STCs under greenhouse conditions the results of a 240 year long greenhouse warming simulation (*Roeckner et al., 1999*) of the ECHAM4/ OPYC model are analyzed. The increase in the CO_2 concentration is prescribed from observations from 1860 up to present and follows the IPCC 1992a scenario until 2100 (figure 25a).

Additionally, the control and 1% integrations (1% increase in the CO_2 concentration per

year) from the coupled model intercomparison project (CMIP2) were used. These integrations have a length of 80 years (corresponding to a doubling of the CO_2 concentration) and the output was averaged over 20 year intervals. For the Pacifc (Atlantic), meridional overturning data are available from 10 (13) models.

All data used in this study (except the results from the CMIP2 integrations) are monthly values with the mean annual cycle removed. Especially the northern TC in the Pacific shows a pronounced seasonal cycle related to the shift in the Intertropical Convergence Zone (ITCZ), being strongest (weakest) in the boreal winter (summer).

3. Pacific Ocean

3.1. Observed variability in Niño4 SST

Observations indicate that the decadal SST variability is particularly strong in the western central equatorial Pacific (e.g. *Trenberth and Hurrell, 1994, Graham, 1994*). Therefore the Niño4 region (160^{o}E - 150^{o}W, 5^{o}N - 5^{o}S) is chosen to begin the analysis of the decadal variability. Furthermore, the influence of the tropical (TCs) and subtropical (STCs) cells is larger in the western tropical Pacific than in the Niño3 region (see chapter 3.2).

Figure 3 shows the observed sea surface temperature anomalies (SSTAs) averaged over the Niño4 region from 1870 onwards. The timeseries exhibits rather strong decadal fluctuations with strong interannual variability superimposed. In order to highlight the decadal variability a five year running mean (red curve) is also shown. It is interesting that the relatively strong change in the mid 1970s is not unusual in the context of the last 130 years. It is also noteworthy that there is a rather strong trend in the Niño4 SSTAs during the last few decades.

The monthly Niño4 SSTA timeseries is decomposed by means of a singular spectrum analysis (SSA). The reconstructed Niño4 SSTAs using the first two SSA modes (pairs) are shown in figure 4. The leading temporal mode, accounting for about 25% of the variance of the Niño4 index, has a quasi-decadal timescale (figure 4a). It closely resembles the low-pass filtered curve (five year running mean) shown in figure 3. The second most energetic mode (figure 4b) corresponds to the well-known interannual variability associated with the El Niño/ Southern Oscillation (ENSO) phenomenon. It explains about 20% of the variance. It is noteworthy that the warming trend in the western equatorial Pacific seen in figure 3 projects only onto the decadal, but not onto the ENSO mode. Further discussion of the two timeseries is given in *Lohmann and Latif (2004, submitted)*.

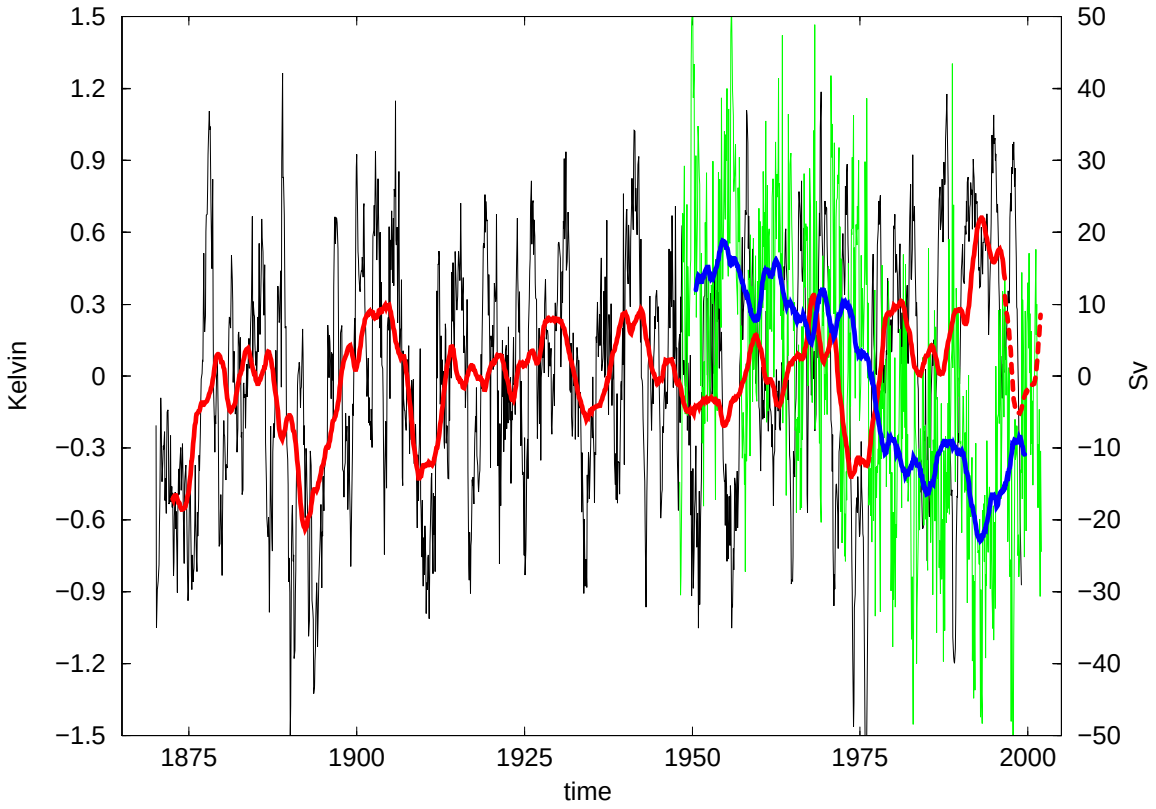

Figure 3: *Timeseries of the observed Niño4 SST anomalies and the anomalous strength of the tropical cells (TCs) taken from the MPI-OM model integration forced with the NCEP reanalysis. For definition of the cell strength see text (chapter 3.2). Shown are monthly values with the annual cycle removed (black for SST, green for TC) and five year running mean (red for SST, blue for TC). The dashed line shows the Niño4 SST anomalies (with a five year running mean applied) from the NCEP reanalysis.*

Next, the spatial structure associated with the temporal modes was computed by means of linear regression. The decadal mode (figure 5a) is El Niño-like, as described in other papers (e.g. *Zhang et al., 1997*). However, there are important differences to the canonical El Niño structure. The regression pattern for the decadal mode is broader in the meridional direction and stronger in the western than in the eastern equatorial Pacific. Near the dateline, the regression coefficients amount to about 0.3^{o}C per standard deviation of the decadal mode timeseries. The associated explained variance (figure 5b) shows a horseshoe-like structure, with maximum values in the western equatorial Pacific and off the equator, but low explained variances in the Niño3 region. It should be noted that the largest explained variance must occur in the Niño4 region, since the corresponding SSTA timeseries was used in the SSA. The equatorial horseshoe-like structure is also seen in the correlation pattern between the Niño4 SSTAs and the strength of the (S)TCs (figure 10, 20).

The regression pattern for the interannual or ENSO mode (not shown) shows the typical El

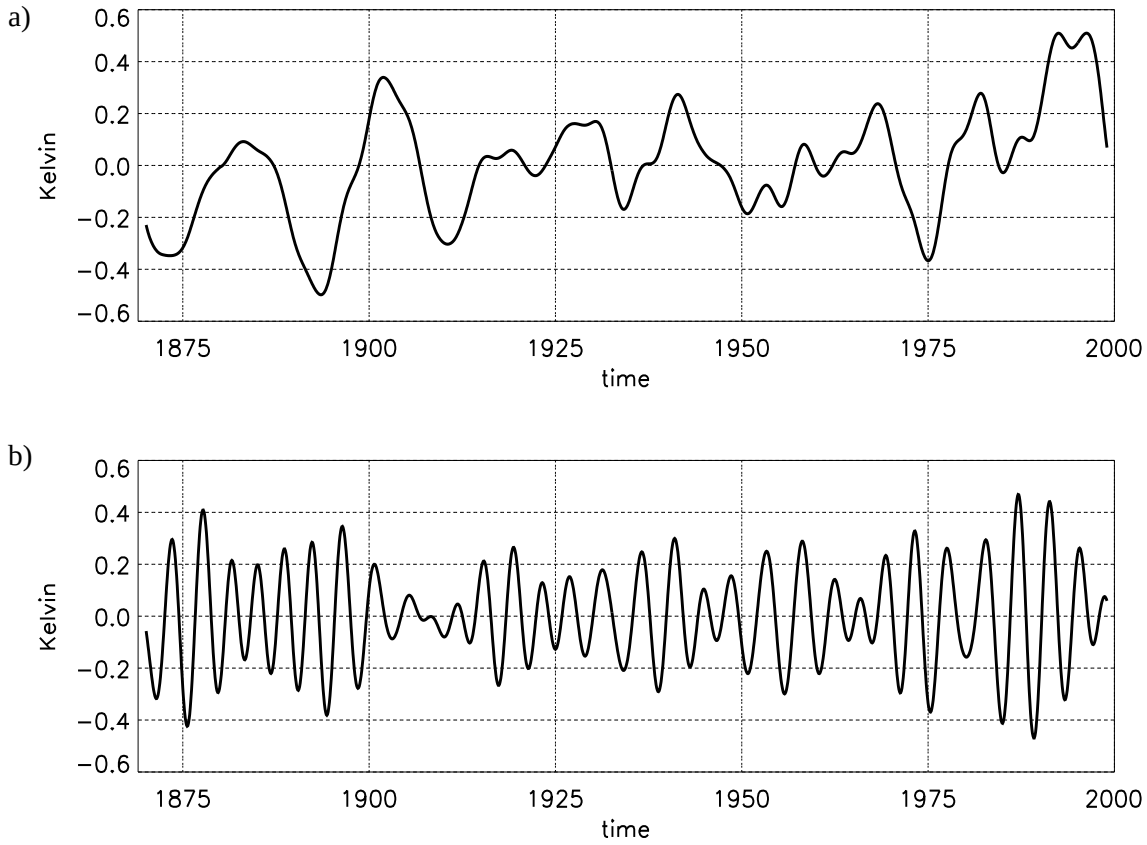

Figure 4: *Reconstruction of the monthly observed Niño4 SST anomalies (black curve in figure 3) from singular spectrum analysis using (a) mode 1 and 2 and (b) mode 3 and 4.*

Niño structure, with strongest anomalies in the eastern and central equatorial Pacific. Maximum regression coefficients reach 0.4^{o}C per standard deviation of the interannual mode timeseries. The ENSO mode explains most variance at the equator.

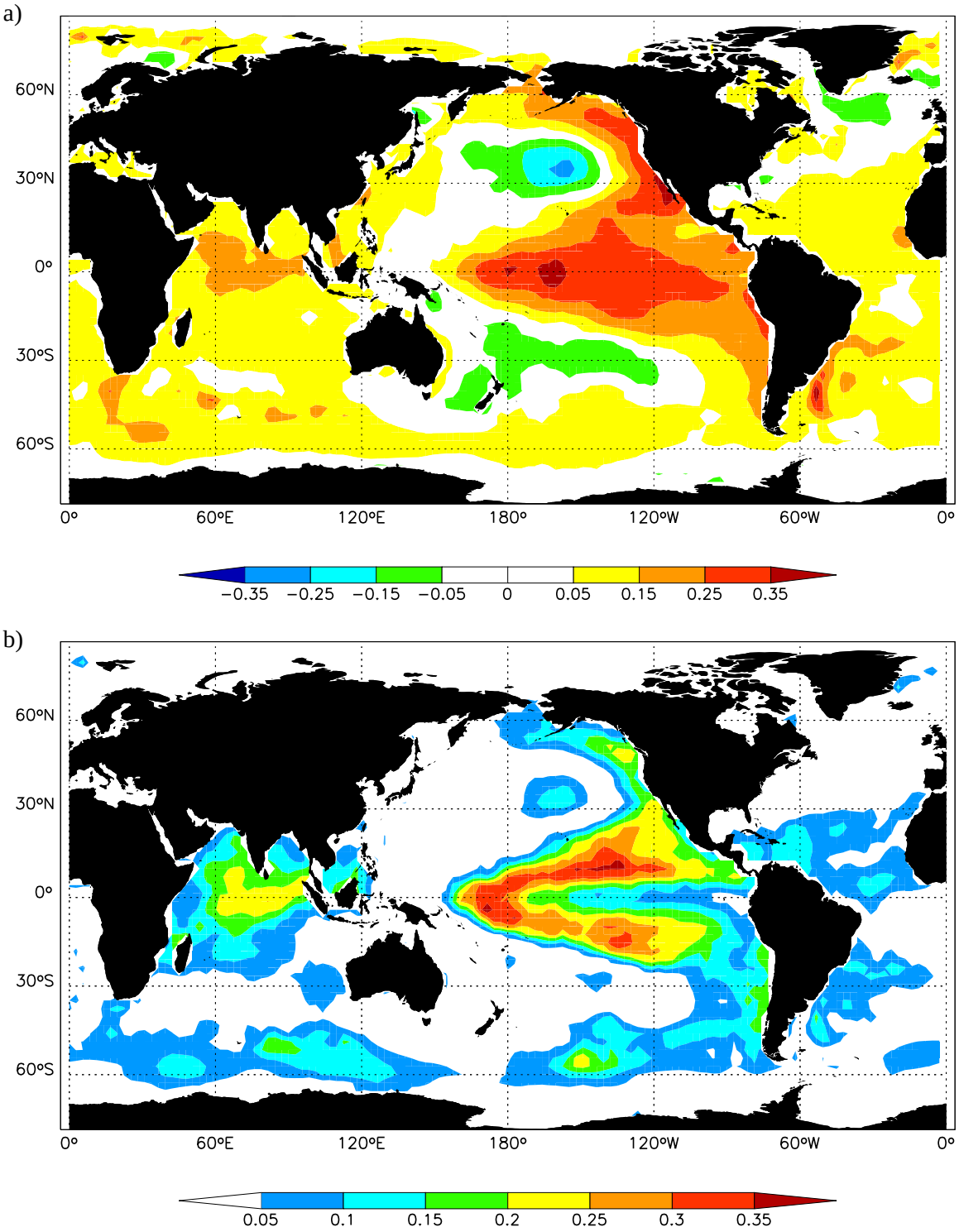

Figure 5: *(a) Linear regression of the monthly global observed SST onto the decadal Niño4 SST mode shown in figure 4a. Unit is Kelvin per standard deviation Niño4 SST (0.21K). (b) Explained variance of the regression pattern shown in (a).*

3.2. Relation of the observed Niño4 SST to the TCs and STCs

In this chapter the relationship between the observed decadal SST variability in the Niño4 region and the variability of the Pacific TCs and STCs derived from the MPI-OM model integration forced with the NCEP reanalysis is discussed.

Indices for the strength of the TCs and the STCs were defined by taking for each timestep $psi_{max}(5^oS \text{ to } 5^oN, \text{ upper } 250m) - psi_{min}(5^oS \text{ to } 5^oN, \text{ upper } 250m)$ and $psi_{max}(10^oN, \text{ upper } 250m) - psi_{min}(10^oS, \text{ upper } 250m)$ respectively, where *psi* is the Pacific meridional overturning streamfunction (the overturning is negative for the southern cell). The STC index is defined at 10^o latitude to be outside the range of the TCs. Further dependance on latitude is discussed below. To account for the fact that the surface branch of the cells is spinning-up and -down quicker than the pycnocline branch (*Liu, 1998, Klinger et al., 2002, Merryfield and Boer, 2004, submitted*), the decadal TC and STC strength variability discussed in this chapter is determined from overturning data to which a five year running mean has been applied.

In figure 3, the TC index is shown in addition to the Niño4 SSTA. The low-pass filtered TC and Niño4 SST timeseries as well as the low-pass filtered STC and Niño4 SST timeseries (not shown) are strongly anticorrelated, so that anomalously warm Niño4 SST goes along with anomalously weak overturning cells. For the TCs, the correlation coefficient amounts to -0.7, with the overturning leading by a few months (solid line in figure 9). The time lag indicates that the variability of the TCs is indeed driving the decadal SST fluctuations in the Niño4 region. Considering the northern and the southern hemispheric TC separately, the lag is about 2 month for the southern and 7 month for the northern cell. The reason for the different lag is not clear, but the fact that the northern cell is weaker than the southern one (figure 1) might play a role.

Considering the STCs, the largest correlation coefficient between the low-pass filtered cell strength index and Niño4 SSTAs amounts to -0.6 (long dashed line in figure 9), which is lower compared to the TCs but statistically significant at the 95% level (threshold value -0.44 according to a t-test). The changes in the STC strength lead the changes in SST by about 15 months. Compared to the TCs the lag is increasing, indicating that the STCs spin-up and -down slower than the narrow TCs. The lag is consistent with *Nonaka et al. (2002)* who found a lag of about 2 years between the equatorial temperature anomalies simulated by an ocean model forced with no equatorial winds and those from an ocean model forced by only

equatorial winds. Therefore one can suggest that the STCs have an influence on the (western) equatorial SST. Also the cross-correlation function between the low-pass filtered Niño4 SSTAs and indices of the decadal STC strength computed from different latitudes (short dashed and dashed dotted line in figure 9) has been determined. With increasing distance from the equator the correlation coefficient decreases and the lag between STC and SST anomalies increases. However, poleward of 15^o latitude, the correlation drops to a value close to the significance level. The fact that the trend in the STC strength vanishes at about 15^o latitude might contribute to the low correlations. Also figure 11a does not show a signal in the overturning poleward of 15^o latitude during phases of anomalously warm (cold) Niño4 SST.

The spatial correlation pattern (figure 10) between the decadal TC strength index and the monthly observed SSTs as well as between the decadal STC strength index and the monthly observed SSTs (not shown) closely resembles the equatorial horseshoe-like structure shown in figure 5b in the tropical Pacific, indicating that the influence of the STCS is higher in the western than in the eastern equatorial Pacific.

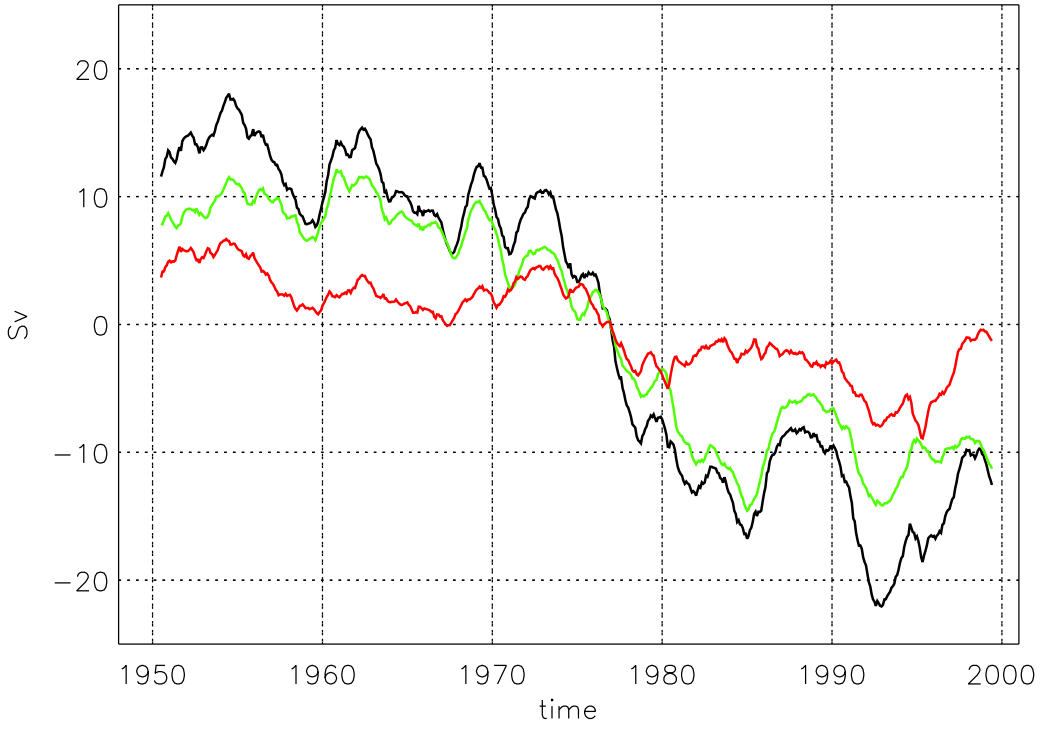

Figure 6: *Timeseries of the anomalous strength of the TCs taken from the MPI-OM model integration forced with the NCEP reanalysis: northern hemispheric cell (red), southern hemispheric cell (green) and combined index (black, corresponding to the blue curve in figure 3). For definition of the cell strength see text.*

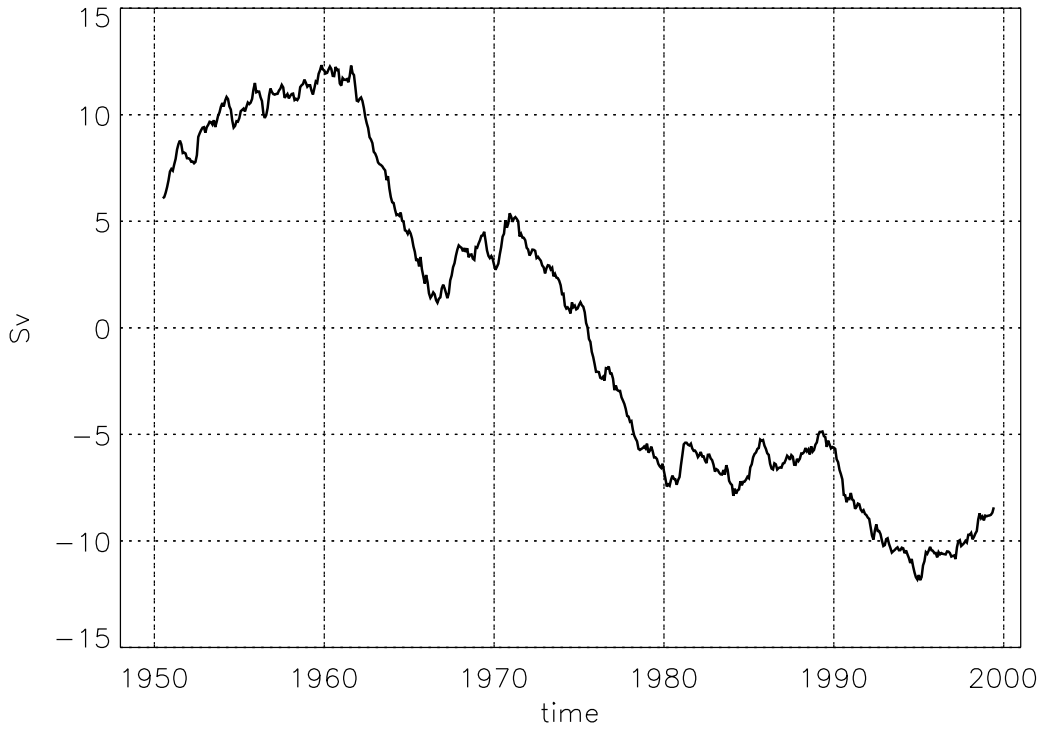

Figure 7: *Timeseries of the anomalous strength of the STCs taken from the MPI-OM model integration forced with the NCEP reanalysis. For definition of the cell strength see text.*

The most striking feature in the OGCM simulation is the spin-down of the TCs (figure 3) and STCs (figure 7) over the last 50 years which goes along with a warming of the Niño4 SST. This decreasing trend is seen in both the northern and southern hemispheric cell (figure 6 for the TCs). *Wu and Xie (2003*) call for caution in studies of the tropical Pacific climate variability based on ocean model integrations forced with the NCEP reanalysis due to differences in NCEP and COADS (comprehensive ocean and atmosphere dataset) winds. This trend, however, has been also found by *McPhaden and Zhang (2002)* using hydrographic data. They determined the convergence of the pycnocline transports at about 9^{o} latitude to obtain a measure of the strength of the STCs and found a decrease of about 12 Sv between the 1960s and 1990s. The trend in the strength of the STCs in the OGCM simulation is of comparable order (figure 7).

Furthermore, the trend is simulated in each individual member of an ensemble of integrations with the MPI-OM model, run with a coarser horizontal (but higher vertical) model grid resolution, in which the initial conditions were varied (figure 8). It is therefore unlikely that the strong downward trend seen in the model simulations forced with the NCEP reanalysis

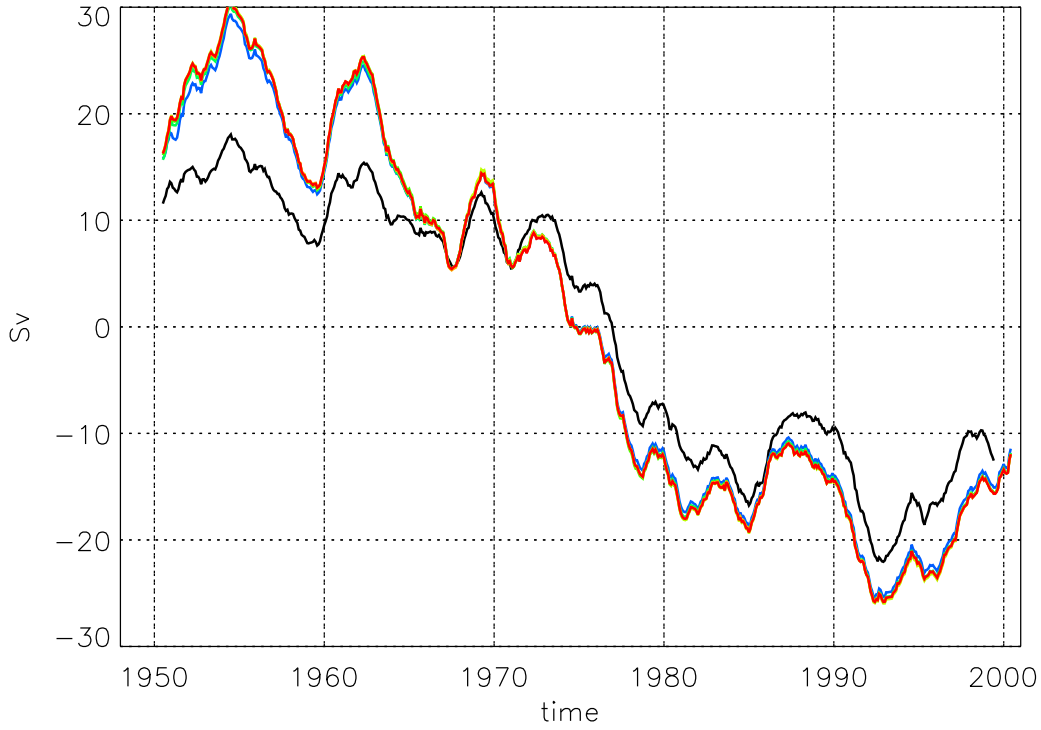

Figure 8: *Timeseries of the anomalous strength of the TCs taken from the MPI-OM model integration forced with the NCEP reanalysis. The black curve corresponds to the blue curve in figure 3, the coloured curves are six ensemble members from an integration with a different grid resolution. For definition of the cell strength see text.*

arises from problems associated with the initialization of the OGCM. Figure 8 also shows that different resolutions of the model grid lead to differences in the amplitude of the cell variability.

Figure 11a shows the pattern for the regression of the Pacific meridional overturning streamfunction onto the decadal Niño4 SST mode (figure 4a). It shows a rather broad pattern indicating that not only the TCs but also the STCs have some influence onto the decadal SST variability. This is in contrast to the interannual Niño4 SST mode (figure 4b) for which the overturning regression pattern is limited to about 5^{o} latitude (figure 18a). Again, this indicates that the STCs need more time to spin-up and -down than the TCs. Figure 11a also suggests an influence from both hemispheric cells. Note that for the southern hemisphere the mean overturning is negative, i.e. positive anomalies correspond to a weakening. The slightly weaker values for the northern hemisphere might be partly due to the fact that the overturning is weaker in the mean (25 Sv compared to 40 Sv for the southern hemisphere, figure 1). It follows from the regression pattern that a change of about 0.2 ^{o}C (standard deviation of the decadal

Niño4 SST mode) goes along with a change of the cells by about 15 -20%.

To further investigate the dynamics of the decadal Niño4 SST variability, various atmospheric and oceanic fields from the MPI-OM model integration forced with the NCEP reanalysis are regressed onto the decadal mode timeseries (figure 4a). The regression patterns are shown in figure 11.

A warming (cooling) in the Niño4 region goes along with a weakening (strengthening) of the trade winds over nearly the whole tropical Pacific domain (vectors in figure 11b). The changes are of the order of 0.01 to 0.02 Nm^{-2} per one standard deviation change in the decadal Niño4 SSTA. In the following, all described changes in the atmospheric and oceanic fields are per standard deviation change of the decadal SSTA index, even if this is not stated explicitly. Furthermore, only the warming case is described.

Weaker trade winds will lead to a reduced Ekman transport divergence in the ocean which will in turn decrease the equatorial upwelling of colder subsurface water (figure 11c). The strongest vertical velocity changes occur in the central Pacific, where the wind stress changes

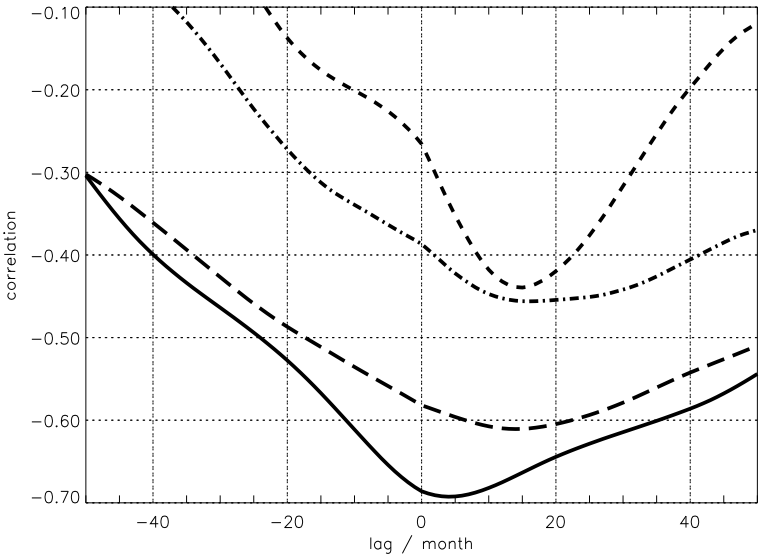

Figure 9: *Cross-correlation function between the decadal observed Niño4 SST (figure 3, years 1948-1998) and the strength of the TCs and STCs (at different latitudes) taken from an ocean model forced with the NCEP reanalysis: TC (solid line), STC at 10^o latitude (long dashed line), STC at 17.5^o latitude (short dashed line) and STC at 25^o latitude (dashed dotted line). For definition of the cell strength see text. The 95% significance level according to a t-test is -0.44. A positive (negative) lag indicates that the Niño4 SST is lagging (leading).*

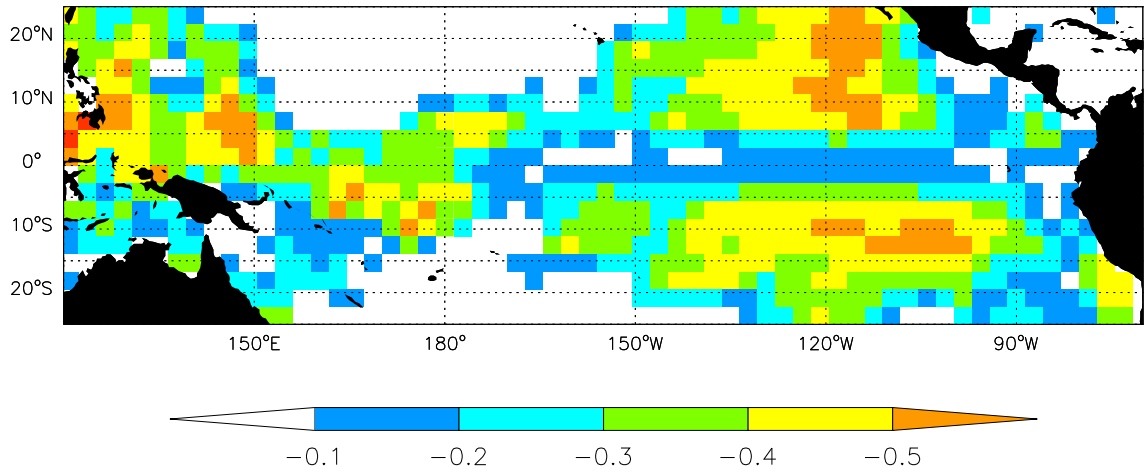

Figure 10: *Correlation pattern between the anomalous strength of the TCs taken from the MPI-OM model integration forced with the NCEP reanalysis (blue curve in figure 3) and the monthly observed SST. For definition of the cell strength see text.*

are largest. In the Niño4 region, a reduction of up to 50 cm/day or about 25% of the mean upwelling is simulated. This is consistent with the study of *McPhaden and Zhang (2002)* who describe a strong decrease in the upwelling from the 1970s to the 1990s. The effect of the (off)equatorial wind stress onto the variability of the TCs and STCs is discussed below.

A weakening in the trade winds will not only affect the vertical velocity, but will also weaken the wind-driven horizontal circulation. Figure 11e (vectors) shows a weakening of the South and North Equatorial Currents (SEC, NEC) of the order of 10 cm/s. Close to the equator, relatively strong meridional velocity anomalies are simulated, which reflect the weaker Ekman divergence during anomalously warm Niño4 SST. If one considers the mean horizontal SST gradients in the tropical Pacific (figure 12), the current anomalies will advect water from the warm pool area zonally towards the east and also meridionally into the equatorial cold tongue. The horizontal temperature advection by the anomalous currents (colour-shaded in figure 11e) is determined from $-u'd\overline{T}/dx\ -v'd\overline{T}/dy$, where the horizontal current anomalies are taken from the corresponding regression pattern (vectors in figure 11e), and the mean temperature gradients from the observed SST data (figure 12). This horizontal advection contribution of the anomalous currents exhibits the strongest warming tendency in the region of the SEC. Splitting the advection of the mean temperature up into the zonal and meridional part (figure 11f and g) reveals the same order of magnitude for the two components in the Niño4 region (up to about $3x10^{-8}$ Ks^{-1}).

For comparison, an estimate of the vertical advection by the anomalous vertical velocity has been calculated according to $-w'_{65m}\ (T_{surface}-T_{90m})/90m$. At model level 65 meter, the

upwelling anomalies reach their maximum, but values of about 25 cm/day are simulated down to a depth of 90 meter. The vertical temperature gradient is estimated from the Levitus data to be 1 to 1.5 Kelvin over the upper 90 meter in the warm pool area, which gives (taking w'_{65m} = 25 cm/day) a value of about 4×10^{-8} Ks^{-1}. This value is quite similar to the estimate of the horizontal advection of the mean temperature by the anomalous horizontal currents in the Niño4 area.

The subsurface circulation weakens also during periods of anomalously warm Niño4 SST (figure 11h). The Equatorial Undercurrent (EUC) is reduced by the order of 10 cm/s. Shown are the horizontal current anomalies at 150 meter depth, i.e. the core depth of the EUC in the central Pacific. *Goes and Wainer (2003)* found in an OGCM integration forced with the NCEP reanalysis similar reductions for the Atlantic Ocean. The EUC and SEC transports decrease (increase) for an anomalously warm (cold) equatorial Atlantic SST. It may be noteworthy that the western boundary currents show, in contrast to the interior pycnocline transport, a strengthening during phases of anomalously warm Nino4 SST. This is consistent with *Lee and Fukumori (2003)* who also describe an anticorrelation between the variations of the boundary currents and those of the interior pycnocline transport.

In addition to the ocean dynamics, the surface heatflux can change the SST. Figure 11i suggests a damping effect of the heatflux onto the SST over most of the equatorial Pacific. In the northern hemispheric part of the Niño4 region, however, the heatflux contributes to the warming.

The wind stress curl anomalies are also shown in figure 11b (colour-shaded). A wind stress curl anomaly favouring Ekman upwelling (according to $w_e \sim curl\tau / f$) is simulated between about 10^o and 15^o latitude in both hemispheres during phases of anomalously warm Niño4 SST. In the southwest, the negative anomalies are due to a shift in the South Pacific Convergence Zone (SPCZ), as is clearly seen in the regression pattern for the precipitation (figure 11j). The effect of the off-equatorial wind stress curl anomalies is also visible in the vertical velocity (figure 11c) and the depth of the thermocline (figure 11d). Anomalous upwelling and a shoaling of the thermocline are found at about 10^o to 15^o latitude during anomalously warm Niño4 SST. *Capotondi et al. (2003)*, using an OGCM forced with fluxes of momentum, heat and freshwater based on the NCEP reanalysis for the period 1958 to 1997, describe strong thermocline variability along 10^oS and 13^oN and suggest that it is associated with long first-mode baroclinic Rossby waves. The changes in the depth of the thermocline might contribute to the spin-down of the STCs. *Merryfield and Boer (2004, submitted)* suggest

a)

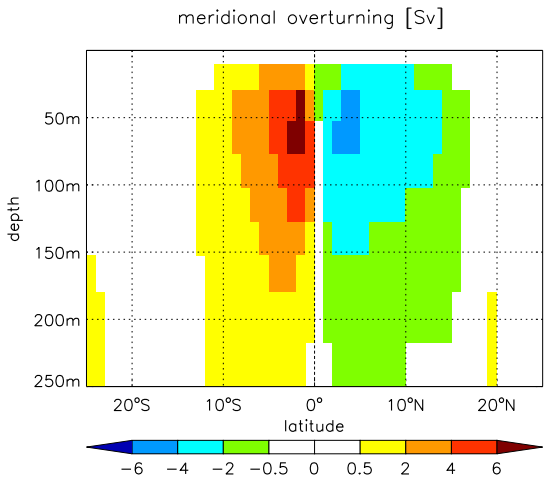
meridional overturning [Sv]
depth
50m
100m
150m
200m
250m
20°S
10°S
0°
10°N
20°N
latitude
−6 −4 −2 −0.5 0 0.5 2 4 6

b)

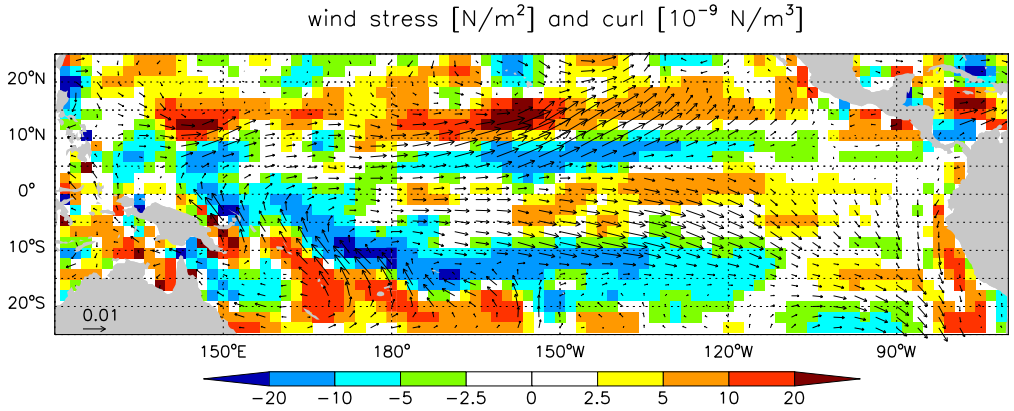
wind stress [N/m²] and curl [10⁻⁹ N/m³]
20°N
10°N
0°
10°S
20°S
0.01
150°E
180°
150°W
120°W
90°W
−20 −10 −5 −2.5 0 2.5 5 10 20

c)

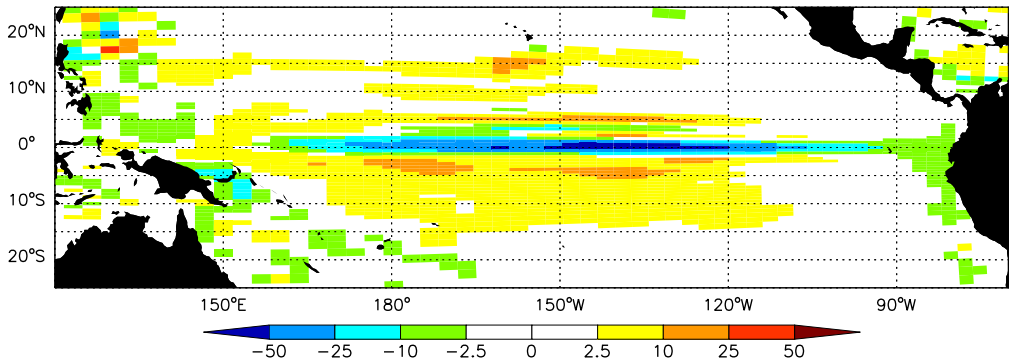
vertical velocity at 65m [cm/day]
20°N
10°N
0°
10°S
20°S
150°E
180°
150°W
120°W
90°W
−50 −25 −10 −2.5 0 2.5 10 25 50

d)

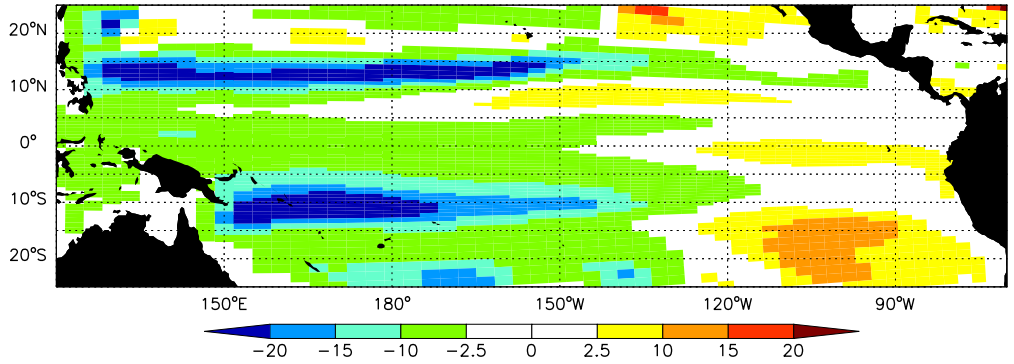
depth of thermocline [m]
20°N
10°N
0°
10°S
20°S
150°E
180°
150°W
120°W
90°W
−20 −15 −10 −2.5 0 2.5 10 15 20

e)

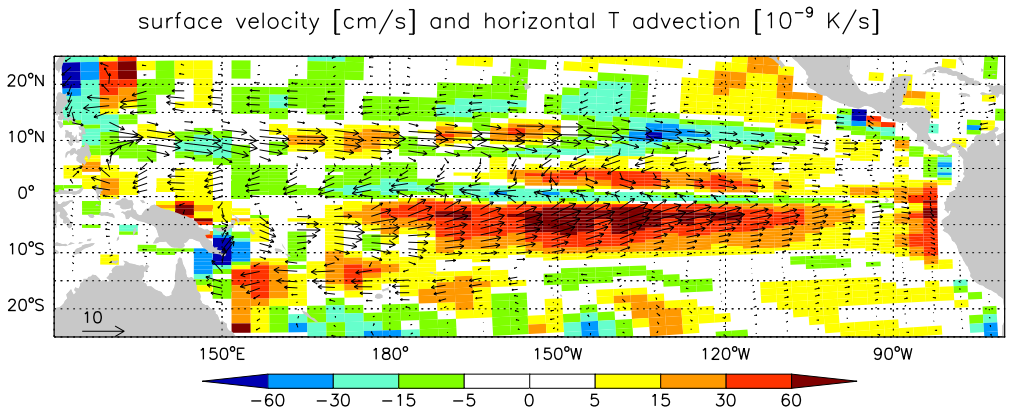
surface velocity [cm/s] and horizontal T advection [10^{-9} K/s]
20°N
10°N
0°
10°S
20°S
10
150°E
180°
150°W
120°W
90°W
−60 −30 −15 −5 0 5 15 30 60

f)

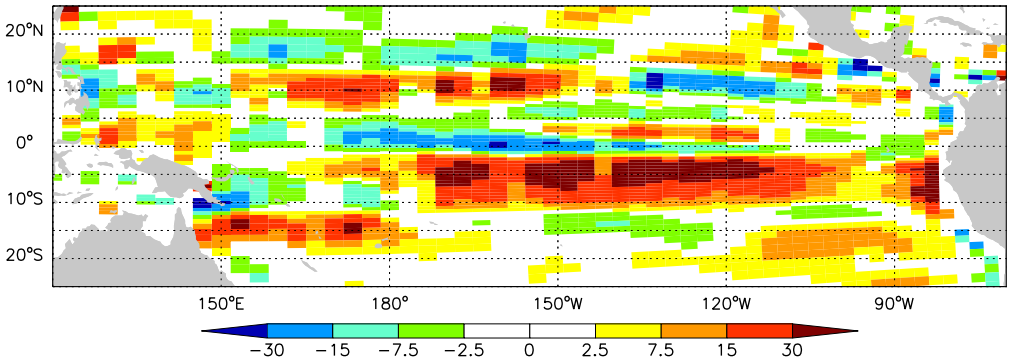
zonal T advection [10^{-9} K/s]
20°N
10°N
0°
10°S
20°S
150°E
180°
150°W
120°W
90°W
−30 −15 −7.5 −2.5 0 2.5 7.5 15 30

g)

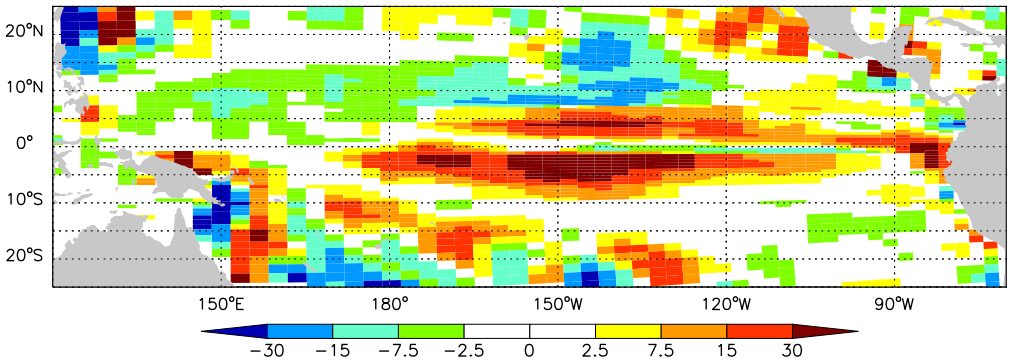
meridional T advection [10^{-9} K/s]
20°N
10°N
0°
10°S
20°S
150°E
180°
150°W
120°W
90°W
−30 −15 −7.5 −2.5 0 2.5 7.5 15 30

h)

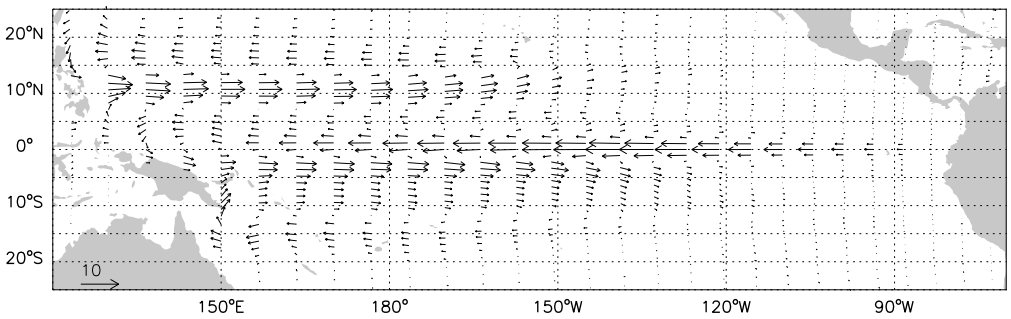
velocity in 150m [cm/s]
20°N
10°N
0°
10°S
20°S
10
150°E
180°
150°W
120°W
90°W

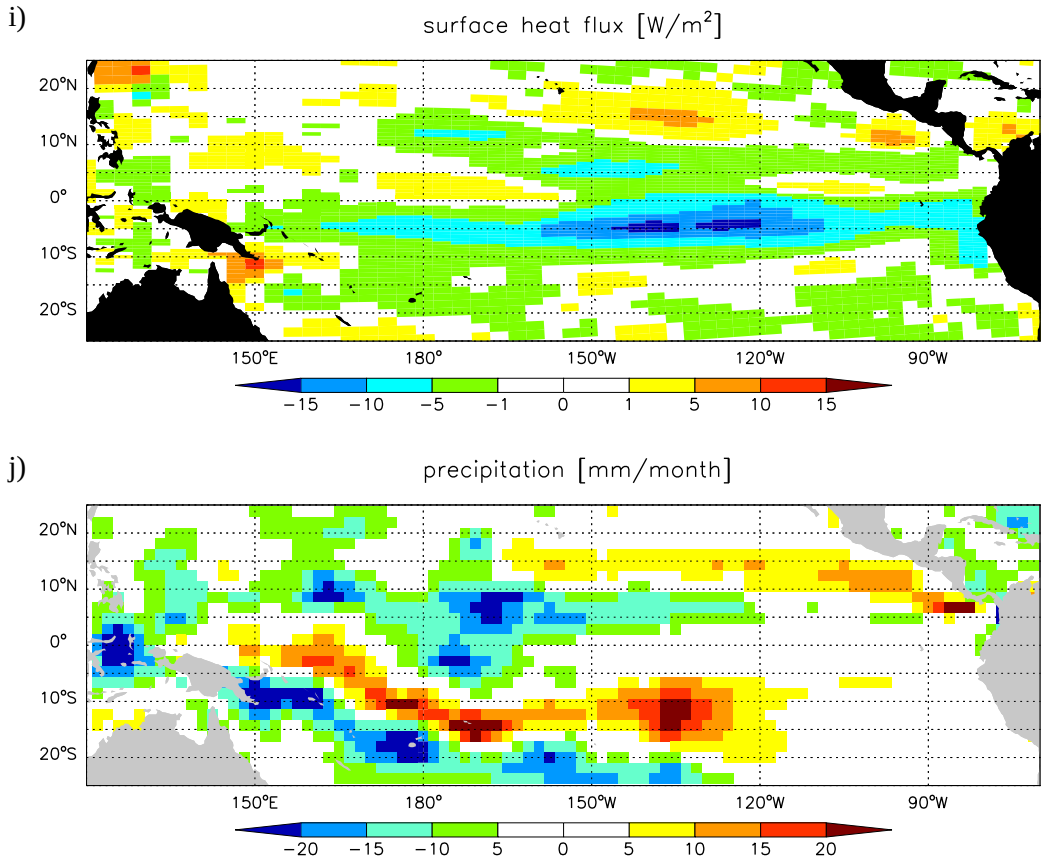

Figure 11: *Linear regression of various atmospheric and oceanic fields from the MPI-OM model integration forced with the NCEP reanalysis onto the observed decadal Niño4 SST mode (figure 4a). The fields are monthly values with the annual cycle removed. All values are per standard deviation of the SST index (0.21K). (a) Pacific meridional overturning streamfunction (in Sv), (b) wind stress (vectors, in Nm^{-2}) and wind stress curl (contours, in 10^{-9} Nm^{-3}), (c) vertical velocity at model level 65 meters (in cm/day), (d) depth of the thermocline (in m), (e) horizontal velocity at the surface (vectors, in cm/s) and horizontal temperature advection (contours, in 10^{-9} Ks^{-1}), (f) zonal temperature advection (in 10^{-9} Ks^{-1}), (g) meridional temperature advection (in 10^{-9} Ks^{-1}), (h) horizontal velocity at model level 150 meters (in cm/s), (i) downward net surface heat flux (in Wm^{-2}), (j) precipitation (in mm/month)*

a controlling of the pycnocline transport changes due to the wind stress curl. Apart from the weakening of the off-equatorial downwelling, the shoaling of the thermocline in the west will decrease the zonal slope of the thermocline, which itself might reduce the equatorward flow within the thermocline. Timeseries of the tilt of the thermocline at about 10^{o} latitude show a decreasing trend consistent with the decreasing strength of the STCs. Correlation coefficients between the anomalous thermocline depth and the STC strength at 10^{o} latitude as well as between the anomalous wind stress curl and the STC strength amount to about 0.7 for the northern and to about 0.6 for the southern hemisphere.

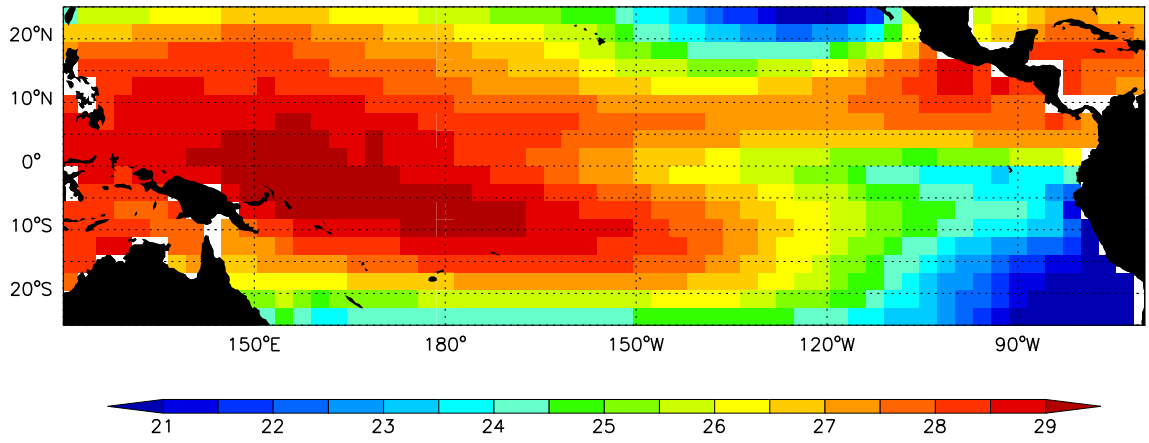

Figure 12: *Mean observed SST (in ^{o}C) taken from the HadISST1.1 dataset encompassing the years 1948 to 1998.*

To investigate the effects of the equatorial and off-equatorial wind stress variability onto the variability of the TCs and STCs, the results from two wind sensitivity experiments with the MPI-OM model forced with the NCEP reanalysis have been analyzed. In the two experiments climatological wind stress forcing is prescribed between 5^{o}S and 5^{o}N or poleward of 5^{o} latitude respectively. Indices have been calculated for the decadal strength of the TCs and the STCs in the same way as described for the control run at the beginning of this chapter.

Figure 13a shows the results for the TCs. Nearly all variability of the cell strength seen in the control run (black curve) is simulated with wind stress variability restricted only to the equatorial region (green curve). The off-equatorial wind stress fluctuations (blue curve) do not significantly affect the TCs.

In contrast, the variability of the strength of the STCs (figure 13b) is generated mostly by wind stress (curl) fluctuations poleward of 5^{o} latitude (blue curve compared to the black one). This indicates that the off-equatorial winds have an influence on the equatorial SST in the western tropical Pacific. The STC strength has been calculated at 10^{o} latitude but similar results are obtained for 15^{o} and 20^{o} latitude. It is noteworthy that for the variability of the STCs the effect of the equatorial and off-equatorial wind stress are adding up linearly (the sum (red dashed curve in figure 13b) of the STC indices from the two wind sensitivity experiments resembles the index from the control integration).

Indices for the strength of the TCs and STCs have also been calculated for MPI-OM model integrations with only wind stress and only heat/freshwaterflux forcing variability respectively. The results clearly show (figure 14) that the variability of the cell strength simulated in the control run (black curve) is driven by the wind stress forcing variability alone (red curve).

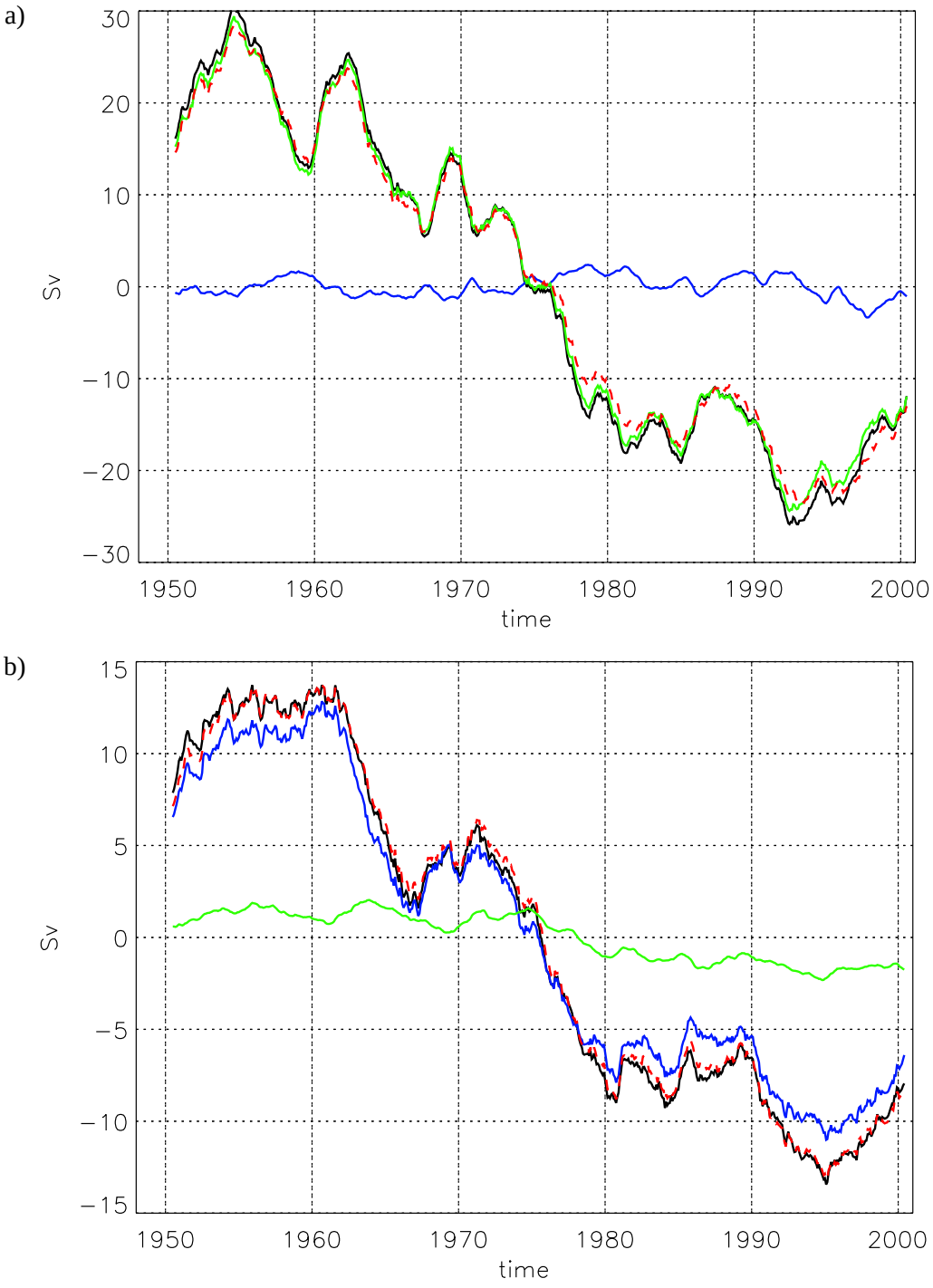

Figure 13: *Timeseries of the anomalous strength of (a) the TCs and (b) the STCs taken from MPI-OM model integrations forced with the NCEP reanalysis: control run (black), climatological wind stress forcing poleward of 5^o latitude (green) and climatological wind stress forcing between 5^{o}S and 5^{o}N (blue). The red dashed line is the sum of the blue and the green curve. For definition of the cell strength see text.*

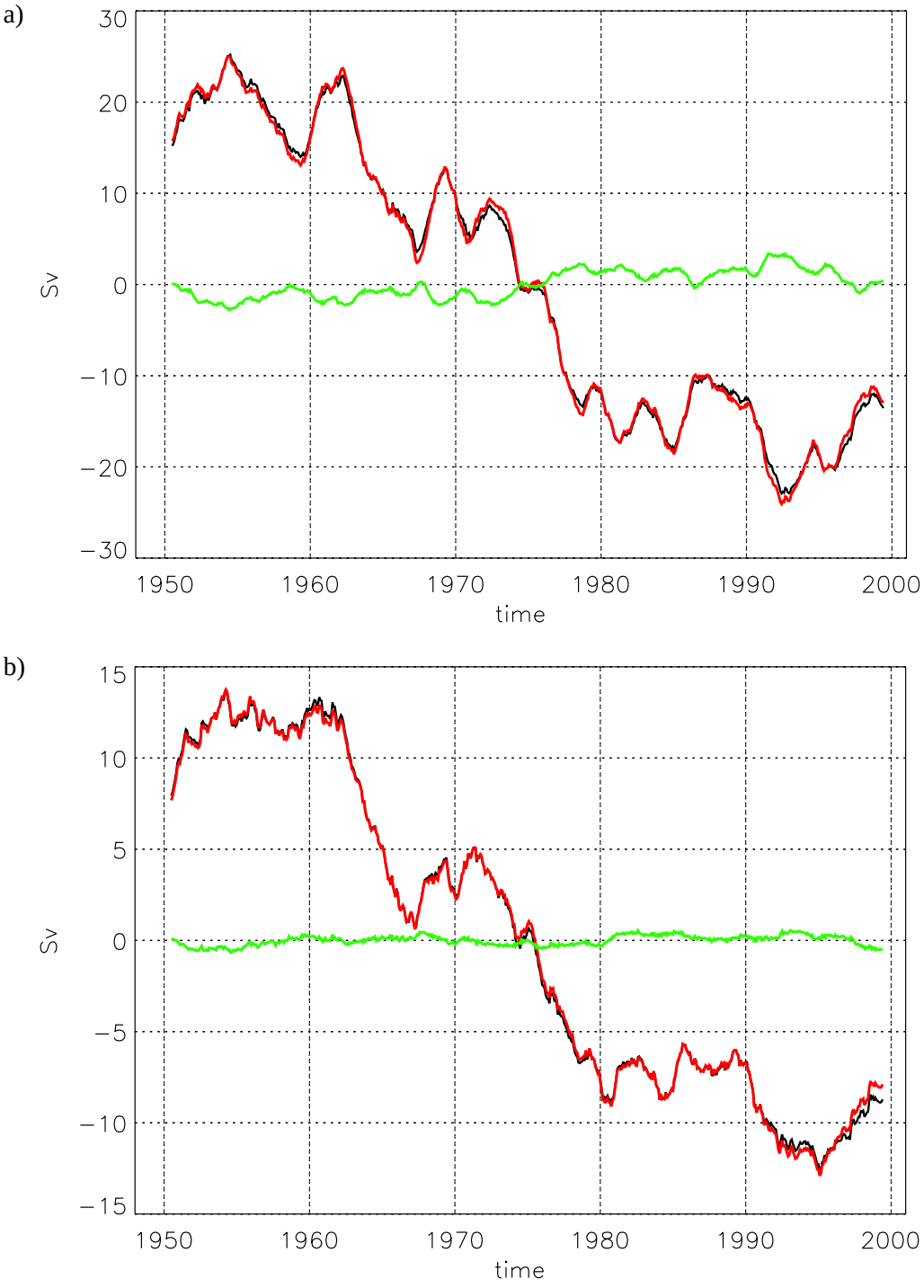

Figure 14: *Timeseries of the anomalous strength of (a) the TCs and (b) the STCs taken from MPI-OM model integrations forced with the NCEP reanalysis: control run (black), climatological heat/freshwater forcing (red) and climatological wind stress forcing (green).*

Apart from the western equatorial Pacific, a strong correlation between the decadal TC as well as STC variability and the monthly observed SST is found off-equatorial in the eastern Pacific (figure 10). The correlation is even higher than in the western equatorial Pacific. The cross-correlation function between the decadal strength of the cells and the observed SST averaged over the region 150^{o}W to 90^{o}W and 5^{o} to 15^{o} latitude shows that, as for the Niño4 region, the cell variability is leading the SST fluctuations, indicating that also the off-equatorial SST variability is driven by the variability of the (S)TCs.

The warming (cooling) of the off-equatorial eastern Pacific during phases of weak (strong) cells should mainly be caused by horizontal temperature advection. The regression pattern for the decadal eastern off-equatorial SST index closely resembles figure 11e. The anomalously weak (strong) Ekman transport will advect anomalously less (much) water from the equatorial cold tongue polewards. For the southern hemisphere also a strong zonal temperature gradient exists (figure 12). During phases of weak (strong) cells, the weakened (strengthened) SEC will advect anomalously less (much) colder water from the east westwards.

The relationship between the tropical SST and the strength of the TCs and STCs might give rise to some predictability at decadal timescales. In figure 15, the potential predictability, defined by decadal variance divided by total variance, of the observed SST in the tropical Pacific is shown. While the potential predictability is close to zero in the typical ENSO region, the eastern and central equatorial Pacific, it is significant in some parts of the western equatorial Pacific and off the equator. These are basically the regions, in which the decadal mode explains most of the variance (figure 5b). Furthermore, classical predictability studies

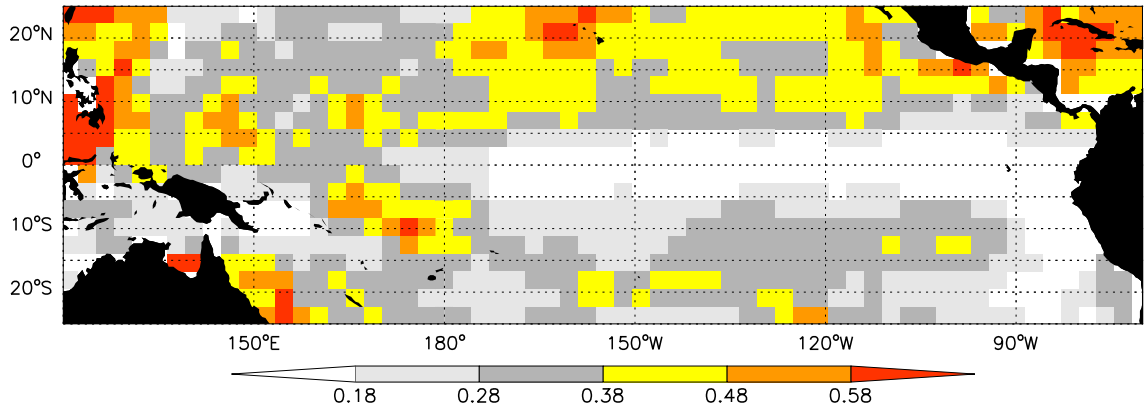

Figure 15: *Potential predictability for decadal observed SST defined by variance of decadal means divided by total variance. Significant values according to an F-test are shown in color.*

with a coupled general circulation model in which the MPI-OM model is used as the ocean component, confirm the results of the potential predictability analysis and show predictive skill in exactly the same regions (*Pohlmann et al., 2004*,).

In the following, shortly the relationship between the observed Niño4 SST and the strength of the TCs on interannual timescales is discussed. Since e.g. *Klinger et al. (2002)* have shown that the surface limb of the cells is spinning-up and -down quicker than the return flow within the pycnocline here only the relatively narrow TCs are considered. Furthermore, the regression of the interannual Niño4 SST mode (figure 4b) onto the Pacific meridional overturning streamfunction shows an influence onto the SST mainly from the TCs (figure 18a).

In figure 16 the monthly Niño4 SSTAs and the anomalous strength of the TCs are shown. The timeseries have been detrended and a one year running mean has been applied (so that the correlation becomes more clear). Also on shorter timescales the Niño4 SST and the strength of the TCs are correlated with a correlation coefficient of about -0.75 which is comparable to what is found on decadal timescales (solid line in figure 9). Again, the cell variability is leading, i.e. indeed driving, the SST anomalies (figure 17).

As for the decadal timescale, the regression onto the interannual Niño4 SST mode (figure 4b) shows a contribution to the Niño4 SSTAs not only from changes in the strength of the upwelling (figure 18b) but also from horizontal temperature advection by anomalous currents (figure 18c). However, the net surface heatflux (not shown) has a damping effect over the entire Niño4 area.

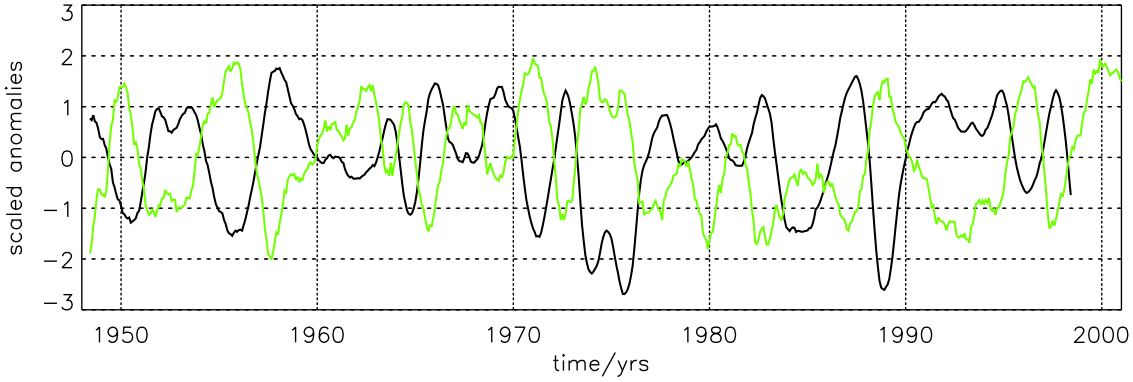

Figure 16: *Timeseries of the observed Niño4 SSTAs (black) and the anomalous strength of the TCs (green) taken from the MPI-OM model integration forced with the NCEP reanalysis. Both timeseries have been detrended and a one year running mean has been applied. For definition of the cell strength see text.*

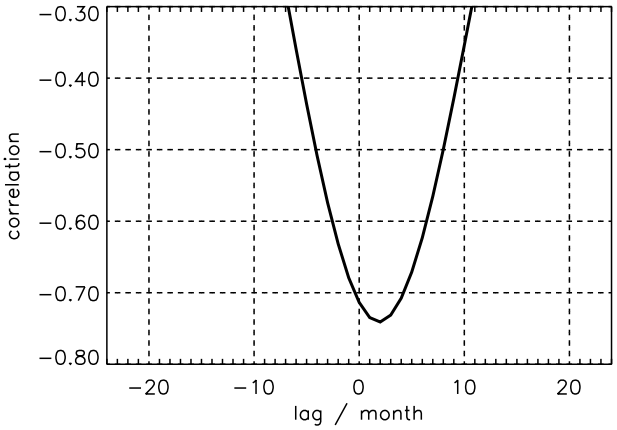

Figure 17: *Cross-correlation function between the two timeseries in figure 16. The 95% significance level according to a t-test is -0.28. A positive (negative) lag indicates that the Niño4 SST is lagging (leading) the strength of the TCs.*

In the west, a wind driven eastward (westward) flowing equatorial jet is simulated during phases of warm (cold) Niño4 SST. Due to this jet and a strengthening (weakening) of the North Equatorial Countercurrent (NECC), the horizontal temperature advection (colour-shaded in figure 18c) contributes, in contrast to figure 11e, to a warming (cooling) in the west north of the equator. The reason for this difference is at least partly the strong trend in the mid-1970s which is not seen in the interannual SSA mode (figure 4b). If the decadal SSA mode (as well as the simulated velocities) are detrended prior to the regression analysis, an equatorial jet in the west is found on decadal timescales too.

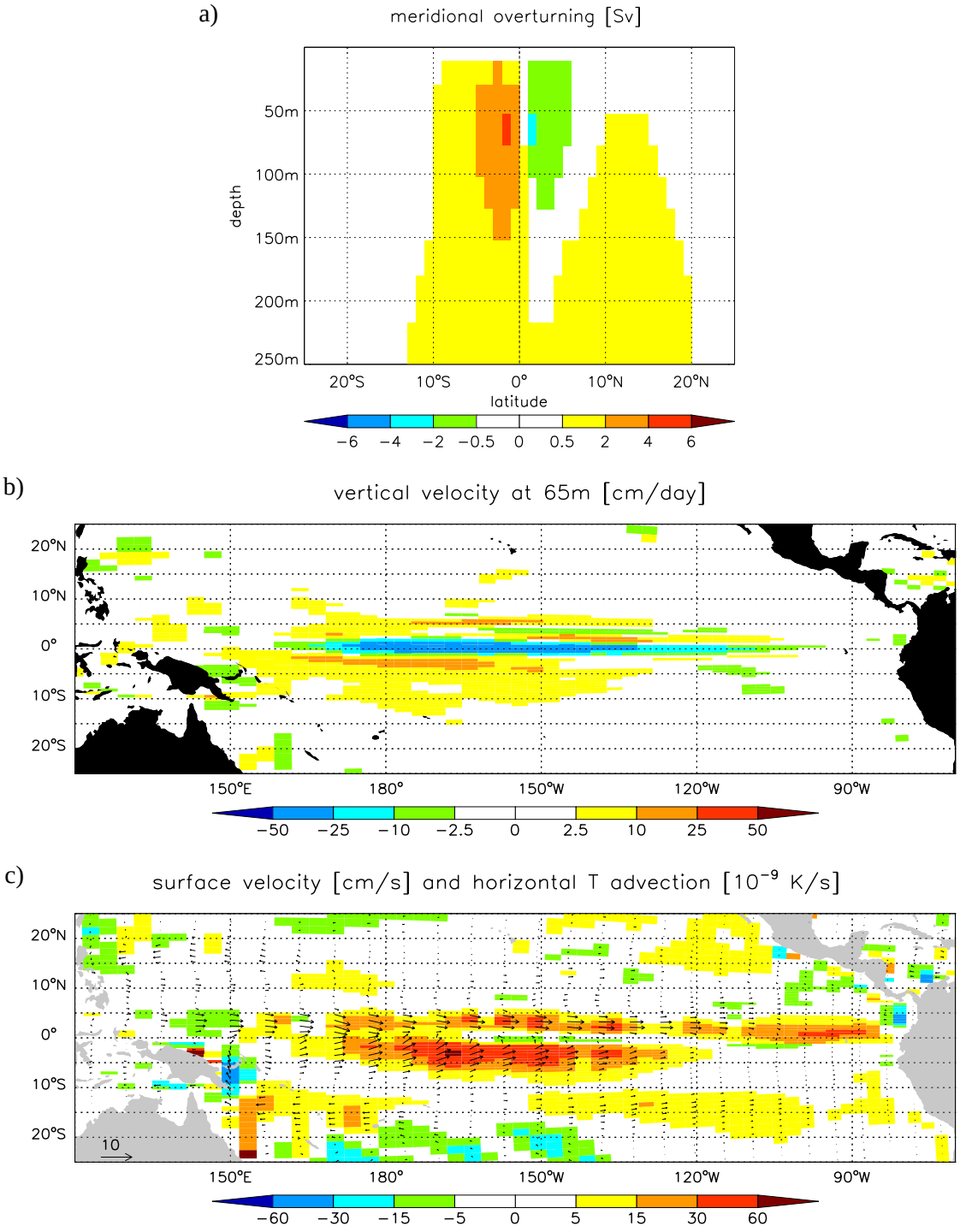

Figure 18: *Linear regression of various fields from the MPI-OM model integration forced with the NCEP reanalysis onto the observed interannual Niño4 SST mode (figure 4b). The fields are monthly values with the annual cycle removed. All values are per standard deviation of the SST index (0.20K). (a) Pacific meridional overturning streamfunction (in Sv), (b) vertical velocity at model level 65 meters (in cm/day), (c) horizontal velocity at the surface (vectors, in cm/s) and horizontal temperature advection (contours, in 10^{-9} Ks^{-1})*

3.3. Simulations with a coupled general circulation model

In this chapter the decadal variability in the tropical Pacific as simulated by a 300 year long integration of the coupled ocean/atmosphere general circulation model ECHAM4/OPYC is described.

Figure 19 shows the low-pass filtered (applying a five year running mean) model timeseries of the Niño4 SSTAs and the maximum strength of the TCs derived from Pacific meridional overturning streamfunction data with a five year running mean applied (as described in chapter 3.2). The level of the simulated SST variability is of the order of the observed one (figure 3). However, no strong trend is found in the control integration with the coupled model. The fluctuations of the TCs and the STCs (not shown) are comparable to those from the MPI-OM model integration forced with the NCEP reanalysis, in the following denoted as MPI-OM, before and after 1975. However, a change of the cell strength like the one which occured in the mid-1970s is not found in the coupled model integration. This is in accord with *Merryfield and*

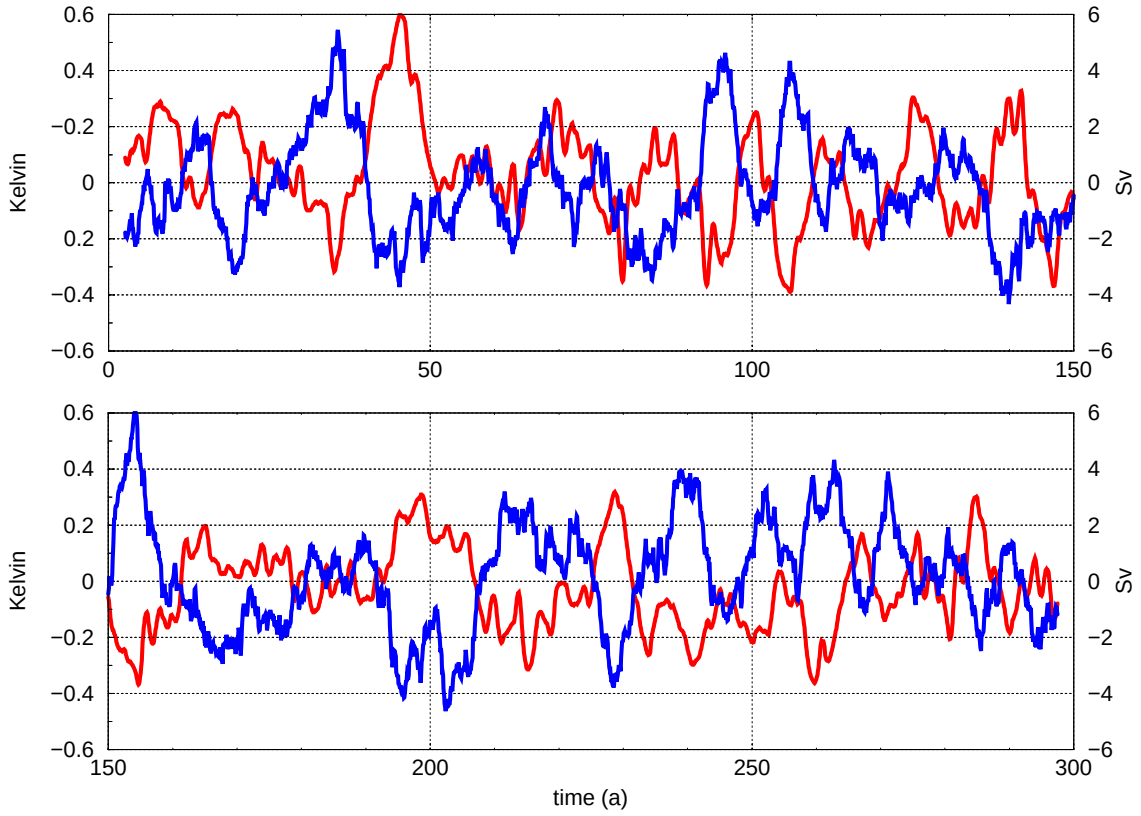

Figure 19: *Timeseries of the Niño4 SST anomalies and the anomalous strength of the TCs taken from the ECHAM4/OPYC model. For definition of the cell strength see text. Shown are only values with a five year running mean applied (red for SST, blue for TC).*

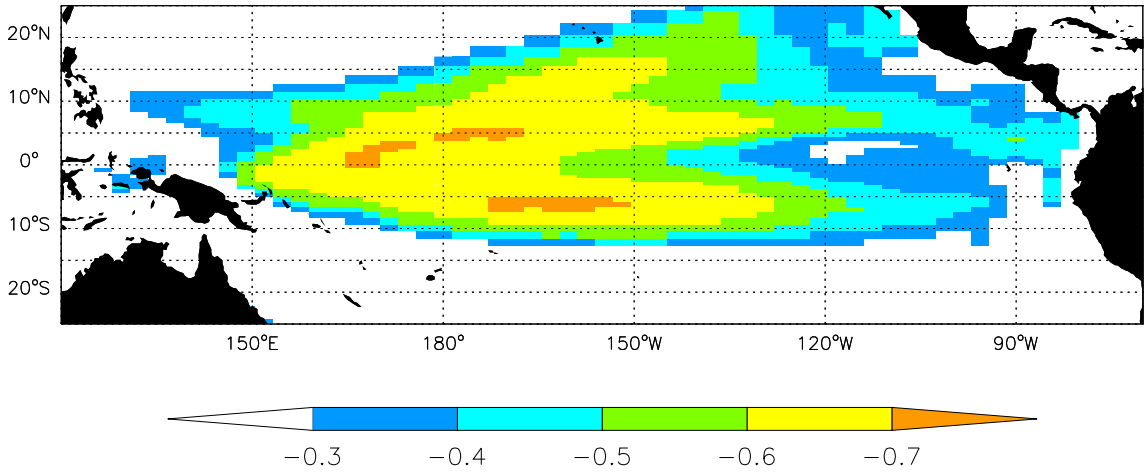

Figure 20: *Correlation pattern between the anomalous strength of the TCs (blue curve in figure 19) and the decadal (five year running mean applied) SST from the ECHAM4/OPYC model. For definition of the cell strength see text.*

Boer (2004, submitted) who also found less pycnocline transport variability in their coupled control integration than *McPhaden and Zhang (2002)* estimated from hydrographic observations. It should be mentioned, however, that the mean strength of the cells is weaker in ECHAM4/OPYC than in MPI-OM (30 Sv compared to 40 Sv for the southern and 11 Sv compared to 25 Sv for the northern hemispheric TC).

Also for the coupled integration, the low-pass filtered Niño4 SST and timeseries of the strength of the TCs and STCs (not shown) are anticorrelated. For the TCs, the maximum correlation coefficient amounts to -0.7. The same correlation is found for the decadal observed Niño4 SSTAs and STC strength anomalies from MPI-OM. However, in ECHAM4/OPYC the maximum correlation is found at lag zero. This lag is influenced from both hemispheric cells. While the northern TC is leading the SST by about 6 month, no such lag is found for the southern TC. The reason for this is not yet clear.

Considering the decadal strength of the STCs, the strongest (anti-) correlation amounts to about -0.45 (figure 21), which is weaker than for MPI-OM, but still statistically significant at the 95% level (threshold value -0.21 according to a t-test). The fact that the cells are weaker compared to MPI-OM might contribute to the lower correlation, although the correlation is similar if the TCs are considered.

The regression pattern (figure 24a) of the Pacific meridional overturning streamfunction onto the decadal Niño4 SST mode (figure 23) also suggests a weaker influence from off-equatorial regions than in MPI-OM, even if the lag between the STC variability and the SST is taken into account. As in MPI-OM, the strongest (anti-)correlation is found if the strength of

the STCs is leading the Niño4 SST by about one year (figure 21). Thus, the coupled integration supports the notion that the low-frequency variability in the strength of the STCs is important in driving western equatorial and off-equatorial SST anomalies. For the STCs, the lag is similar for both hemispheric cells.

A secondary extreme is found in the cross-correlation function, when the Niño4 SSTAs are leading the strength of the STCs. This suggests that changes in the SST contribute (via changes in the trade winds) to changes in the cell strength. Such a feedback is not seen in the uncoupled OGCM integration (long dashed line in figure 9). It is found, however, if the MPI-OM model is coupled to the atmosphere model ECHAM5 as seen from the cross-correlation function (figure 22).

The correlation pattern between the decadal SST in the tropical Pacific and the TC index (figure 20) as well as the STC index (not shown) shows a horseshoe-like structure with maximum correlation in the western equatorial Pacific and off the equator also for the coupled model integration, resembling the pattern shown in figures 5b and 10.

Also for the coupled integration, a singular spectrum analysis (SSA) of the monthly Niño4 SSTAs is performed. In contrast to the observed SST, the leading SSA mode of the coupled model has an interannual timescale representing the ENSO mode, while only a less energetic mode (modes 5 and 6 or modes 3 and 4 depending on the window length) has a quasi-decadal

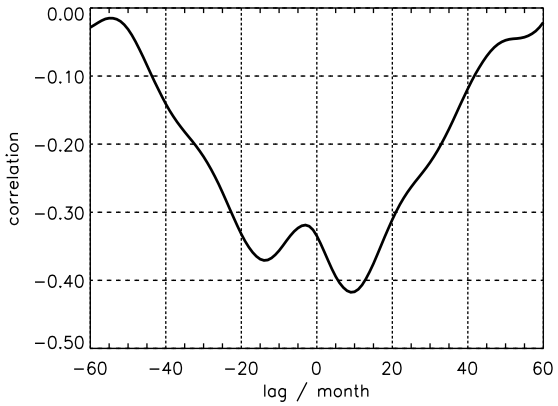

Figure 21: *Cross-correlation function between the decadal Niño4 SST (red curve in figure 19) and the strength of the STCs taken from the ECHAM4/OPYC model. For definition of the cell strength see text. The 95% significance level according to a t-test is -0.21. A positive (negative) lag indicates that the Niño4 SST is lagging (leading).*

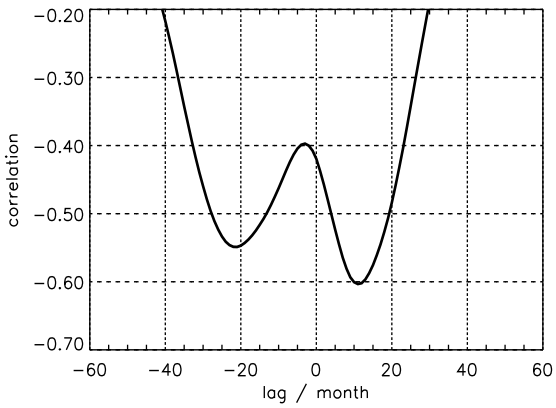

Figure 22: *As figure 21 but for the ECHAM5/ MPI-OM model. The 95% significance level according to a t-test is -0.39.*

timescale (figure 23). This might be due to the fact that the coupled model simulates an El Niño period of only two years and slightly too strong ENSO variability. If the SSA is calculated from annual values rather than from monthly values so that the ENSO frequency is not fully resolved, the decadal mode turns out to be the leading one. The decadal SSA mode closely resembles the SST anomalies with a five year running mean applied (red curve in figure 19). As for the observed SST (figure 5a) the decadal Niño4 SST mode is El Niño-like (figure 24l).

Again, various atmospheric and oceanic fields are regressed onto the decadal Niño4 SST mode. The regression patterns derived from the coupled simulation (figure 24) are similar to the ones derived from MPI-OM (figure 11) in many aspects. There are, however, significant differences which will be discussed below. If one takes into account the different standard deviations of the decadal Niño4 SST modes (0.13^{o}C for ECHAM4/OPYC compared to 0.21^{o}C for the observed one), the regression coefficients have the same order of magnitude. Note that the scale in figure 24 is different to that in figure 11 and that in both cases the regression coefficients are expressed per standard deviation of the SST index. Again, only the case of anomalously warm Niño4 SST is described.

The weakening of the surface wind stress (vectors in figure 24b) as well as the upwelling favourable curl at about 10^{o} latitude (contours in figure 24b) during an increase in the Niño4 SST are confined to the western part of the basin. This is also the case, if the SST index is averaged over the entire width of the Pacific. In MPI-OM, the dominating change is the relatively strong

trend in the mid-1970s (e.g. figure 3). If the observed Niño4 SST index as well as the wind stress (curl) from the NCEP reanalysis are detrended prior to the calculation of the regression coefficients, also the regression pattern for MPI-OM shows a weakening of the trades between about 15^oS and 15^oN as well as an upwelling favourable curl at about 10^o latitude only in the western part of the Pacific. According to the wind stress pattern in ECHAM4/OPYC (vectors in figure 24b), the maximum equatorial upwelling anomalies are simulated in the west (figure 24c) where the mean vertical velocity is relatively small.

Considering the horizontal surface circulation during phases of anomalously warm Niño4 SST (figure 24e) the weakening of the South Equatorial Current (SEC) is quite strong in the east. This is at least partly due to the fact that the mean SEC is relatively strong in the east in the ECHAM4/OPYC model (70 cm s^{-1} compared to 50 cm s^{-1} in MPI-OM). In the west, a wind driven equatorial jet is simulated by the CGCM, flowing eastwards during anomalously warm Niño4 SST. Due to this jet and the strengthening of the North Equatorial Countercurrent (NECC), the horizontal temperature advection (contours in figure 24e) contributes, in contrast to MPI-OM, to an increase of the Niño4 SST north of the equator. The strong NECC during phases of warm Niño4 SST (and weak cells) might reflect the fact that the intertropical convergence zone weakens the northern hemispheric cell by providing a potential vorticity barrier

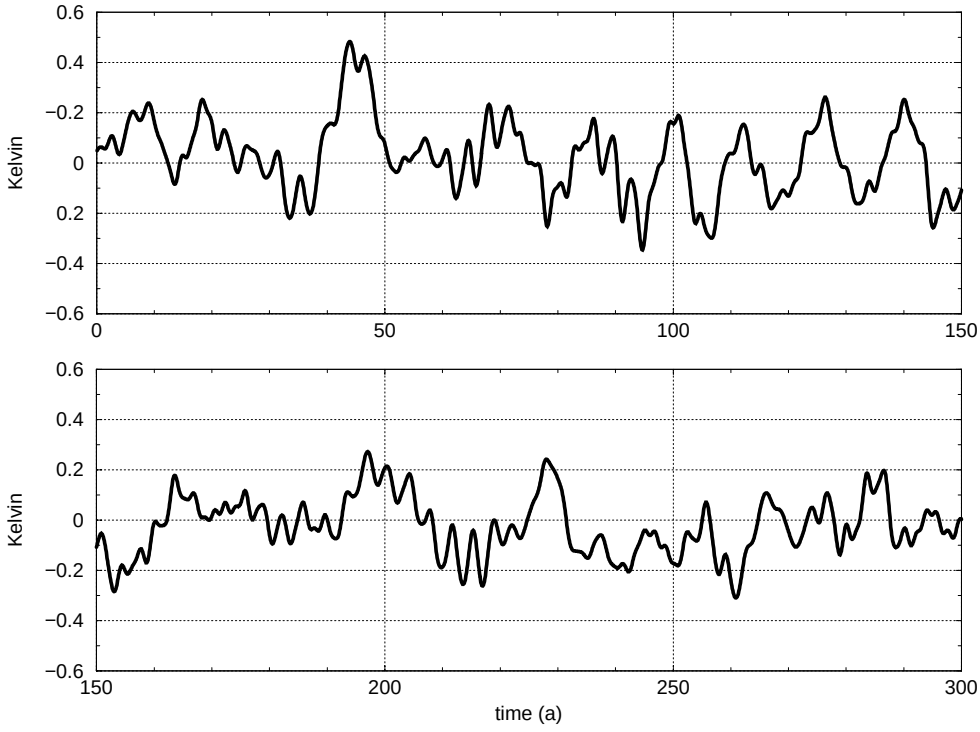

Figure 23: *Reconstruction of the ECHAM4/OPYC monthly Niño4 SST anomalies from singular spectrum analysis using mode 5 and 6.*

which prevents the subducted water to flow to the equator in the interior ocean (*Lu and McCreary, 1995, Johnson and McPhaden, 1999*). As for the wind stress pattern, the difference between the two simulations seems to be due to the relatively strong trend found in the MPI-OM simulation. If the observed Niño4 SST index as well as the simulated horizontal velocities are detrended prior to the regression analysis, the regression pattern for MPI-OM shows an equatorial jet in the west too.

For the subsurface circulation (figure 24h) it should be mentioned that the Equatorial Undercurrent (EUC) is reduced over the whole width of the basin. Since the EUC core rises towards the east, the changes in the east are visible in the regression patterns for model levels 50 and 100 meters (not shown).

The net surface heat flux (figure 24j) in ECHAM4/OPYC also contributes to the warming in the north western equatorial Pacific, although this contribution is confined to the region west of of the dateline.

Considering the changes in the depth of the thermocline during anomalously warm Niño4 SST (figure 24d), the shoaling of the thermocline in the western and central part is much weaker in ECHAM4/OPYC than in MPI-OM. In contrast, the deepening of the thermocline in the east is more pronounced in the CGCM simulation. As discussed before, the main reason for the difference between the two simulations is the relatively strong trend found in MPI-OM. Timeseries of the depth of the thermocline at about 10^{o} latitude in the western and central tropical Pacific in MPI-OM show decreasing trends of 50 to 80 meters in the 1970s. Such a signal is not found in the ECHAM4/OPYC control simulation. Again, if the observed Niño4 SST index and the simulated thermocline depth are detrended prior to the calculation of the regression coefficients, the regression pattern for MPI-OM also shows much weaker shoaling of the thermocline in the western and central parts and stronger deepening of the thermocline in the area of the cold tongue.

As a summary it can be said that the coupled integration (using also a different ocean model) supports the results described in the previous chapter for the uncoupled integration.

a)

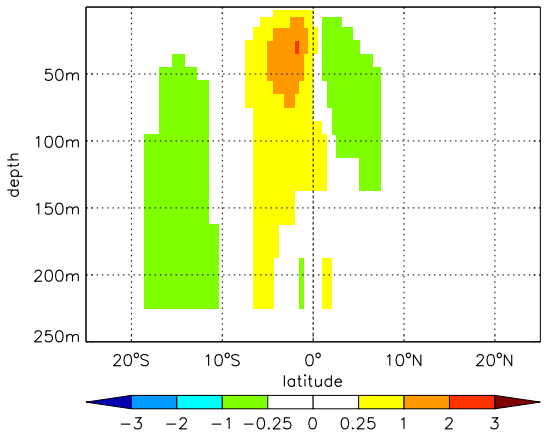
meridional overturning [Sv]
depth
50m
100m
150m
200m
250m
20°S
10°S
0°
10°N
20°N
latitude
−3 −2 −1 −0.25 0 0.25 1 2 3

b)

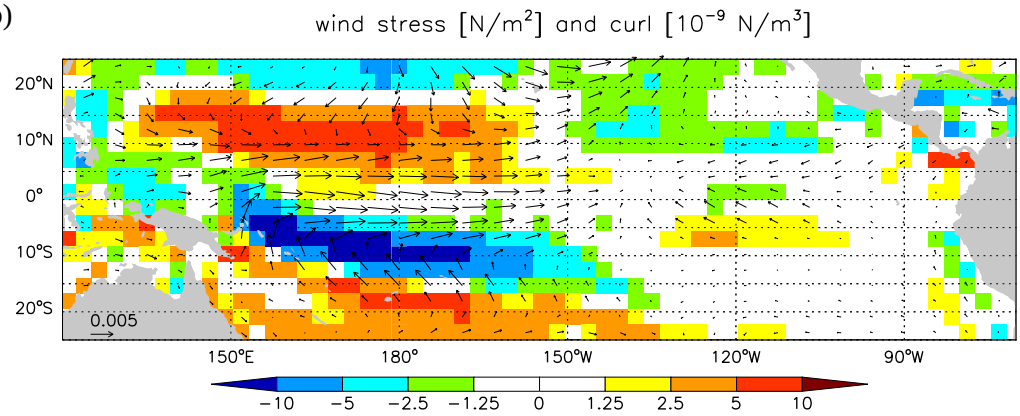
wind stress [N/m²] and curl [10⁻⁹ N/m³]
20°N
10°N
0°
10°S
20°S
0.005
150°E
180°
150°W
120°W
90°W
−10 −5 −2.5 −1.25 0 1.25 2.5 5 10

c)

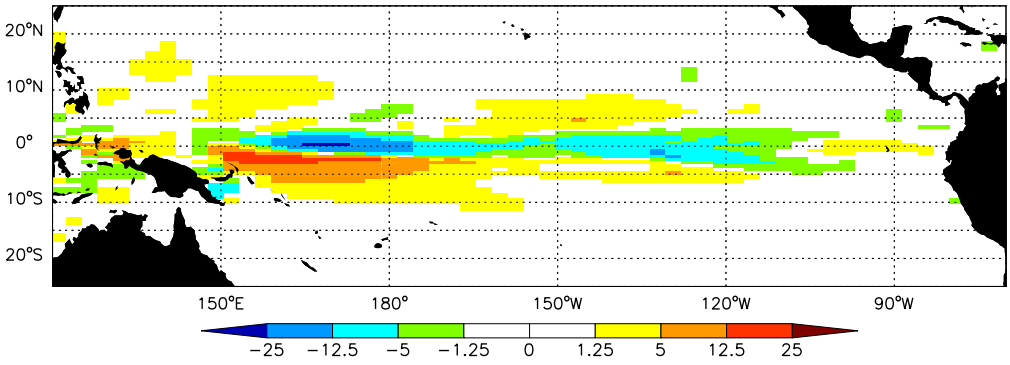
vertical velocity at 50m [cm/day]
20°N
10°N
0°
10°S
20°S
150°E
180°
150°W
120°W
90°W
−25 −12.5 −5 −1.25 0 1.25 5 12.5 25

d)

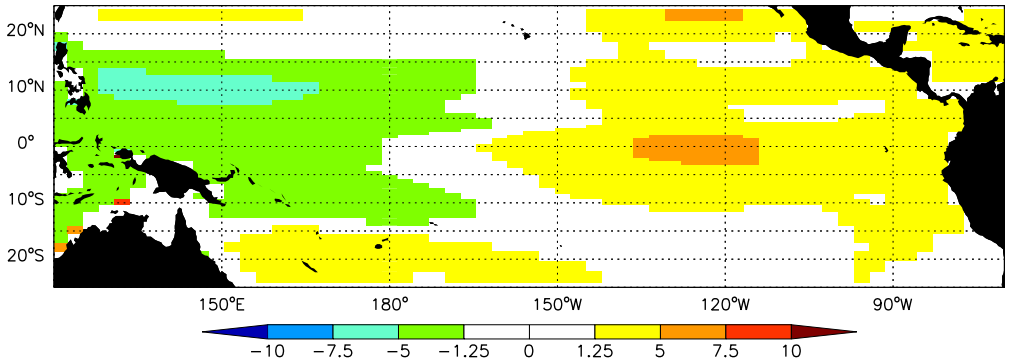
depth of thermocline [m]
20°N
10°N
0°
10°S
20°S
150°E
180°
150°W
120°W
90°W
−10 −7.5 −5 −1.25 0 1.25 5 7.5 10

e)

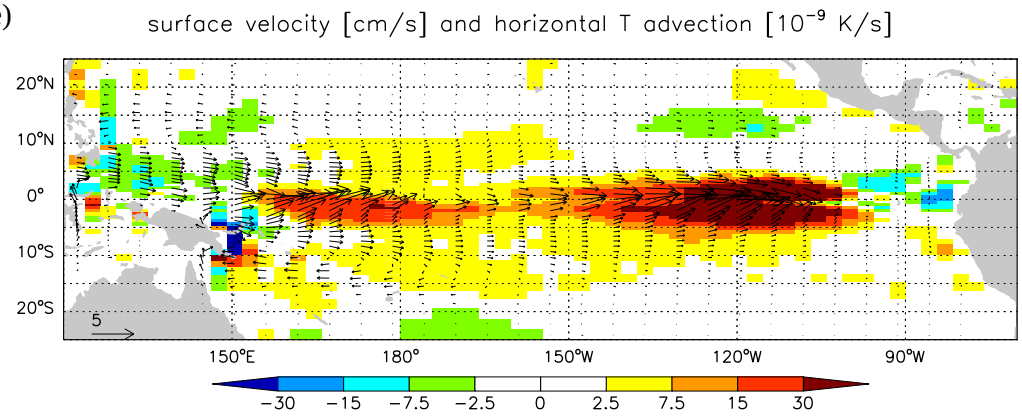
surface velocity [cm/s] and horizontal T advection [10⁻⁹ K/s]
20°N
10°N
0°
10°S
20°S
5
150°E
180°
150°W
120°W
90°W
−30 −15 −7.5 −2.5 0 2.5 7.5 15 30

f)

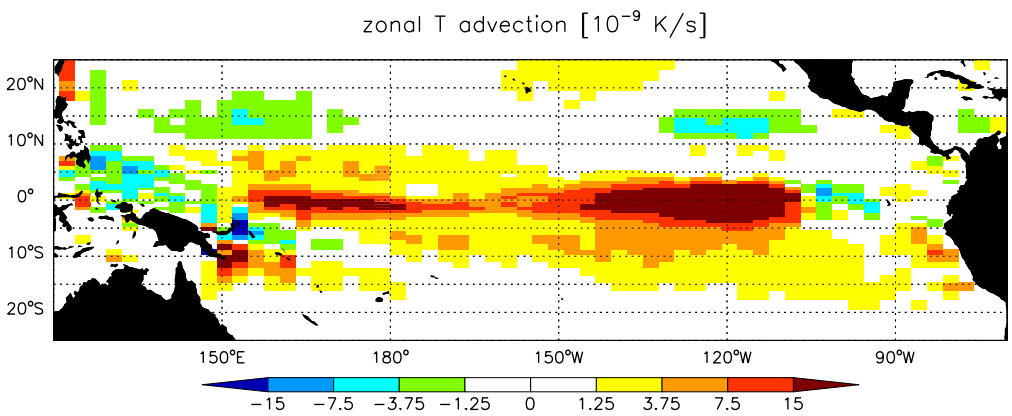
zonal T advection [10⁻⁹ K/s]
20°N
10°N
0°
10°S
20°S
150°E
180°
150°W
120°W
90°W
−15 −7.5 −3.75 −1.25 0 1.25 3.75 7.5 15

g)

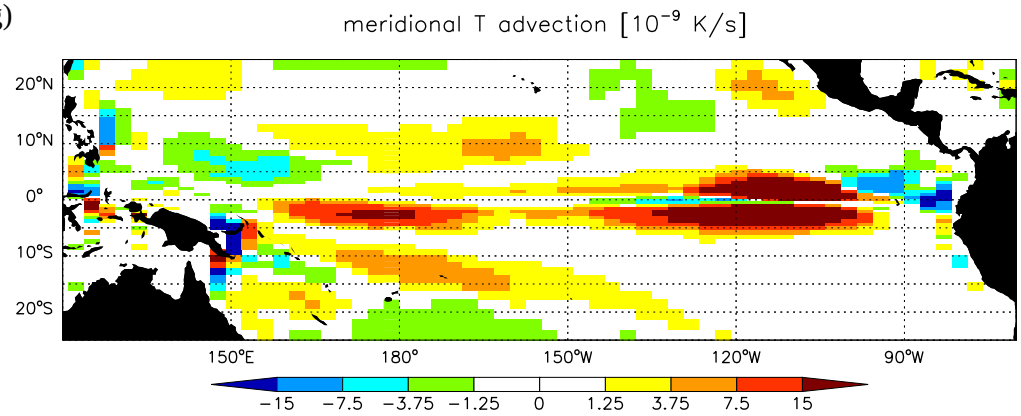
meridional T advection [10⁻⁹ K/s]
20°N
10°N
0°
10°S
20°S
150°E
180°
150°W
120°W
90°W
−15 −7.5 −3.75 −1.25 0 1.25 3.75 7.5 15

h)

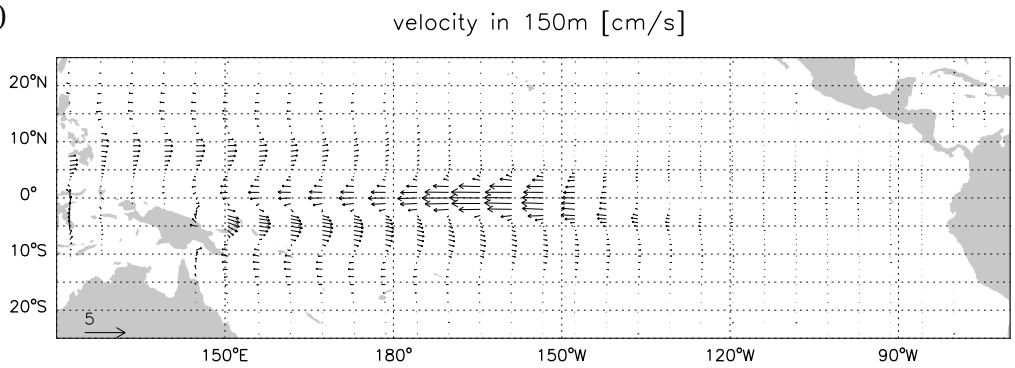
velocity in 150m [cm/s]
20°N
10°N
0°
10°S
20°S
5
150°E
180°
150°W
120°W
90°W

i)

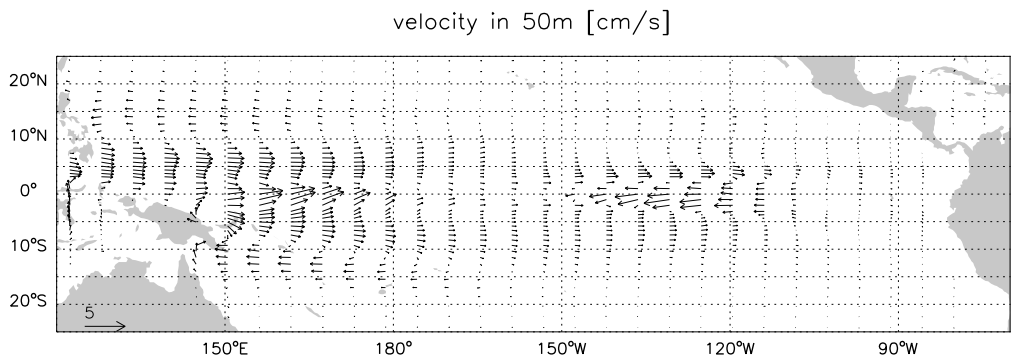
velocity in 50m [cm/s]
20°N
10°N
0°
10°S
20°S
5
150°E
180°
150°W
120°W
90°W

j)

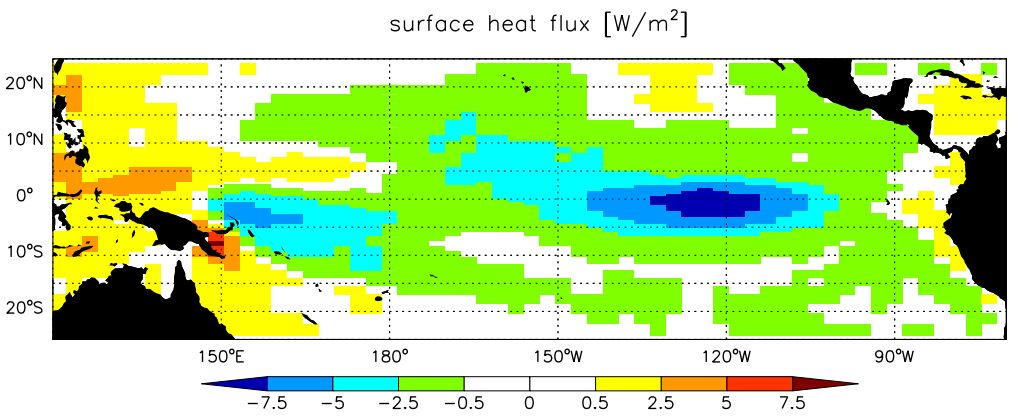
surface heat flux [W/m²]
20°N
10°N
0°
10°S
20°S
150°E
180°
150°W
120°W
90°W
−7.5
−5
−2.5
−0.5
0
0.5
2.5
5
7.5

k)

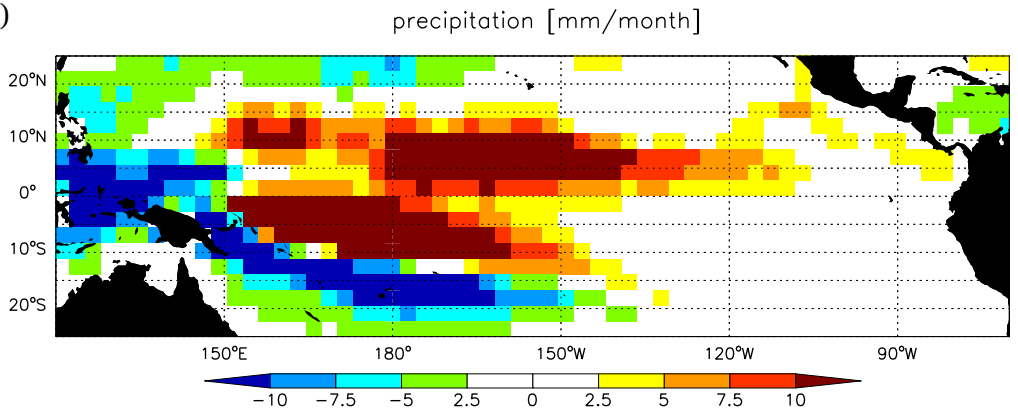
precipitation [mm/month]
20°N
10°N
0°
10°S
20°S
150°E
180°
150°W
120°W
90°W
−10
−7.5
−5
2.5
0
2.5
5
7.5
10

l)

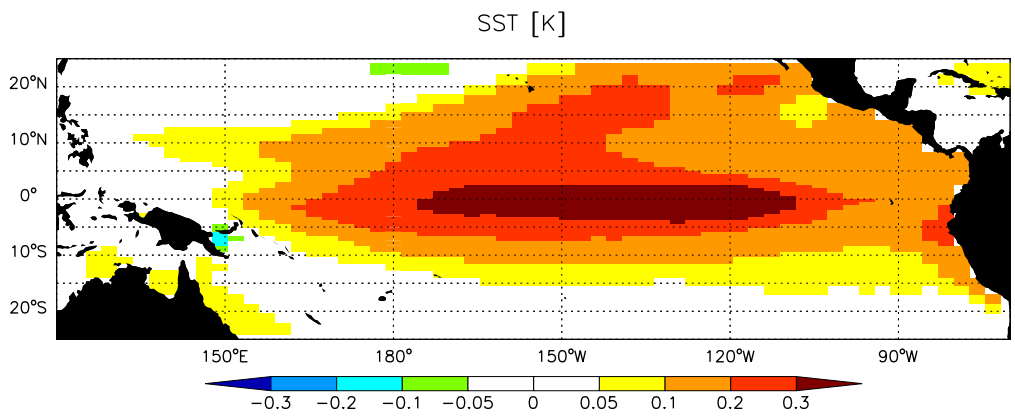
SST [K]
20°N
10°N
0°
10°S
20°S
150°E
180°
150°W
120°W
90°W
−0.3
−0.2
−0.1
−0.05
0
0.05
0.1
0.2
0.3

Figure 24: *Linear regression of various atmospheric and oceanic fields from the ECHAM4/OPYC model integration onto the decadal Niño4 SST mode (figure 23). The fields are monthly values with the annual cycle removed. All values are per standard deviation of the SST index (0.13K). (a) Pacific meridional overturning streamfunction (in Sv), (b) wind stress (vectors, in Nm^{-2}) and wind stress curl (contours, in 10^{-9} Nm^{-3}), (c) vertical velocity at model level 65 meters (in cm/day), (d) depth of the thermocline (in m), (e) horizontal velocity at the surface (vectors, in cm/s) and horizontal temperature advection (contours, in 10^{-9} Ks^{-1}), (f) zonal temperature advection (in 10^{-9} Ks^{-1}), (g) meridional temperature advection (in 10^{-9} Ks^{-1}), (h) horizontal velocity at model level 150 meters (in cm/s), (i) horizontal velocity at model level 50 meters (in cm/s), (j) downward net surface heat flux (in Wm^{-2}), (k) precipitation (in mm/month), (l) sea surface temperature (in K)*

3.4. Greenhouse gas simulations

In this chapter a scenario integration of the ECHAM4/OPYC model is analyzed to study the sensitivity of the TCs and STCs to greenhouse warming. The integration is forced by observed greenhouse gas concentrations from 1860 to present and the concentrations follow the IPCC 1992a scenario until 2100 (figure 25a).

As for the control integration, indices for the strength of the TCs and STCs are computed in the same way as described at the beginning of chapter 3.2. Additionally, an STC index at 15^o latitude is calculated. Figure 25b shows the timeseries of the strength of the TCs in the scenario integration. The strength of the TCs is increasing under greenhouse conditions. The increase is about 15% for a doubling of the CO_2 concentration. Such a trend is not seen in the control integration (blue curve in figure 19). Considering the strength of the STCs, the model simulates a decreasing trend poleward of 10^o latitude. This is seen clearly at 15^o latitude (figure 25c), where the transport weakens during the 21st century by about 10%.

If one calculates the trend in the Pacific merdional overturning streamfunction over the last 110 years (where the CO_2 concentration approximately doubles, figure 25a), a quite complex response of the tropical circulation to global warming is found (figure 26a). While the TCs intensify, the off-equatorial and deeper parts of the overturning spin-down. The latter is consistent with *Merryfield and Boer (2004, submitted)* who found a decrease of the pycnocline transport at 10^o latitude under global warming conditions.

The trend in the SST (figure 26b) shows an increase in temperature over the entire tropical Pacific. However, the warming trend is smaller in the western than in the eastern tropical Pacific. Since the influence of the TCs onto the SST (stronger cells leading to colder SST) is largest in the west (figure 20), the increase in the strength of the TCs might contribute to the pattern in the SST trend.

Additionally to the scenario integration of the ECHAM4/OPYC model, the response of the TCs and STCs to global warming in the 1% integrations (1% increase of the CO_2 concentration per year) of the coupled model intercomparison project (CMIP2) is analyzed.

Figure 28 shows the timeseries of the strengths of the TCs and the STCs at 15^o latitude for the different models. Note that for the meridional overturning streamfunction in the CMIP2 integrations only output averaged over 20 year intervals is available. Since partly also the

control integrations show a trend in the strength of the cells and to account for the quite different mean strength of the cells in the different models (figure 27) the strength of the (S)TCs is expressed as the difference between the strengths in the 1% and the control integration divided by the mean strength of the cells in the control integration (between 5^oS and 5^oN and at 15^o latitude respectively).

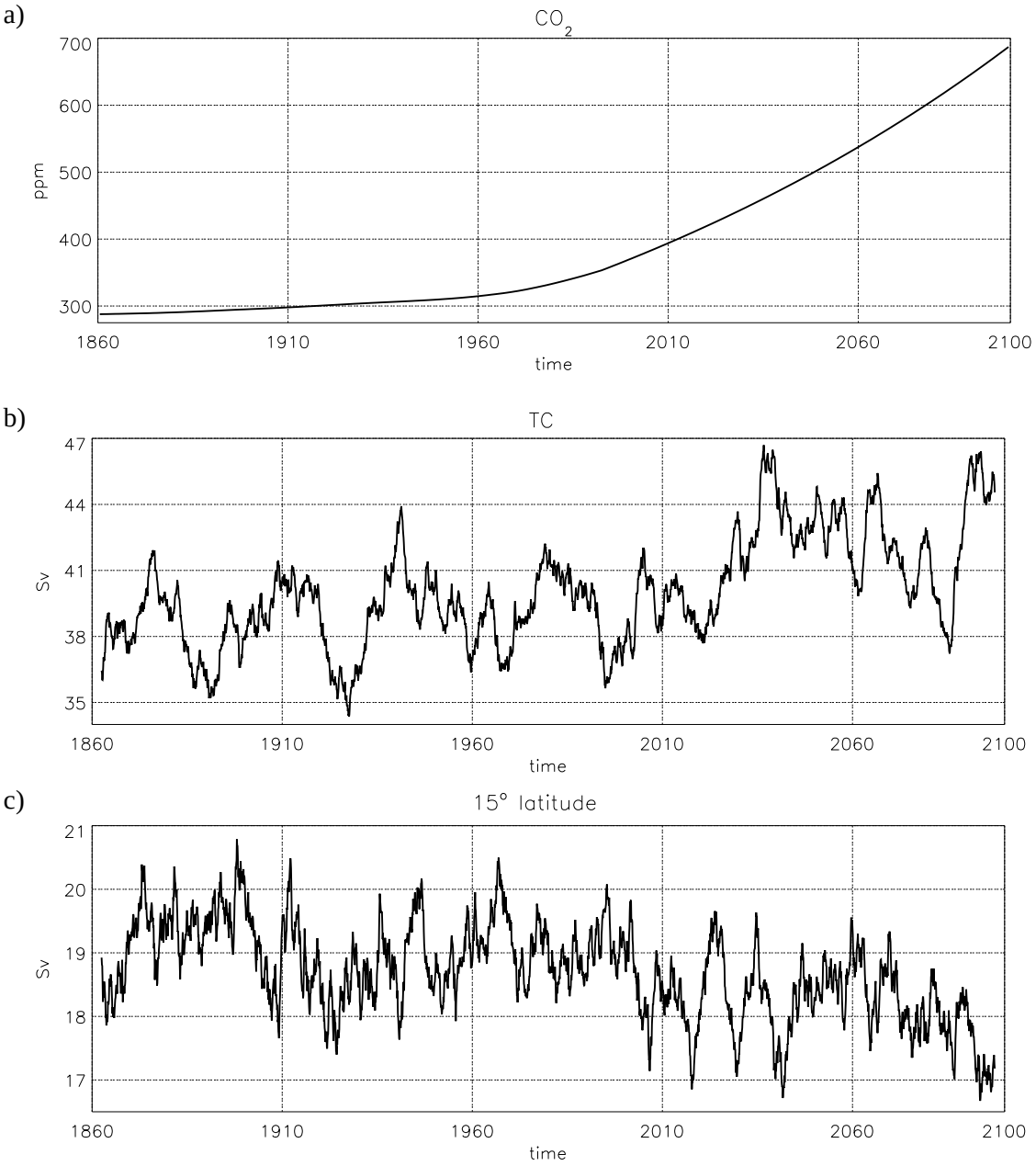

Figure 25: *(a) Increase in the CO_2 concentration in the scenario integration of the ECHAM4/OPYC model and timeseries of the strength of (b) the TCs and (c) the STCs at 15^o latitude as simulated in the scenario integration. For definition of the cell strength see text.*

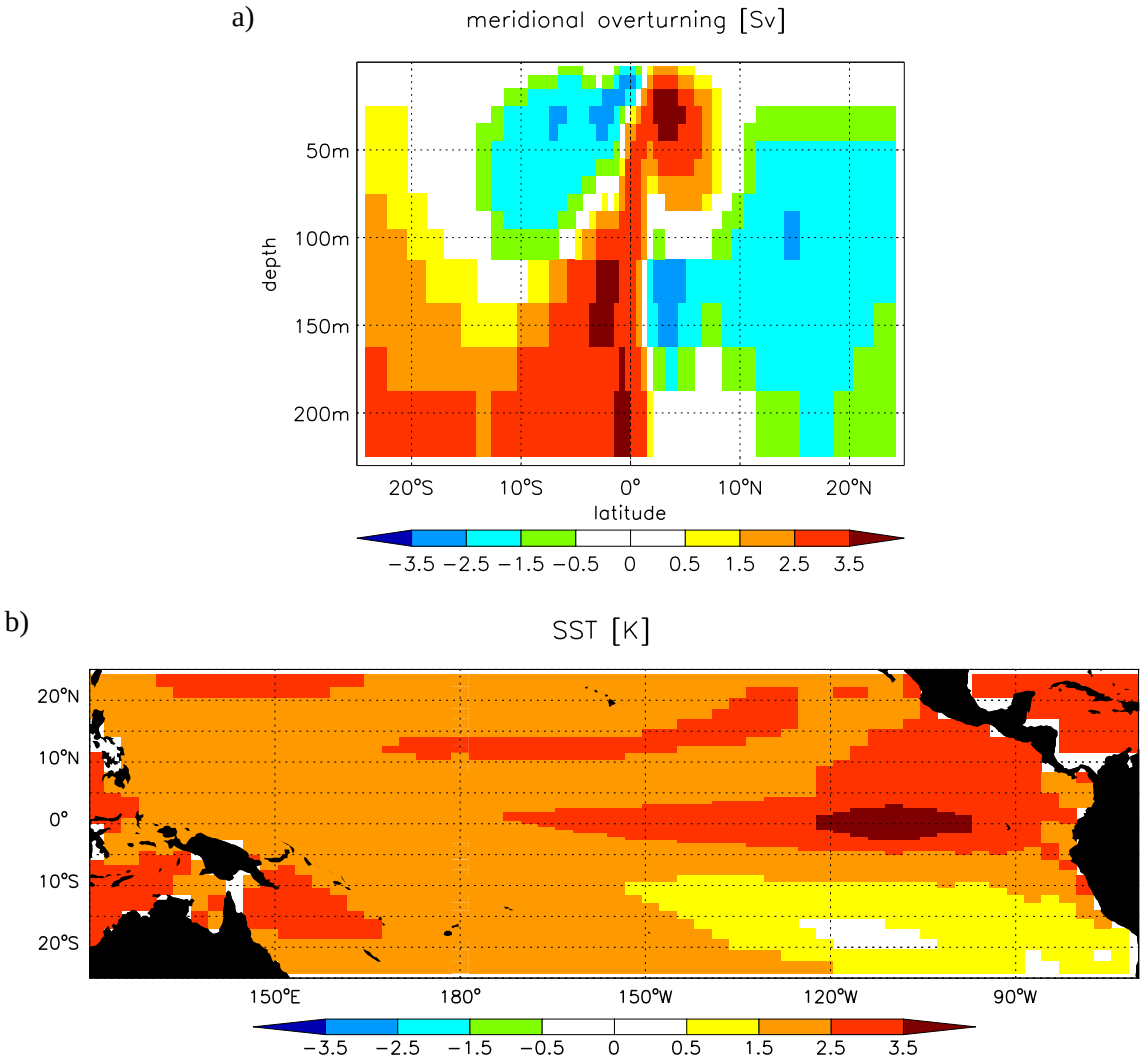

Figure 26: *Trend in (a) the Pacific meridional overturning streamfunction and (b) the SST in the scenario integration of the ECHAM4/OPYC model. Unit is (a) Sv and (b) ^{o}C over the last 110 years of the run (1990-2100). Note in (a) that for the southern hemisphere the mean is negative, i.e. negative (positive) values correspond to a strengthening (weakening) of the overturning.*

Within the different CMIP2 models no uniform response of the cell strength to an increase in the CO_2 concentration is found neither for the TCs nor for the STCs. Furthermore, many models simulate only a rather weak trend, especially in the strength of the STCs. The latter is shown at 15^{o} latitude (as in figure 25) but a similar picture is obtained at 10^{o} and 20^{o} latitude. For the TCs it should be mentioned that they are not simulated in some of the models (figure 27, e.g. IAP and GFDL).

The different response shows that a prediction of the (S)TC sensitivity to an increase in the CO_2 concentration is difficult from the CMIP2 model integrations.

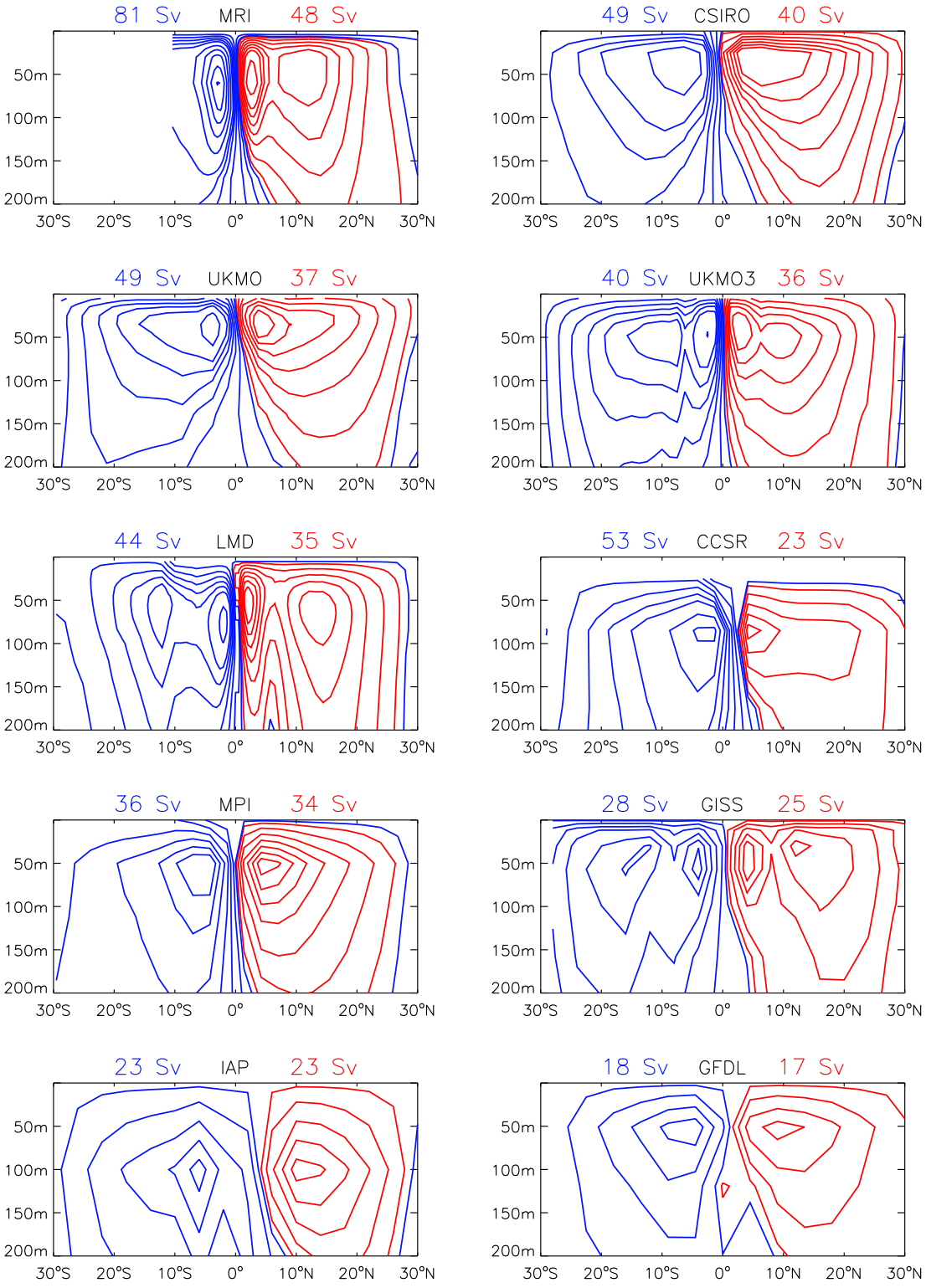

Figure 27: *Mean Pacific meridional overturning streamfunction in different models of the coupled model intercomparison project (CMIP2), averaged over the 80 year long control integrations. Red (blue) contourlines represent (anti)clockwise flow. Contour levels are 1, 5, 10, 15, 20, 25, 30, 40, 50, 60, 70 and 80 Sv. The numbers give the maximum strength of the cells. The model from MPI is the ECHAM3/LSG model.*

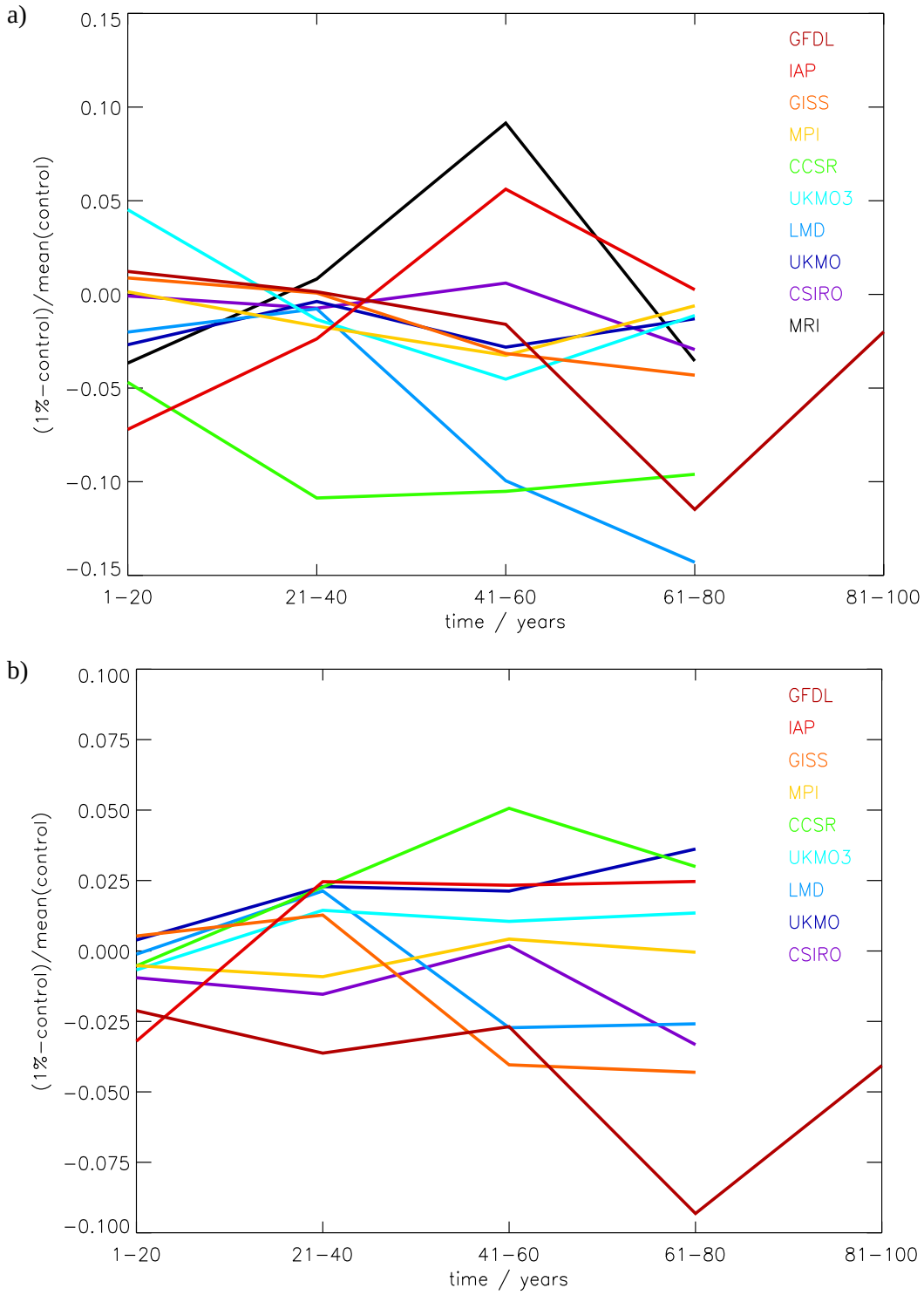

Figure 28: *Timeseries of the strength of (a) the TCs and (b) the STCs at 15^o latitude in the different CMIP2 models. For definition of the cell strength see text. The cell strength is expressed as timeseries of the 1% run minus timeseries of the control run divided by the mean of the control run. Note that only 20 year means of the overturning from the CMIP2 integrations are available and that for the MRI model no overturning is calculated south of 10^{o}S.*

4. Atlantic Ocean

4.1. Relation between TC/STC and tropical SST

Also in the Atlantic Ocean a (southern hemispheric) subtropical (STC) and tropical (TC) cell exists (figure 2). In the following the variability of these cells and their relation to the tropical Atlantic climate variability is investigated.

Figure 29 shows the observed SST anomalies (taken from the HadISST1.1 dataset) in the equatorial Atlantic in the last 130 years. The variability is weaker compared to the Pacific (figure 3 for the Niño4 region). As in the western equatorial Pacific the leading SST mode from a singular spectrum analysis has a quasi-decadal timescale (figure 30), closely resembling the timeseries with the five year running mean applied (red curve in figure 29). In the tropical Atlantic there has also been an increase in SST over the last decades.

The decadal variability of the strength of the TC taken from the MPI-OM integration forced with the NCEP reanalysis is shown in figure 31 (blue curve). Here the (southern hemispheric) TC strength index is defined by taking for each timestep $-psi_{min}(5^oS - 0^o, upper\ 150m)$ where *psi* is the Atlantic meridional overturning streamfunction with a five year running mean applied (note that the mean overturning is negative for the Atlantic TC). As for the Pacific TC index, a five year running mean is applied to account for the fact that the surface branch of the cells spins-up and -down quicker than the pycnocline branch (e.g. *Klinger et al., 2002*).

The anomalies in the strength of the TC (as well as the mean strength) are much weaker compared to the Pacific (figure 3, note that here the index is based on both hemispheric cells). Also no strong trend, as simulated in the Pacific TCs in the mid-1970s, is found in the Atlantic TC variability. The simulated cell variability is similar in the individual members of an ensemble of integrations with the same ocean model, run with a coarser horizontal and higher

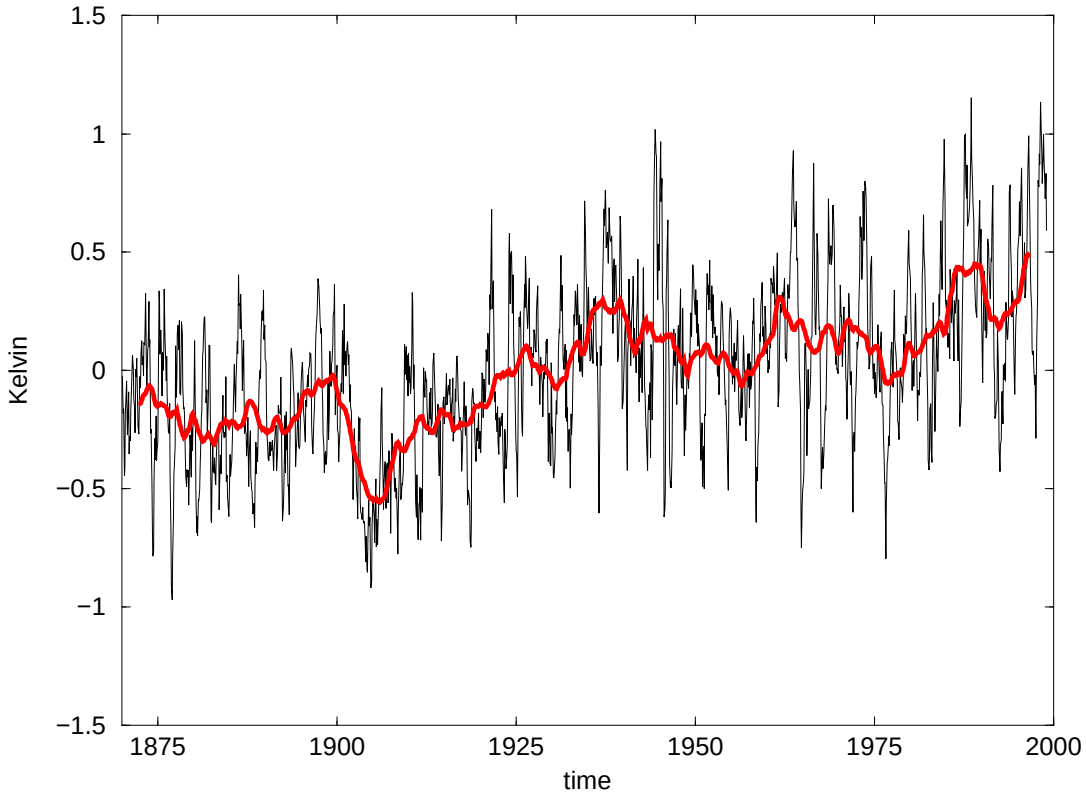

Figure 29: *Observed SST anomalies (taken from the HadISST1.1 dataset) averaged over the equatorial Atlantic Ocean (5^oS to 5^oN, whole Atlantic basin width) for the last 130 years. Shown are monthly values (with the annual cycle removed, black) and five year running mean (red).*

vertical resolution (figure 32). As for the Pacific (figure 8), the amplitude of cell strength variability is different for the different model set-ups.

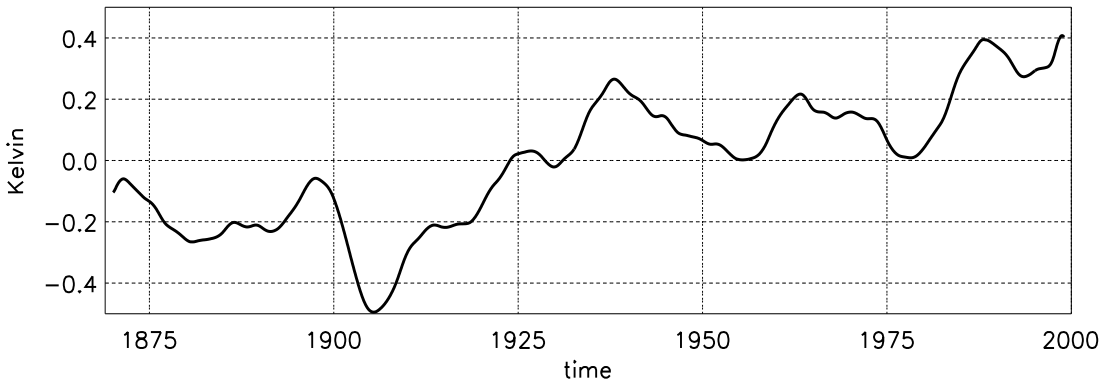

Figure 30: *Reconstruction of the monthly observed SST anomalies in the equatorial Atlantic (black curve in figure 29) from singular spectrum analysis using mode 1 and 2.*

In figure 31 the decadal observed SST variability in the eastern equatorial Atlantic is shown together with the TC strength anomalies from the MPI-OM model integration forced with the NCEP reanalysis. The SSTAs are averaged over the region 5^{o}S to 5^{o}N and 20^{o}W to 10^{o}E. This index has been chosen because the correlation pattern between the TC index and the observed SST shows higher correlation in the eastern tropical Atlantic (figure 33).

In contrast to the Pacific, however, the cross-correlation function between the TC and SST timeseries does not show an influence of the cell variability onto the SST anomalies (figure 34). The maximum correlation coefficient of -0.6 is found with the SST leading the TC index by about 15 months. If the SST timeseries is detrended prior to the calculation of the cross-correlation function the maximum correlation amounts to -0.75. This suggests that changes in the tropical SST can have (via changes in the trade winds) an effect onto the strength of the TC.

Considering an index for the strength of the (southern hemispheric) STC, defined by taking for each timestep *-psi$_{min}$(10^{o}S, upper 150m)*, no correlation between the Atlantic STC and SST anomalies is found in the NCEP forced integration. This is also true if the STC index is calculated at 15^{o}S or 20^{o}S.

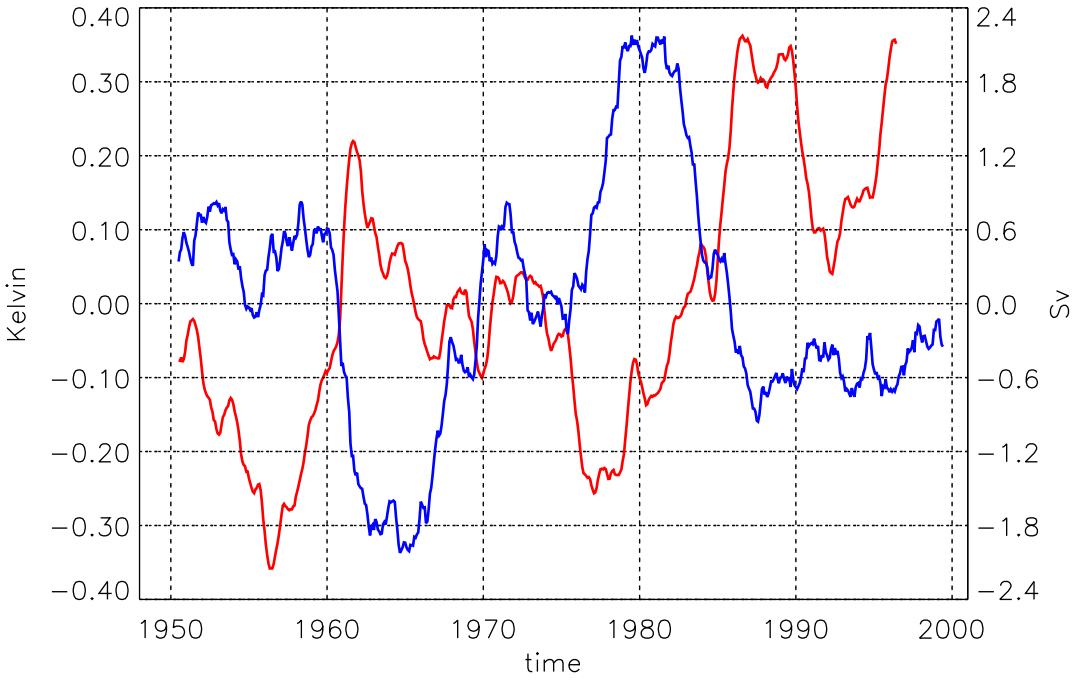

Figure 31: *Timeseries of the observed SST anomalies (taken from the HadISST1.1 dataset) in the eastern tropical Atlantic Ocean (averaged over the region 5^{o}S to 5^{o}N, 20^{o}W to 10^{o}E) and the anomalous strength of the southern hemispheric TC taken from the MPI-OM model integration forced with the NCEP reanalysis. For definition of the cell strength see text. Shown are monthly values with a five year running mean applied (red for SST, blue for TC).*

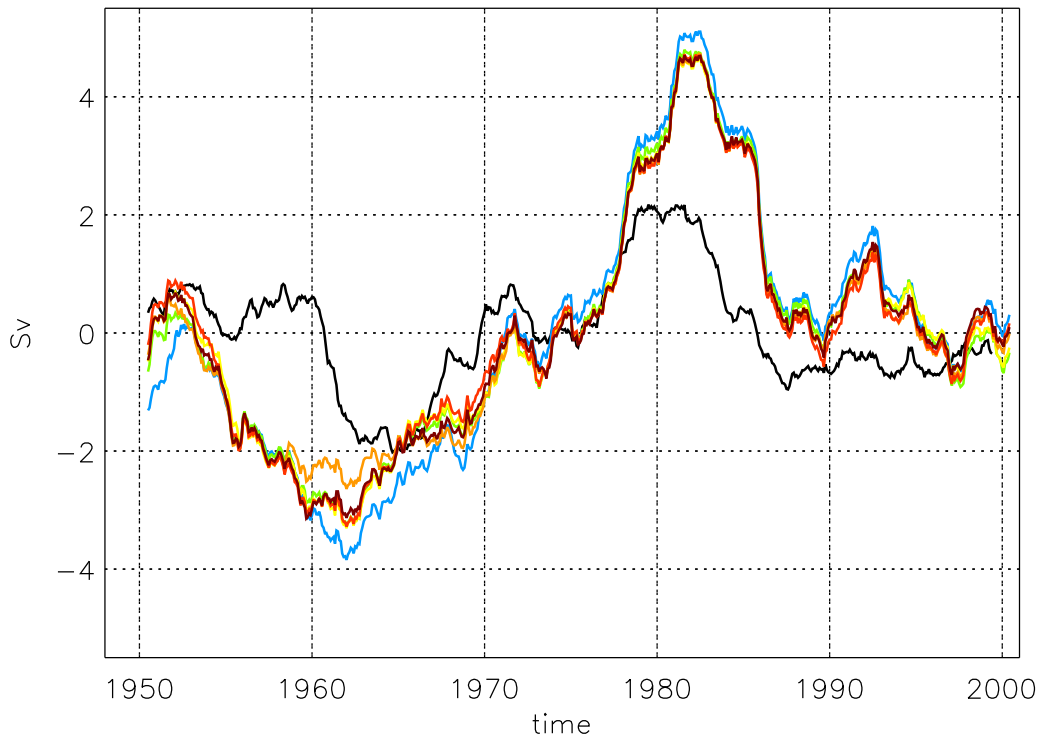

Figure 32: *Timeseries of the anomalous strength of the TC taken from the MPI-OM model integration forced with the NCEP reanalysis. The black curve corresponds to the blue curve in figure 31, the coloured curves are six ensemble members from an integration with a different resolution of the model grid. For definition of the cell strength see text.*

On interannual timescales, *Goes and Wainer (2003)* suggest from an OGCM forced with the NCEP reanalysis that years of warm (cold) eastern tropical SST go along with a decrease (increase) in the South Equatorial Current (SEC) and the Equatorial Undercurrent (EUC).

Figure 35 shows the composite differences for warm minus cold monthly observed eastern equatorial SST for various atmospheric and oceanic fields from the MPI-OM model integration forced with the NCEP reanalysis. The composite difference is calculated to take into account only stronger warm and cold events since the correlation between the SST index and the strength of the TC is low (figure 36). As a threshold value for the composites one standard deviation of the SST index has been taken. The positive (warm) and negative (cold) composite patterns are very similar with the opposite sign for the cold years.

During years of warm (cold) eastern tropical SST (figure 35f), the TCs are weakened (strengthened). Interestingly this signal is seen in both hemispheric cells (figure 35a). While an STC exists only in the southern hemisphere, a TC can be found also north of the equator (figure 2). Note that for the southern cell the mean overturning is negative, i.e. positive anomalies correspond to a weakening of the cell. The change in the strength of the TCs

between years with warm and cold eastern equatorial SST is about 20% of the mean strength of the cells.

The decrease (increase) in the strength of the TCs is also seen in the vertical velocity (figure 35d). The equatorial upwelling is reduced (enlarged) during phases of warm (cold) eastern tropical SST, while anomalous upwelling (downwelling) is found at about 5^o latitude respectively.

The changes in the strength of the cells (and the vertical velocity) go along with changes in the trade winds (figure 35b). During years of warm (cold) SST index , weaker (stronger) trades are found in the western part of the basin on the equator and in the southern hemisphere leading to a reduced (enlarged) Ekman transport divergence (seen in figure 35c close to the equator). Upwelling (downwelling) favourable curl is found at about 5^o latitude.

The changes in the trade winds also lead to changes in the zonal currents (vectors in figure 35c and e). The decrease of the SEC and the EUC by the order of 10 cm/s between years with warm and cold eastern equatorial SST is in agreement with *Goes and Wainer (2003)*. The changes in the currents also contribute to the increase (decrease) in the SST by horizontal temperature advection (colour-shaded in figure 35c).

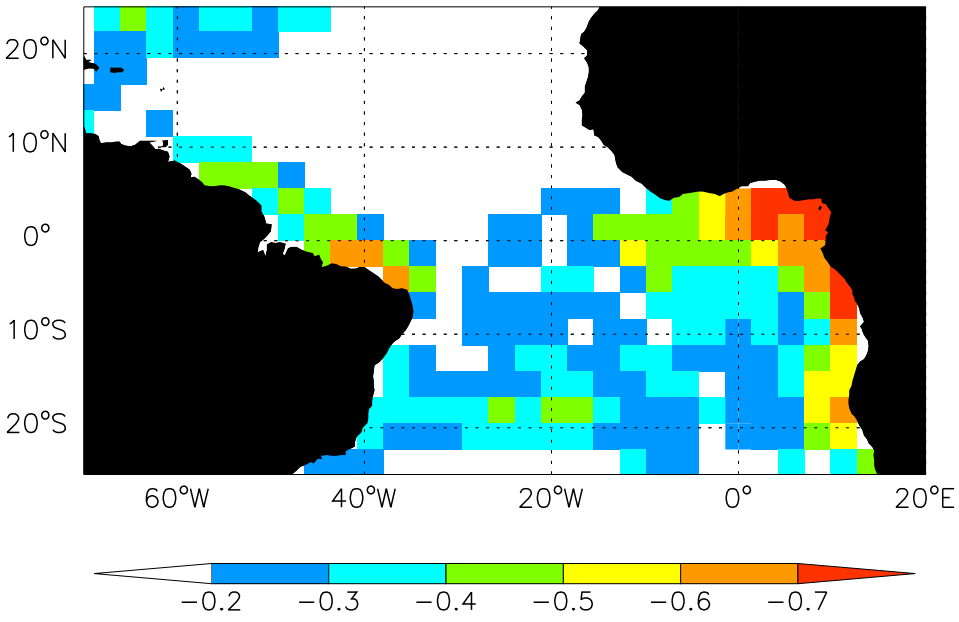

Figure 33: *Correlation pattern between the anomalous strength of the TC from the MPI-OM model integration forced with the NCEP reanalysis (blue curve in figure 31) and the decadal (five year running mean applied) observed SST (taken from the HadISST1.1 dataset). For definition of the cell strength see text.*

The net surface heatflux (figure 35g) acts to damp the SST over most of the region. Only at the northern edge the heatflux contributes to the warming (cooling).

The cross-correlation function between the SST index and the monthly strength of the TCs (figure 36) suggests that on interannual timescales changes in the strength of the TCs are leading changes in the eastern equatorial SST. Here the TC index is calculated by taking for each timestep $psi_{max}(5^oS - 5^oN, upper\ 150m) - psi_{min}(5^oS - 5^oN, upper\ 150m)$ where *psi* is the monthly Atlantic meridional overturning streamfunction assuming that the TCs are narrow enough to spin-down (or -up) at the same time. Southern as well as northern TC are considered because figure 35a suggests an influence onto the SST from both hemispheric cells. The correlation is quite low although statistically significant. One reason might be that the SST variability is relatively low. The highest variability is found in boreal summer (figure 37). If only the SST anomalies from june and july are considered the correlation coefficient amounts to -0.6.

As for the Pacific, also the output from the coupled atmosphere/ocean general circulation model ECHAM4/OPYC has been analyzed.

If the TC is considered, no significant connection to the SST can be found neither for decadal nor for interannual timescales. This is also true if only the months of highest SST

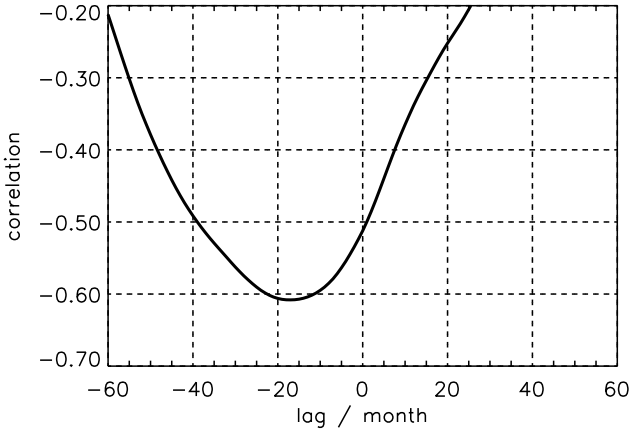

Figure 34: *Cross-correlation function between the SST and TC anomalies in figure 31. The 95% significance level according to a t-test is -0.44. A positive (negative) lag indicates that the SST is lagging (leading).*

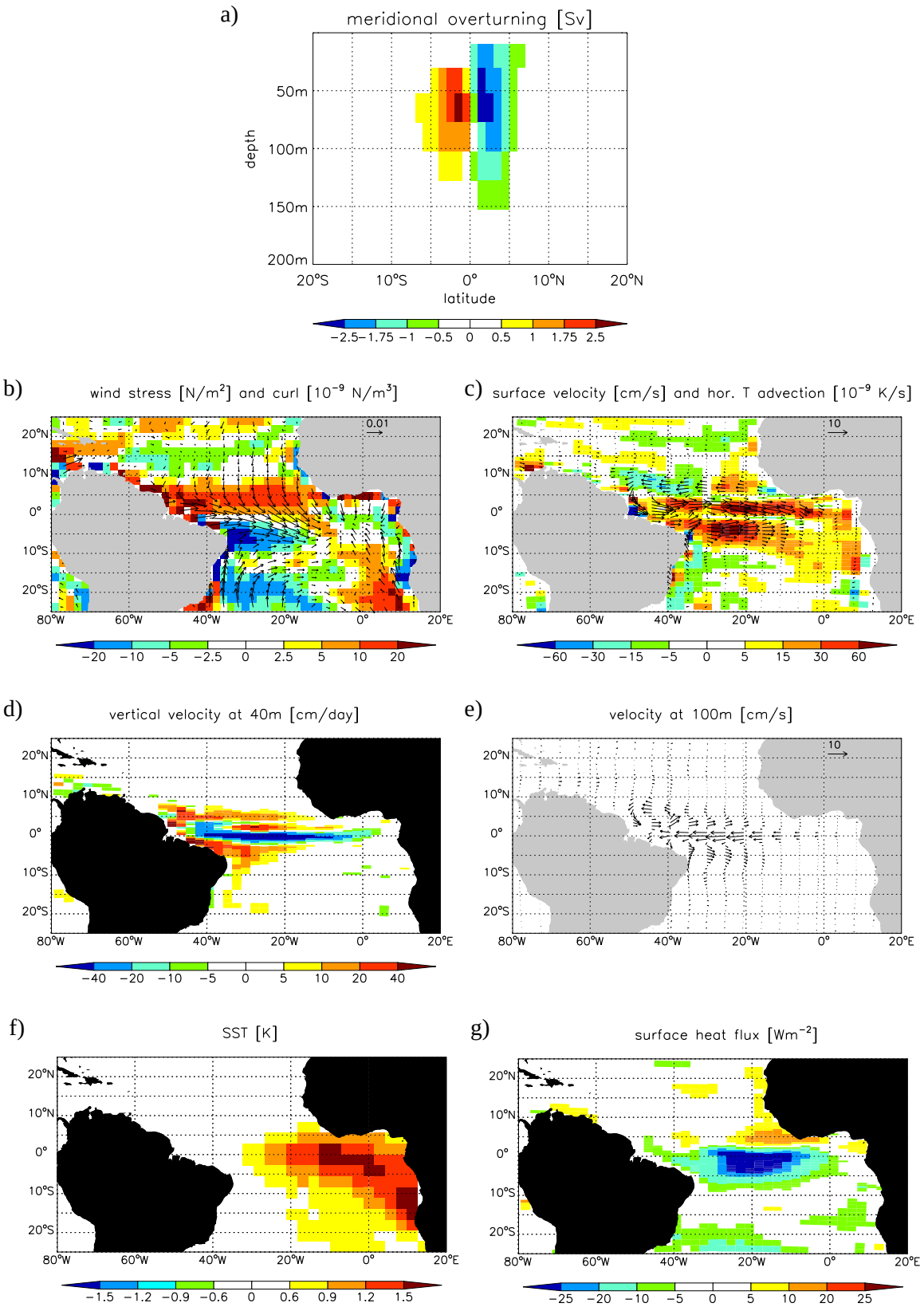
a)
meridional overturning [Sv]
depth
50m
100m
150m
200m
20°S
10°S
0°
10°N
20°N
latitude
−2.5 −1.75 −1 −0.5 0 0.5 1 1.75 2.5
b)
wind stress [N/m²] and curl [10⁻⁹ N/m³]
0.01
20°N
10°N
0°
10°S
20°S
80°W
60°W
40°W
20°W
0°
20°E
−20 −10 −5 −2.5 0 2.5 5 10 20
c)
surface velocity [cm/s] and hor. T advection [10⁻⁹ K/s]
10
−60 −30 −15 −5 0 5 15 30 60
d)
vertical velocity at 40m [cm/day]
−40 −20 −10 −5 0 5 10 20 40
e)
velocity at 100m [cm/s]
10
f)
SST [K]
−1.5 −1.2 −0.9 −0.6 0 0.6 0.9 1.2 1.5
g)
surface heat flux [Wm⁻²]
−25 −20 −10 −5 0 5 10 20 25

Figure 35: *Composite differences for warm minus cold observed eastern equatorial SST (5^oS - 5^oN, 20^oW - 10^oE) of various atmospheric and oceanic fields from the MPI-OM model integration forced with the NCEP reanalysis. SST index and fields are monthly values with the annual cycle removed and have been detrended prior to the composite calculation. The threshold value for the composites is one standard deviation of the SST index. (a) Atlantic meridional overturning streamfunction (in Sv), (b) wind stress (vectors, in Nm^{-2}) and wind stress curl (contours, in 10^{-9} Nm^{-3}), (c) horizontal velocity at the surface (vectors, in cm/s) and horizontal temperature advection (contours, in 10^{-9} Ks^{-1}), (d) vertical velocity at model level 40 meters (in cm/day), (e) horizontal velocity at model level 150 meters (in cm/s), (f) observed SST (in K), (g) downward net surface heat flux (in Wm^{-2})*

variability (March to May in this model integration) are considered. The very low SST variability (about one half of the observed SST range) as well as the weak cell strength (6 Sv compared to 12 Sv in the MPI-OM model integration forced with the NCEP reanalysis) might contribute to this.

However, considering the strength of the STC suggests some influence of the STC onto the equatorial SST for decadal timescales. The maximum correlation coefficient of -0.5 is found with the cell strength leading the SST by about 8 months which is comparable to what is found in the Pacific (figure 21). The correlation pattern shows the highest correlations south of the equator in the western part of the basin.

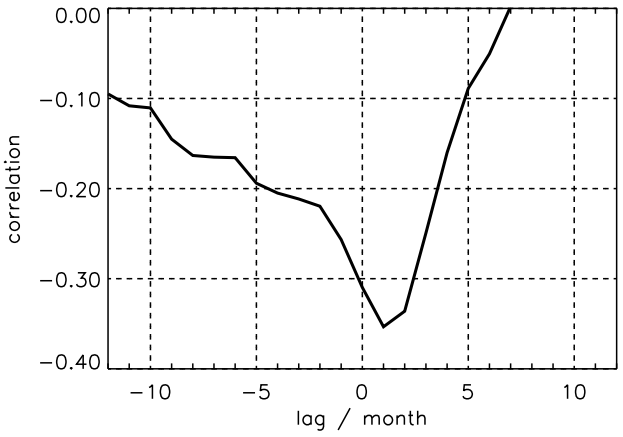

Figure 36: *Cross-correlation function between the monthly observed eastern equatorial SST index (5^oS - 5^oN, 20^oW - 10^oE) and the monthly strength of the TCs taken from the MPI-OM model integration forced with the NCEP reanalysis. For definition of the cell strength see text. The 95% significance level according to a t-test is -0.28. A positive (negative) lag indicates that the SST is lagging (leading).*

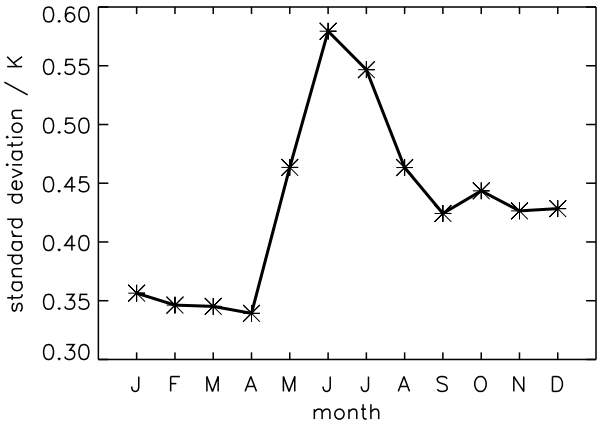

Figure 37: *Annual cycle of the standard deviation of the monthly observed eastern equatorial SST index (5^oS - 5^oN, 20^oW - 10^oE).*

It is noteworthy that the analysis of the coupled general circulation model ECHAM5/MPI-OM, which simulates more realistical tropical SST variability and cell strength, leads to similar results.

4.2. Influence of El Niño onto the TC/STC

Previous studies (e.g. *Wu et al., 2002*) have shown that the trade winds over the tropical Atlantic are influenced by the Niño3 SST (5^{o}S - 5^{o}N, 150^{o}W - 90^{o}W). Since the TCs and STCs are mainly wind driven, it will be investigated in this chapter if an influence of the tropical Pacific onto the Atlantic (S)TC can be found.

Figure 39a shows the composite difference for warm minus cold observed monthly Niño3 SST (threshold value one standard deviation) of the Atlantic meridional overturning streamfunction taken from the MPI-OM integration forced with the NCEP reanalysis. The composite difference is calculated to take into account only stronger El Niño and La Niña events since the correlation between the Niño3 SST and the strength of the Atlantic TC is low (figure 38). For years with a anomalously warm (cold) eastern equatorial Pacific the Atlantic (S)TC is strengthened (weakened). Note that for the southern hemisphere the mean overturning is negative, i.e. negative (positive) anomalies correspond to a strengthening (weakening). The change in the strength of the (S)TC between El Niño and La Niña years is about 15 to 20% of the mean cell strength. For decadal timescales (five year running mean applied) no influence

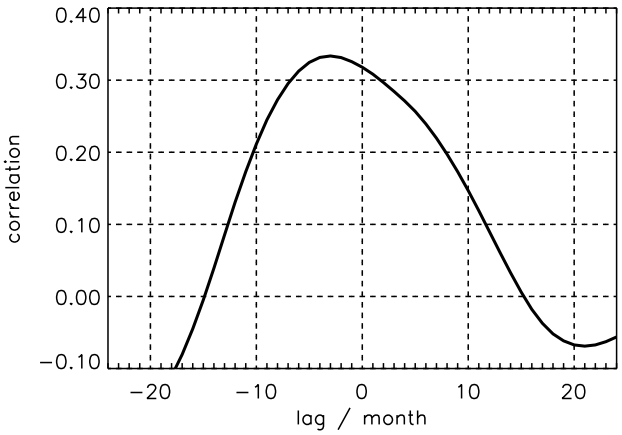

Figure 38: *Cross-correlation function between the monthly observed Niño3 SST index (with a one year running mean applied and detrended) and the monthly strength of the southern hemispheric Atlantic TC taken from the MPI-OM model integration forced with the NCEP reanalysis. For definition of the cell strength see text. The 95% significance level according to a t-test is -0.28. A positive (negative) lag indicates that the Niño3 SST is lagging (leading).*

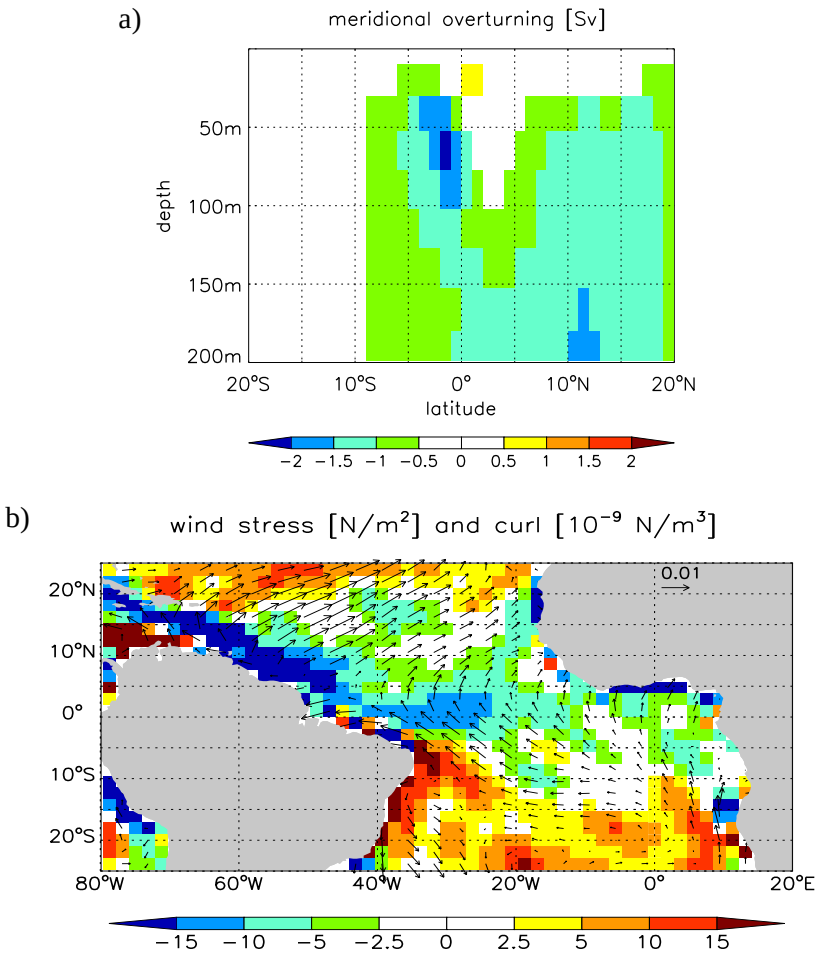

Figure 39: *Composite differences for warm minus cold Niño3 SST of fields from the MPI-OM model integration forced with the NCEP reanalysis. The Niño3 SST is leading by four months. All timeseries are monthly values with a one year running mean applied and have been detrended prior to the composite calculation. The threshold value for the composites is one standard deviation of the Niño3 SST index. (a) Atlantic meridional overturning streamfunction (in Sv), (b) wind stress (vectors, in Nm^{-2}) and wind stress curl (contours, in 10^{-9} Nm^{-3})*

from the tropical Pacific is found.

In figure 39 the Niño3 SST is leading the Atlantic overturning by four months. This lag is taken from the cross-correlation function between the Niño3 SST and the strength of the southern hemispheric Atlantic TC (figure 38). The latter has been determined from monthly Atlantic meridional overturning streamfunction data with a one year running mean applied. Only the TC index is considered in the cross-correlation function assuming that the narrow TCs spin-up (or -down) at the same time. For the northern hemispheric TC no influence from the Niño3 region is seen in figure 39a.

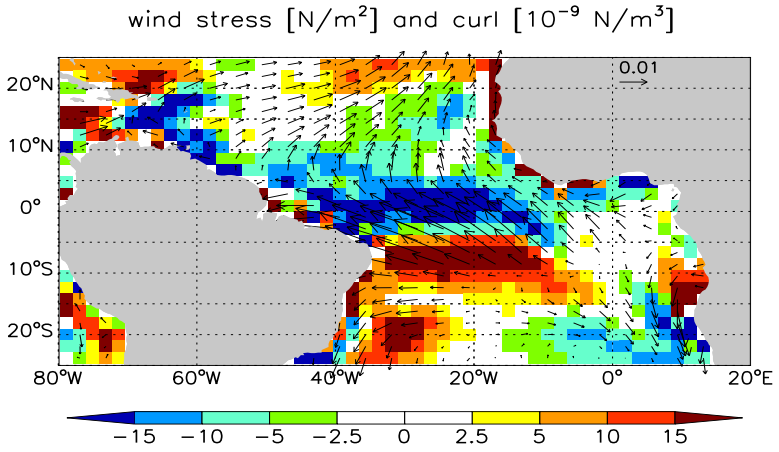

Figure 40: *Composite difference for strong minus weak Atlantic TC index (taken from the MPI-OM model integration forced with the NCEP reanalysis) of the wind stress (vectors, in Nm^{-2}) and wind stress curl (contours, in 10^{-9} Nm^{-3}) from the NCEP reanalysis. For definition of the cell strength see text. All timeseries are monthly values with a one year running mean applied and have been detrended prior to the composite calculation. The threshold value for the composite is one standard deviation of the TC index.*

The strengthening (weakening) of the Atlantic (S)TC goes along with a strengthening (weakening) of the south easterly trade winds during years with anomalously warm (cold) Niño3 SST (figure 39b, here with the Niño3 SST leading by four months, but the picture is similar for lag zero). The north easterly trades, in contrast, are weakened (strengthened) which is consistent with *Wu et al. (2002)*.

Figure 40 shows the composite difference for strong minus weak Atlantic TC index of the wind stress taken from the NCEP reanalysis. Note that the pattern for lag zero is shown, but a similar picture is obtained if the wind is leading the cell index by a few months. The pattern resembles the wind stress pattern seen for warm minus cold Niño3 SST (figure 39b).

To investigate which winds are driving the variability of the TC and STC, cell strength indices have been calculated for MPI-OM integrations forced with the NCEP reanalysis with climatological wind stress forcing within and poleward of the equatorial region respectively. The cell strength indices are calculated from meridional overturning streamfunction data with a five year running mean applied. As for the Pacific (S)TCs (figure 13) nearly all variability of the TC seen in the control run (figure 41a, black curve) can be simulated with wind stress variability restricted only to the equatorial region (green curve), while the variability of the STC is mainly caused by the wind stress (curl) fluctuations poleward of 5^{o} latitude (figure 41b,

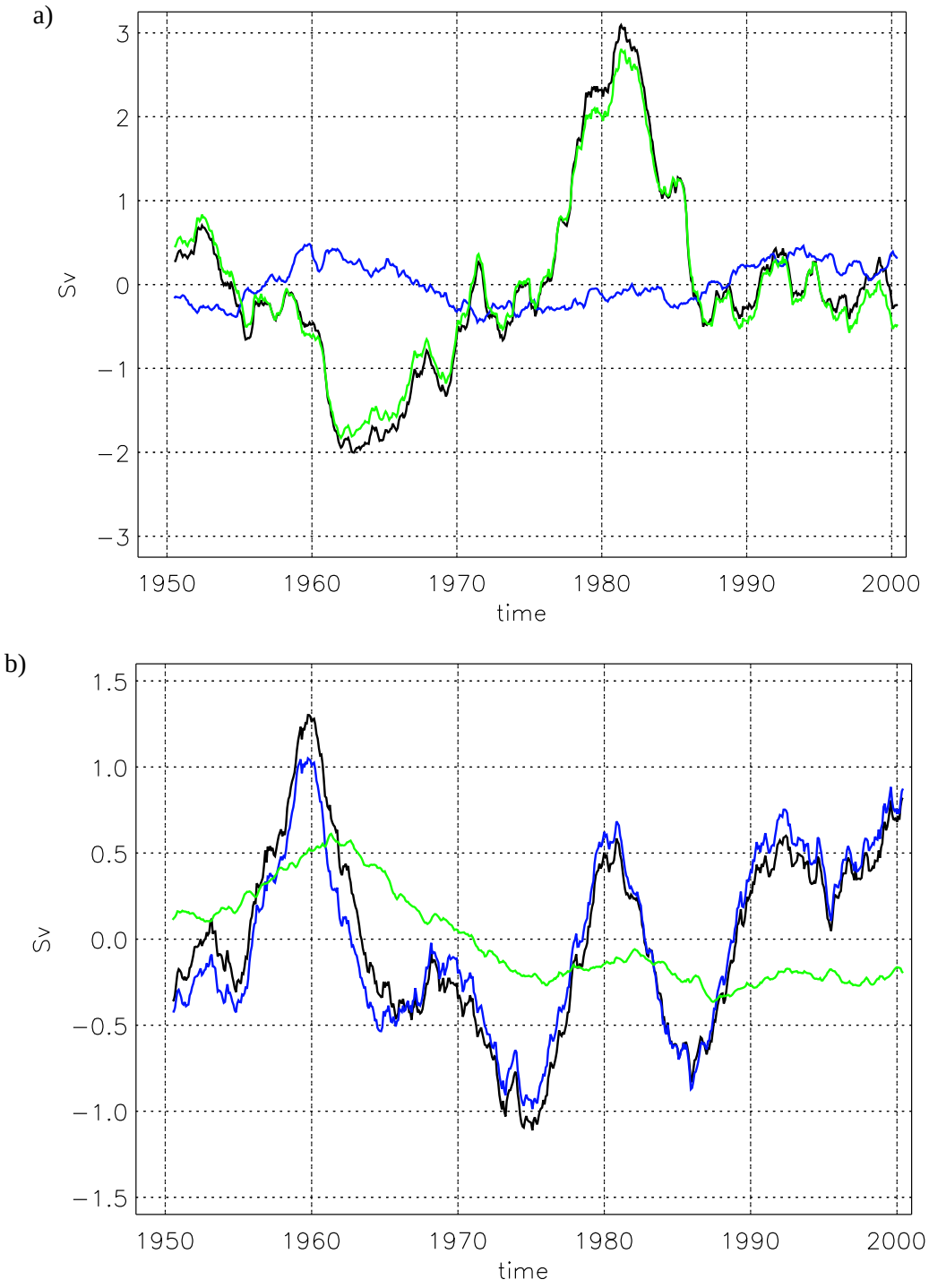

Figure 41: *Timeseries of the anomalous strength of (a) the TC and (b) the STC taken from MPI-OM integrations forced with the NCEP reanalysis: control run (black), climatological wind stress forcing poleward of 5^o latitude (green) and climatological wind stress forcing between 5^oS and 5^oN (blue). For definition of the cell strength see text.*

blue curve).

Considering integrations with coupled general circulation models, no significant correlation between the Atlantic TC and the Niño3 SST can be found in the ECHAM4/OPYC model. The weak strength of the cell in this model might contribute to this.

For the ECHAM5/MPI-OM integration, however, the strength of the TC increases (decreases) during years with anomalously warm (cold) Niño3 SST with a lag of about four months (figure 42), which is consistent with figure 38. The correlation coefficient between the Atlantic TC index and the Niño3 SST is higher than for the NCEP forced integration. The change in the strength of the (S)TC between El Niño and La Niña years in the ECHAM5/MPI-OM integration is about 25 to 30% of the mean cell strength.

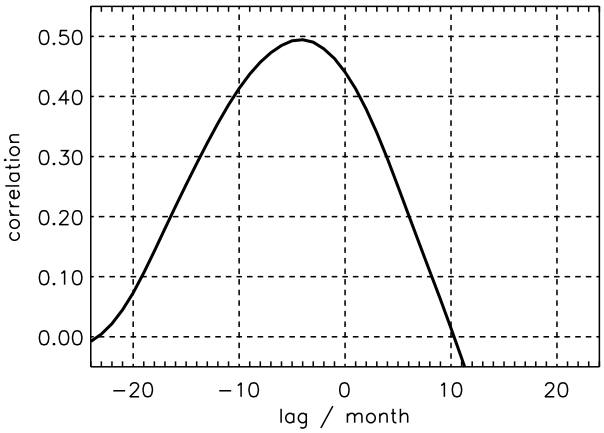

Figure 42: *Cross-correlation function between the monthly Niño3 SST index (with a one year running mean applied) and the monthly strength of the Atlantic TC taken from the coupled atmosphere/ocean general circulation model ECHAM5/MPI-OM. For definition of the cell strength see text. The 95% significance level according to a t-test is -0.25. A positive (negative) lag indicates that the Niño3 SST is lagging (leading).*

4.3. Greenhouse gas simulations

In chapter 3.4 it has been shown that the strength of the Pacific (S)TCs simulated by the ECHAM4/OPYC model changes under greenhouse warming conditions (figure 25). Here the response of the Atlantic TC and STC to an increase in the CO_2 concentration is investigated.

Figure 43b shows the strength of the southern hemispheric Atlantic TC in the scenario integration of the ECHAM4/OPYC model. In this integration the CO_2 concentration is increasing according to observations from 1860 to present and the IPCC 1992a scenario afterwards (figure 43a). The TC index has been calculated in the same way as described in chapter 4.1.

In contrast to the Pacific TCs (figure 25b), the strength of the Atlantic TC is decreasing in the ECHAM4/OPYC scenario integration due to a weakening in the south easterly trade winds over the Atlantic Ocean. The weakening is about 15% for a doubling of the CO_2 concentration.

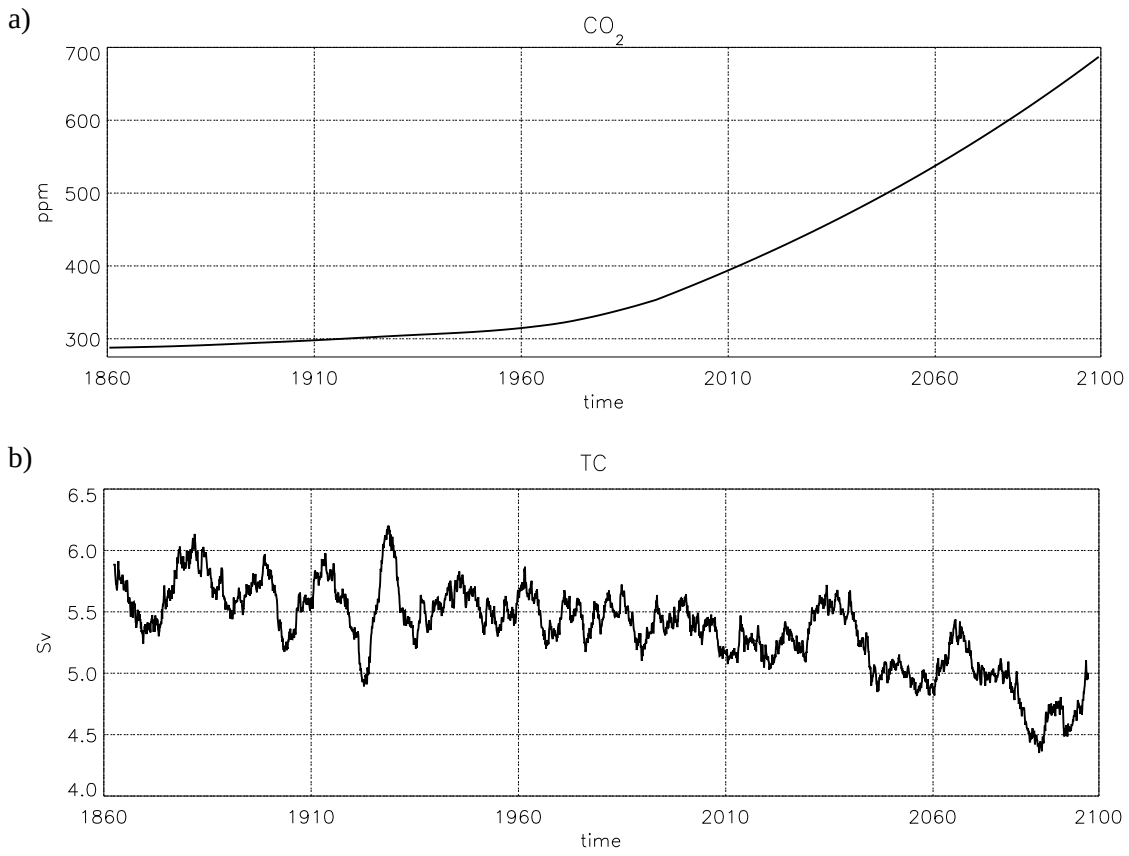

Figure 43: *(a) Increase in the CO_2 concentration for the scenario integration of the ECHAM4/OPYC model and (b) timeseries of the strength of the southern hemispheric Atlantic TC from the integration. For definition of the cell strength see text.*

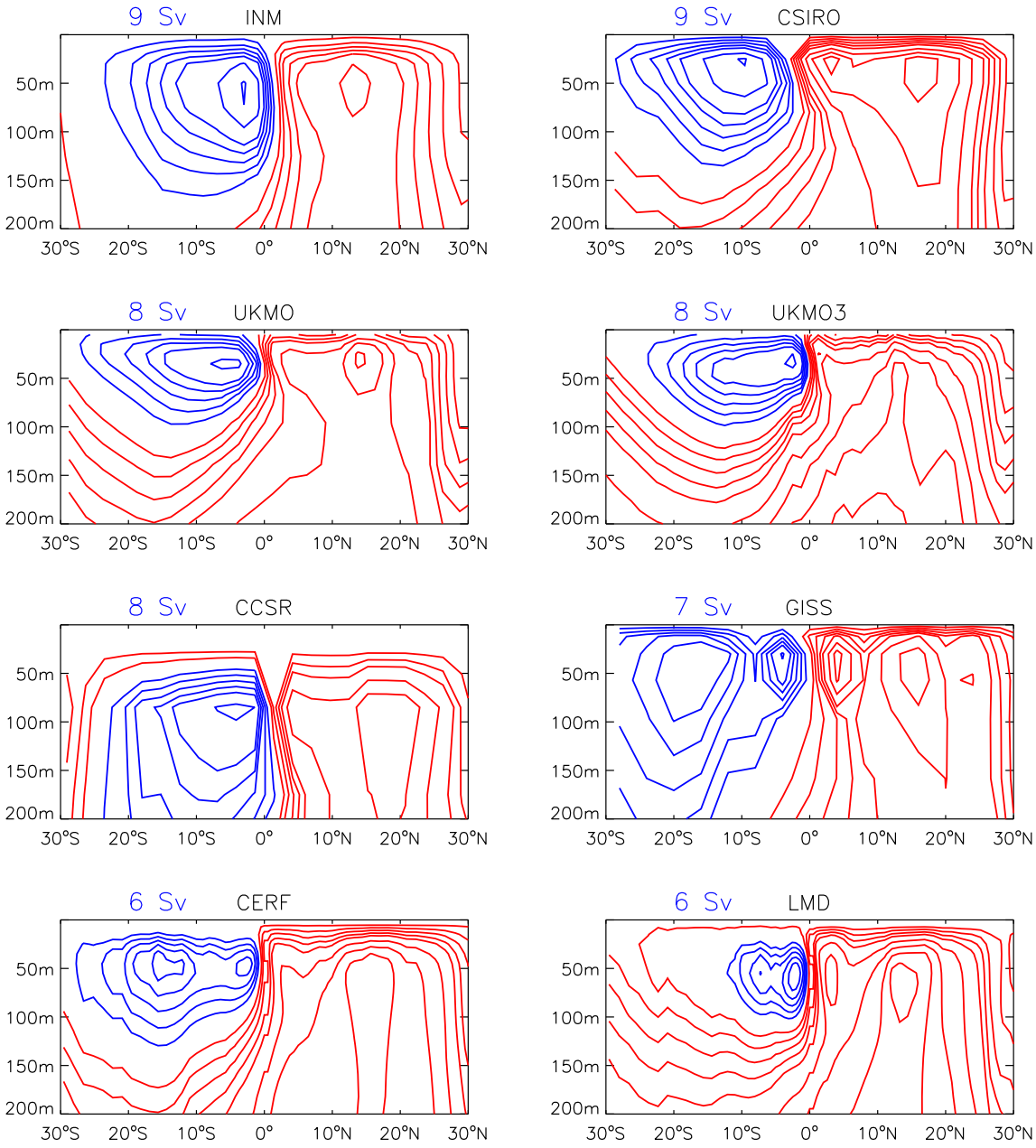

Figure 44: *Mean Atlantic meridional overturning streamfunction from different models of the coupled model intercomparison project (CMIP2), averaged over the 80 year long control integrations. Red (blue) contourlines represent (anti)clockwise flow. Contour levels are 1, 2, 3, 4, 5, 7 and 9 Sv. The numbers give the maximum strength of the cell.*

In the control integration no trend in the strength of the TC is found (not shown).

Considering the strength of the STC (not shown), no trend is found in the scenario integration. The fact that the Atlantic STC in the ECHAM4/OPYC integration is quite weak (about 2 Sv poleward of 5^{o}S) might contribute to this.

In addition to the scenario integration of the ECHAM4/OPYC model, changes in the strength of the (S)TC in the 1% integrations (1% increase of the CO_2 concentration per year) of the coupled model intercomparison project (CMIP2) were investigated.

In figure 45 the strengths of the TC in the different CMIP2 models are shown. The set of models slightly differs from those of the Pacific (S)TC analysis (figure 28) since some of the models do not simulate a reasonable Atlantic STC and also for some no Pacific meridional overturning was available. Note also that the available meridional overturning streamfunction output has been averaged over 20 year intervals. As for the Pacific the strength in the TC is expressed as the difference between the strengths in the 1% and in the control integration divided by the mean TC strength in the control integration (to take into account the different mean strength of the cells (figure 44) and trends in the cell strength of the control runs).

Also for the Atlantic TC no uniform response to greenhouse conditions is found within the different CMIP2 models. Furthermore, most models simulate only a rather weak trend. The same is true for the Atlantic STC (not shown). Therefore, it is difficult to estimate the Atlantic (S)TC sensitivity to global warming from the CMIP2 models.

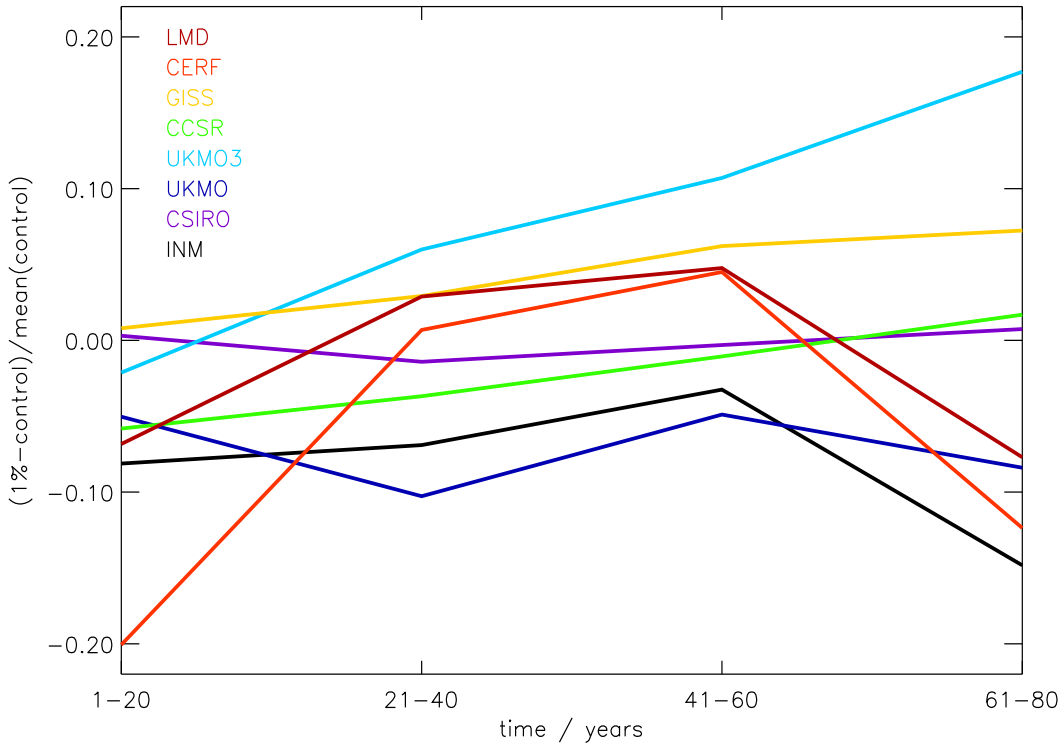

Figure 45: *Timeseries of the Atlantic TC strength for different CMIP2 models. For definition of the cell strength see text. The cell strength is expressed as timeseries of the 1% run minus timeseries of the control run divided by the mean of the control run. Note that only 20 year means are available for the meridional overturning streamfunction in CMIP2.*

5. Summary and Outlook

In this study the decadal variability of the SST in the tropical Pacific is investigated. The leading SST mode in the western equatorial Pacific (the Niño4 region) is a decadal mode. The analysis suggests that the decadal variability is closely connected to the variability of the wind driven subtropical (STCs) and tropical (TCs) overturning cells. Changes in the strength of the (S)TCs lead the changes in the SST. The lag becomes larger with increasing latitude, indicating that the STCs adjust slower than the narrow TCs. The correlation pattern between the index for the strength of the (S)TCs and the SST in the tropical Pacific shows an equatorial horseshoe-like pattern, which indicates that the influence of the cells is larger in the Niño4 than in the Niño3 region.

Different processes play important roles in the connection between (S)TCs and SST. Apart from the anomalous upwelling of colder subsurface water the zonal and meridional advection of water from the cold tongue by anomalous currents contributes to the changes in SST. In the warm pool area where the vertical temperature gradient in the upper layer is relatively weak, the horizontal temperature advection is of the same order as the vertical one. The surface heat flux acts in most regions as a damping. Thus, it is the ocean dynamics that drive the decadal SST variability in large regions of the tropical Pacific.

In the eastern equatorial Pacific, the variability of the (S)TCs does not explain much of the SST variability. The SST in this region is mainly determined by the depth of the thermocline. In the MPI-OM model integration forced with the NCEP reanalysis as well as in the coupled ECHAM4/OPYC integration, correlation coefficients between the eastern tropical SST and the depth of the thermocline are of the order of 0.8 to 0.9 for interannual as well as decadal timescales.

The results of coupled model integrations suggest the existence of a coupled feedback loop between the SST and the off-equatorial part of the STCs. One possible feedback hypothesis is described in the following. Start the loop with anomalously strong (weak) STCs. These in turn

will drive colder (warmer) SSTs in the equatorial Pacific that are La Niña- (El Niño)-like. The SST anomalies will force characteristic off-equatorial wind stress (curl) anomalies, eventually weakening (strengthening) the STCs, which completes the phase reversal.

Additionally to the tropical Pacific, the variability in the tropical Atlantic connected to the (S)TC has been investigated. Considering the influence of the (S)TC onto the equatorial Atlantic SST, no uniform results are found for different models and timescales. Since the variability in the tropical Atlantic is relatively small compared to the Pacific, one reason might be that mainly noise is considered here.

Some influence from the tropical Pacific onto the Atlantic (S)TC (via changes in the trade winds over the Atlantic Ocean) can be found. During years with anomalously warm (cold) Niño3 SST the strength of the cell increases (decreases). Also a warming of the tropical Atlantic during El Niño years is described (e.g. *Latif and Groetzner, 2000*). An increase in the strength of the (S)TC (and the equatorial upwelling) will tend to decrease the SST. These two counteracting influences might contribute to the low correlation between the SST and the (S)TC in the Atlantic.

In the following, some questions which have not been addressed within this study will be discussed.

The calculation of the Pacific meridional overturning streamfunction assumes a closed basin. However, there exists the so-called Indonesian throughflow (ITF) which connects the Pacific and the Indian Ocean at about 5^{o}S to 10^{o}S. Its strength is of the order of 10 Sv (e.g. *Gordon and McClean, 1999*).

Lee et al. (2002) performed two ocean general circulation model integrations with and without the ITF respectively. To see using such simulations if the ITF influences our results would be interesting. From their analysis *Lee et al. (2002)* found that if the ITF is blocked off the mean strength of the New Guinea Coastal Undercurrent (the tropical western boundary current in the southern hemisphere) is reduced. The relative variability of western boundary and interior pycnocline flow, however, is insensitive to the presence of the ITF (*Lee and Fukumori, 2002*).

Wu and Xie (2003) associate the climate shift in the tropical Pacific in the mid-1970s simulated by ocean models forced with the NCEP reanalysis with differences between the NCEP and the COADS (comprehensive ocean and atmosphere dataset) winds. Although the decrease in the strength of the Pacific STCs in the mid-1970s is found also in hydrographic observations (*McPhaden and Zhang, 2002*), it would be interesting to determine the strength of the (S)TCs from an ocean model forced with the COADS or other (e.g. ECMWF reanalysis) winds.

An integration of a tropical Pacific version of the MPI-OM model forced with FSU (Florida State University) winds, which was done by Heiko Hansen, shows a decrease in the equatorial upwelling strength in the mid-1970s comparable to the decrease in the upwelling in the MPI-OM model integration forced with NCEP winds which is used in this study. However, the integration forced with FSU winds shows very large variability in the upwelling around 1970 and in the 1990s.

Concerning the trend also the question how the strength of the Pacific (S)TCs will develop in the future is interesting. Will it stay at about the level of the 1980s and 1990s, will it decrease further or is the shift part of a longer timescale oscillation?

A integration of the MPI-OM model forced with the NCEP reanalysis up to 2003 (not 2001 as the integration used in this study) shows an increase in the strength of the cells in the last years. The strength, however, is still much smaller than before 1975. In a recently published paper, *McPhaden and Zhang (2004)* suggest from observations a strengthening of the Pacific STCs during the period 1998 to 2003.

The sensitivity of the Pacific and Atlantic (S)TCs to an increase in the CO_2 concentration is still controversial between different models of the coupled model intercomparison project (CMIP2). Therefore, future CMIP integrations will be of interest. A simulation with the coupled general circulation model ECHAM5/MPI-OM, in which the CO_2 concentration is increased by 1% per year, shows a decrease of the strength of the TCs (and nearly no trend off-equatorial) in the Pacific, contradicting the results of the ECHAM4/OPYC scenario integration. The simulation with the ECHAM5/MPI-OM model, however, has a cold bias of about 1^oC in the central tropical Pacific which (via stronger trade winds) leads to relatively strong (S)TCs. Therefore, under global warming conditions the strength of the cells may reduce.

Wind sensitivity experiments have shown that the variability of the TCs is driven by the equatorial winds while the variability of the STCs can be reproduced without the equatorial winds. These sensitivity experiments could be used to further investigate the (off)-equatorial influence onto the Niño4 SST variability. Since the SST is not free in these uncoupled integrations (the heatflux is calculated according to Bulk formulae), the sea surface height or the heatcontent of the upper ocean could be used instead.

The off-equatorial sensitivity experiment allows wind variability everywhere poleward of 5^o latitude. However, *Nonaka et al. (2002)* found no influence of the winds poleward of about 25^o latitude onto the equatorial SST.

Another interesting analysis is to investigate the influence of the decadal Niño4 SST anomalies onto the atmosphere, e.g. by driving an atmosphere model with SSTs obtained by the observed decadal mode (figure 4a) and the pattern from its regression onto the observed SST (figure 5a).

Considering the influence onto precipitation, contradicting results are found for the tropical North Pacific between the MPI-OM model integration forced with the NCEP reanalysis (figure 11j) and the ECHAM4/OPYC integration (figure 24k).

Also in the Indian Ocean a shallow meridional overturning circulation is found. In contrast to the Pacific and Atlantic (S)TCs , however, the overturning cell is cross-equatorial and shows a pronounced seasonal variability (*Schott et al., 2002, Miyama et al., 2003*). *Lee (2004)* suggests from satellite observations a weakening of the shallow overturning circulation in the Indian Ocean during the last decade. Therefore, it could be interesting to extend the study described in this thesis to the Indian Ocean.

References

Barnett, T., D. Pierce, M. Latif, D. Dommenget and R. Saravanan, 1999: Interdecadal interactions between the tropics and midlatitudes in the Pacific basin. *Geophysical Research Letters*, **26**, 615-618

Boccaletti, G., R. Pacanowski and S. Philander, 2004: A diabatic mechanism for decadal variability in the tropics. *Journal of Climate*, submitted

Capotondi, A., M. Alexander and C. Deser, 2003: Why are there Rossby wave maxima in the Pacific at 10^{o}S and 13^{o}N? *Journal of Physical Oceanography*, **33**, 1549-1563

Fratantoni, D., W. Johns, T. Townsend and H. Hurlburt, 2000: Low-latitude circulation and mass transport pathways in a model of the tropical Atlantic Ocean. *Journal of Physical Oceanography*, **30**, 1944-1966

Giese, B., S. Urizar and N. Fuckar, 2002: Southern hemisphere origins of the 1976 climate shift. *Geophysical Research Letters*, **29**, 1014

Goes, M. and I. Wainer, 2003: Equatorial currents transport changes for extreme warm and cold events in the Atlantic Ocean. *Geophysical Research Letters*, **30**, Cli-6

Gordon, A. and J. McClean, 1999: Thermohaline stratification of the Indonesian seas: Model and observations. *Journal of Physical Oceanography*, **29**, 198-216

Graham, N., 1994: Decadal-scale climate variability in the tropical and north Pacific during the 1970s and 1980s: Observations and model results. *Climate Dynamics*, **10**, 135-162

Gu, D. and S. Philander, 1997: Interdecadal climate fluctuations that depend on exchanges between the tropics and extratropics. *Science*, **275**, 805-807

Hazeleger, W., M. Visbeck, M. Cane, A. Karspeck and N. Naik, 2001: Decadal upper ocean temperature variability in the tropical Pacific. *Journal of Geophysical Research*, **106**, 8971-

8988

Hazeleger, W., P. DeVries and Y. Friocourt, 2003: Sources of the Equatorial Undercurrent in the Atlantic in a high-resolution ocean model. *Journal of Physical Oceanography,* **33**, 677-693

IPCC, Climate change, 1995: The science of climate change, edited by J. Houghton, L. Meira Filho, B. Callendar, N. Harris, A. Kattenberg and K. Maskell. Cambridge University Press, New York, 572pp., 1996

Johnson, G. and M. McPhaden, 1999: Interior pycnocline flow from the subtropical to the equatorial Pacific Ocean. *Journal of Physical Oceanography,* **29**, 3073-3089

Johnson, G., 2001: The Pacific Ocean subtropical cell surface limb. *Geophysical Research Letters*, **28**, 1771-1774

Kalnay, E., M. Kanamitsu, R. Kistler, W. Collins, D. Deaven, L. Gandin, M. Iredell, S. Saha, G. White, J. Woollen, Y. Zhu, M. Chelliah, W. Ebisuzaki, W. Higgins, J. Janowiak, K. Mo, C. Ropelewski, J. Wang, A. Leetmaa, R. Reynolds, R. Jenne and D. Joseph, 1996: The NCEP/NCAR 40-Year Reanalysis Project. *Bulletin of the American Meteorological Society,* **77**, 437-470

Kleeman, R., J. McCreary and B. Klinger, 1999: A mechanism for generating ENSO decadal variability. *Geophysical Research Letters*, **26**, 1743-1746

Klinger, B., J. McCreary and R. Kleeman, 2002: The relationship between oscillating subtropical wind stress and equatorial temperature. *Journal of Physical Oceanography*, **32**, 1507-1521

Latif, M. and A. Groetzner, 2000: The equatorial Atlantic oscillation and its response to ENSO. *Climate Dynamics,* **16**, 213-218

Lazar, A., R. Murtugudde and A. Busalacchi, 2001: A model study of temperature anomaly

propagation from the subtropics to tropics within the South Atlantic thermocline. *Geophysical Research Letters*, **28**, 1271-1274

Lee, T., I. Fukumori, D. Menemenlis, Z. Xing and L.-L. Fu, 2002: Effects of the Indonesian throughflow on the Pacific and Indian Oceans. *Journal of Physical Oceanography*, **32**, 1404-1429

Lee, T. and I. Fukumori, 2003: Interannual-to-decadal variations of tropical-subtropical exchange in the Pacific Ocean: Boundary versus interior pycnocline transports. *Journal of Climate*, **16**, 4022-4042

Lee, T., 2004: Decadal weakening of the shallow overturning circulation in the South Indian Ocean. *Geophysical Research Letters*, **31**, L18305, doi: 10.1029/2004GL020884

Liu, Z., 1994: A simple model of the mass exchange between the subtropical and tropical ocean. *Journal of Physical Oceanography*, **24**, 1153-1165

Liu, Z., 1998: The role of ocean in the response of tropical climatology to global warming: The west-east SST contrast. *Journal of Climate*, **11**, 864-875

Lohmann, K. and M. Latif, 2004: Tropical Pacific decadal variability and the subtropical-tropical cells. *Journal of Climate*, submitted

Lu, P. and J. McCreary, 1995: Influence of the ITCZ on the flow of thermocline water from the subtropical to the equatorial Pacific Ocean. *Journal of Physical Oceanography*, **25**, 3076-3088

Lu, P., J. McCreary and B. Klinger, 1998: Meridional circulation cells and the source waters of the Pacific Equatorial Undercurrent. *Journal of Physical Oceanography*, **28**, 62-84

Marsland, S., H. Haak, J. Jungclaus, M. Latif and F. Roeske, 2003: The Max-Planck-Institute global ocean/sea ice model with orthogonal curvilinear coordinates. *Ocean Modelling*, **5**, 91-127

McCreary, J. and P. Lu, 1994: Interaction between the subtropical and equatorial ocean circulations: the subtropical cell. *Journal of Physical Oceanography*, **24**, 466-497

McPhaden, M. and D. Zhang, 2002: Slowdown of the meridional overturning circulation in the upper Pacific Ocean. *Nature*, **415**, 603-608

McPhaden, M. and D. Zhang, 2004: Pacific Ocean circulation rebounds. *Geophysical Research Letters*, **31**, doi:10.1029/2004GL020727

Merryfield, W. and G. Boer, 2004: Variability of upper Pacific Ocean overturning in a coupled climate model. *Journal of Climate*, submitted

Miyama, T., J. McCreary, T. Jensen, J. Loschnigg, S. Godfrey and A. Ishida, 2003: Structure and dynamics of the Indian Ocean cross-equatorial cell. *Deep Sea Research II*, **50**, 2023-2047

Moura, A. and J. Shukla, 1981: On the dynamics of droughts in northeast Brazil: Observations, theory and numerical experiments with a general circulation model. *Journal of the Atmospheric Sciences*, **38**, 2653-2675

Nonaka, M., S.-P. Xie and J. McCreary, 2002: Decadal variations in the subtropical cells and equatorial Pacific SST. *Geophysical Research Letters*, **29**, 20

Oberhuber, J., 1993: Simulation of the Atlantic circulation with a coupled sea ice - mixed layer - isopycnal general circulation model. Part I: Model description. *Journal of Physical Oceanography*, **23**, 808-829

Pohlmann, H., M. Botzet, M. Latif, A. Roesch, M. Wild and P. Tschuck, 2004: Estimating the decadal predictability of a coupled AOGCM. *Journal of Climate*, **17**, 4463-4472

Rayner, N., D. Parker, E. Horton, C. Folland, L. Alexander, D. Rowell, E. Kent and A. Kaplan, 2003: Global analyses of SST, sea ice and night marine air temperature since the late

nineteenth century. *Journal of Geophysical Research*, **108**, 4407

Roeckner, E., K. Arpe, L. Bengtsson, M. Christoph, M. Claussen, L. Duemenil, M. Esch, M. Giorgetta, U. Schlese and U. Schulzweida, 1996: The atmospheric general circulation model ECHAM-4: Model description and simulation of present-day climate. Report 218, Max-Planck-Institut fuer Meteorologie, Hamburg, Germany

Roeckner, E., L. Bengtsson, J. Feichter, J. Lelieveld and H. Rohde, 1999: Transient climate change simulations with a coupled atmosphere-ocean GCM including the tropospheric sulfur cycle. *Journal of Climate*, **12**, 3004-3032

Schneider, N., S. Venzke, A. Miller, D. Pierce, T. Barnett, C. Deser and M. Latif, 1999: Pacific thermocline bridge revisited. *Geophysical Research Letters*, **26**, 1329-1332

Schott, F., M. Dengler and R. Schoenefeldt, 2002: The shallow overturning circulation of the Indian Ocean. *Progress in Oceanography,* **53**, 57-103

Sloyan, B., G. Johnson and W. Kessler, 2003: The Pacific cold tongue: A pathway for interhemispheric exchange. *Journal of Physical Oceanography*, **33**, 1027-1043

Solomon, A., J. McCreary, R. Kleeman and B. Klinger, 2003: Interannual and decadal variability in an intermediate coupled model of the Pacific region. *Journal of Climate*, **16**, 383-405

Trenberth, K. and J. Hurrell, 1994: Decadal atmosphere-ocean variations in the Pacific. *Climate Dynamics*, **9**, 303-319

Wu, L., Q. Zhang and Z. Liu, 2002: Searching for the role of ENSO in tropical Atlantic variability using a coupled GCM. *Clivar Exchanges*, **7**, 20-24

Wu, R. and S.-P. Xie, 2003: On equatorial Pacific wind changes around 1977: NCEP-NCAR reanalysis versus COADS observations. *Journal of Climate*, **16**, 167-173

Yang, H. and Z. Liu, 2004: Tropical-extratropical and inter-hemispheric climate interaction: Atmospheric bridge and oceanic tunnel. *Journal of Climate*, submitted

Zebiak, S., 1993: Air-sea interaction in the equatorial Atlantic region. *Journal of Climate*, **6**, 1567-1586

Zhang, D., M. McPhaden and W. Johns, 2003: Observational evidence for flow between the subtropical and tropical Atlantic: The Atlantic subtropical cells. *Journal of Physical Oceanography*, **33**, 1783-1797

Zhang, R.-H., L. Rothstein and A. Busalacchi, 1998: Origin of upper-ocean warming and El Nino change on decadal scales in the tropical Pacific Ocean. *Nature*, **391**, 879-883

Zhang, Y., J. Wallace and D. Battisti, 1997: ENSO-like interdecadal variability: 1900-93. *Journal of Climate*, **10**, 1004-1020

Acknowledgements

First of all I want to thank my supervisor Prof. Dr. Mojib Latif for his support throughout my PhD time including his willingness to let me participate in cruises which were completely independent from my work here at MPI.
I also thank Prof. Dr. Jens Meincke from the University of Hamburg for his willingness to be the „Erstgutachter“ of this thesis.

Lots of thanks to Dr. Noel Keenlyside for his help during all stages of this work and for critically reading the first version of this thesis as well as to all members of the Mojib Latif working group for lots of fruitful discussions.

I also want to thank Monika Esch for her help with the ECHAM4/OPYC output, Dr. Helmuth Haak for his support with the MPI-OM model and Dr. Stefan Hagemann for his help with IDL, framemaker and HTML.

To the ocean scientists at the „Bundesamt für Seeschiffahrt und Hydrographie“, especially Prof. Dr. Peter Koltermann, and the crew of RV Gauss many thanks for two wonderful months on sea.

Many thanks also to all my friends here at MPI, especially Stefan Hagemann, Semeena VS, Beena BS and Xiuhua Zhu.

This work was supported by the Ocean-CLIVAR project of the BMBF.

MPI-Examensarbeit-Referenz:

Examensarbeit Nr. 1-82 bei Bedarf bitte Anfragen:
MPI für Meteorologie, Abtlg.: PR, Bundesstr. 53, 20146 Hamburg

Examensarbeit Nr. 83 Juli 2001	**Aggregate models of climate change: development and applications** Kurt Georg Hooss
Examensarbeit Nr. 84 Februar 2002	**Ein Heterodyn-DIAL System für die simultane Messung von Wasserdampf und Vertikalwind: Aufbau und Erprobung** Stefan Lehmann
Examensarbeit Nr. 85 April 2002	**Der Wasser- und Energiehaushalt der arktischen Atmosphäre** Tido Semmler
Examensarbeit Nr. 86 April 2002	**Auswirkungen der Assimilation von Meereshöhen-Daten auf Analysen und Vorhersagen von El Niño** Sigrid Schöttle
Examensarbeit Nr. 87 Juni 2002	**Atmospheric Processes in a young Biomass Burning Plume - Radiation and Chemistry** Jörg Trentmann
Examensarbeit Nr. 88 August 2002	**Model Studies of the Tropical 30 to 60 Days Oscillation** Stefan Liess
Examensarbeit Nr. 89 Dezember 2002	**Influence of Sub-Grid Scale Variability of Clouds on the Solar Radiative Transfer Computations in the ECHAM5 Climate Model** Georg Bäuml
Examensarbeit Nr.90 Mai 2003	**Model studies on the response of the terrestrial carbon cycle to climate change and variability** Marko Scholze
Examensarbeit Nr.91 Juni 2003	**Integrated Assessment of Climate Change Using Structural Dynamic Models** Volker Barth
Examensarbeit Nr.92 Juli 2003	**Simulations of Indonesian Rainfall with a Hierarchy of Climate Models** Edvin Aldrian
Examensarbeit Nr.93 Juli 2003	**ENSO Teleconnections in High Resolution AGCM Experiments** Ute Merkel
Examensarbeit Nr.94 Juli 2003	**Application and Development of Water Vapor DIAL Systems** Klaus Ertel

MPI-Examensarbeit-Referenz:

Examensarbeit Nr. 1-82 bei Bedarf bitte Anfragen:
MPI für Meteorologie, Abtlg.: PR, Bundesstr. 53, 20146 Hamburg

Beginn einer neuen Veröffentlichungsreihe des MPIM, welche die vorherigen Reihen "Reports" und "Examensarbeiten" weiterführt:

„Berichte zur Erdsystemforschung" , „*Reports on Earth System Science*", ISSN 1614-1199
Sie enthält wissenschaftliche und technische Beiträge, inklusive Dissertationen.

Berichte zur Erdsystemforschung Nr.1 Juli 2004	**Simulation of Low-Frequency Climate Variability in the North Atlantic Ocean and the Arctic** Helmuth Haak
Berichte zur Erdsystemforschung Nr.2 Juli 2004	**Satellitenfernerkundung des Emissionsvermögens von Landoberflächen im Mikrowellenbereich** Claudia Wunram
Berichte zur Erdsystemforschung Nr.3 Juli 2004	**A Multi-Actor Dynamic Integrated Assessment Model (MADIAM)** Michael Weber
Berichte zur Erdsystemforschung Nr.4 November 2004	**The Impact of International Greenhouse Gas Emissions Reduction on Indonesia** Armi Susandi
Berichte zur Erdsystemforschung Nr.5 Januar 2005	**Proceedings of the first HyCARE meeting, Hamburg, 16-17 December 2004** Edited by Martin G. Schultz
Berichte zur Erdsystemforschung Nr.6 Januar 2005	**Mechanisms and Predictability of North Atlantic - European Climate** Holger Pohlmann
Berichte zur Erdsystemforschung Nr.7 November 2004	**Interannual and Decadal Variability in the Air-Sea Exchange of CO2 - a Model Study** Patrick Wetzel
Berichte zur Erdsystemforschung Nr.8 Dezember 2004	**Interannual Climate Variability in the Tropical Indian Ocean: A Study with a Hierarchy of Coupled General Circulation Models** Astrid Baquero Bernal
Berichte zur Erdsystemforschung Nr9 Februar 2005	**Towards the Assessment of the Aerosol Radiative Effects, A Global Modelling Approach** Philip Stier
Berichte zur Erdsystemforschung Nr.10 März 2005	**Validation of the hydrological cycle of ERA40** Stefan Hagemann, Klaus Arpe and Lennart Bengtsson


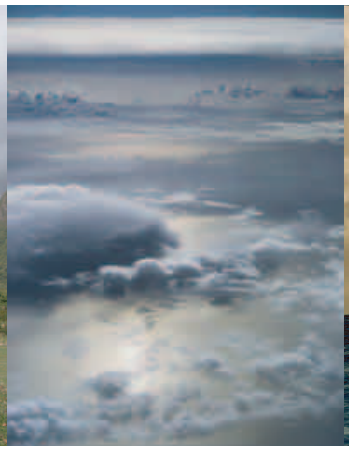


ISSN 1614-1199